

# Thesis

Gravitational wave background  
from cosmic strings and cosmic superstrings

宇宙ひもと宇宙超ひもから放出される  
背景重力波

Yuka NISHIDA

Department of Physics, Nagoya University

February 13, 2020

## Abstract

The universe has been evolving since it was born. One of the biggest goals of cosmology is to understand the evolutionary history of the universe. Although electromagnetic observations in a wide range of wavelengths have made great progress on revealing the evolutionary history, the early epoch of the universe just after the birth cannot be observed directly by electromagnetic waves. Fortunately, we recently have obtained the new observational tool, gravitational wave (GW). The ground-based interferometer LIGO enabled us to observe GWs from black hole binaries and neutron star binaries. Since, unlike the electromagnetic waves, GWs emitted in the early universe propagates until the present, we can probe and constrain the theoretical model of the early universe by observing the GWs. In this thesis, we focus on a cosmic string and cosmic superstring, both of which are considered to be formed in the early universe and emit GWs.

Various phase transitions are considered to occur in the early universe and they predict the formation of cosmic strings. Recently, cosmic superstrings are proposed as a string like an object produced at the end of inflation based on the superstring theory. Although these strings have been searched by using the cosmic microwave background (CMB) temperature anisotropies and the gravitational lensing effects, they have not been found yet.

Cosmic strings and cosmic superstrings move in the space and they form the complex network by repeating intersections and reconnections. Y-junctions where two different strings join and separate appears only in the cosmic superstring network. When these strings reconnect, the sharp structures called kinks are produced. When kinks propagate along the curved strings or collide each other, they emit GWs, which form a GW background by overlapping one another.

In the previous work, although the power spectrum of the GW background from kinks on cosmic strings has been estimated, the time evolution of the number and the sharpness of kinks (distribution function of kinks) on cosmic strings have not been taken into account. In this thesis, first, we solve the time evolution equation of the distribution function of kinks numerically. Second, we extend it for the case of the cosmic superstring considering the two effects; low reconnection probability and Y-junctions. By solving the evolution equation numerically, we find that the distribution function of kinks is determined by the balance of the two effects; the number of kink production is enhanced by low reconnection probability and kinks are blunted by Y-junctions.

Using the distribution of kinks, we estimate the power spectra of the GW background from propagating kinks on cosmic strings and cosmic superstrings numerically. Then, we suggest that we will be able to distinguish the GW background of cosmic string from one of cosmic superstring by the observation because the shapes of these power spectra are different. Moreover, we formulate the power spectra of the GW background from kink-kink collisions on cosmic strings and cosmic superstrings and calculate it numerically. We obtain the result

---

that the amplitude of the GW background from kink-kink collisions on cosmic superstrings is enhanced when the reconnection probability is  $p = 0.1$ , and propose that we may be able to observe the GW background by using future GW experiments.

## Contents

1	Introduction	3
2	Basics of cosmology	7
2.1	Friedmann-Lemaître-Robertson-Walker(FLRW) metric . . . . .	7
2.2	Friedmann equation . . . . .	8
2.3	Evolution of the homogeneous and isotropic universe . . . . .	9
3	Origin of cosmic string and cosmic superstring	12
3.1	Origin of cosmic string . . . . .	12
3.1.1	From phase transition . . . . .	12
3.1.2	From inflation . . . . .	15
3.2	Origin of cosmic superstring . . . . .	17
4	Dynamics of cosmic string and cosmic superstring	19
4.1	Dynamics of strings . . . . .	19
4.1.1	Dynamics of strings in Minkowski spacetime . . . . .	19
4.1.2	Dynamics of strings in Friedmann-Lemaître-Robertson-Walker spacetime . . .	21
4.2	Reconnection of strings . . . . .	25
4.3	Sharp structures . . . . .	25
4.3.1	Cusp . . . . .	25
4.3.2	Kink . . . . .	28
4.4	Y-junction . . . . .	28
4.4.1	Dynamics of cosmic superstring with Y-junction . . . . .	29
4.4.2	Energy conservation of cosmic superstring with Y-junction . . . . .	30
5	String network dynamics	32
5.1	Network of cosmic string . . . . .	32
5.2	Network of cosmic superstring . . . . .	35
5.2.1	Case A: string network with $\mu_1 : \mu_2 : \mu_3 = 1 : 1 : 1$ and $n_p = 1$ . . . . .	38
5.2.2	Case B: string network with $\mu_1 : \mu_2 : \mu_3 = 1 : 1 : 1$ and $n_p = \frac{1}{3}$ . . . . .	38
5.2.3	Case C: string network with $\mu_1 : \mu_2 : \mu_3 = 1 : 10 : 10$ and $n_p = \frac{1}{3}$ . . . . .	39
6	Distribution of kinks	42
6.1	Evolution of sharpness . . . . .	42
6.2	On infinite cosmic strings . . . . .	43
6.3	On infinite cosmic superstrings . . . . .	48
6.3.1	Case A: kink distribution with $\mu_1 : \mu_2 : \mu_3 = 1 : 1 : 1$ and $n_p = 1$ . . . . .	52
6.3.2	Case B: kink distribution with $\mu_1 : \mu_2 : \mu_3 = 1 : 1 : 1$ and $n_p = \frac{1}{3}$ . . . . .	53

6.3.3	Case C: kink distribution with $\mu_1 : \mu_2 : \mu_3 = 1 : 10 : 10$ and $n_p = \frac{1}{3}$ . . . . .	53
6.4	Summary . . . . .	53
7	Gravitational wave background from propagating kinks	55
7.1	Formulation . . . . .	55
7.2	Result . . . . .	60
7.2.1	Case of infinite cosmic string . . . . .	60
7.2.2	Case of infinite cosmic superstring . . . . .	60
7.2.3	Case A: GW background with $\mu_1 : \mu_2 : \mu_3 = 1 : 1 : 1$ and $n_p = 1$ . . . . .	61
7.2.4	Case B: GW background with $\mu_1 : \mu_2 : \mu_3 = 1 : 1 : 1$ and $n_p = \frac{1}{3}$ . . . . .	62
7.2.5	Case C: GW background with $\mu_1 : \mu_2 : \mu_3 = 1 : 10 : 10$ and $n_p = \frac{1}{3}$ . . . . .	62
7.3	Summary . . . . .	63
8	Gravitational wave background from kink-kink collisions	65
8.1	Formulation . . . . .	65
8.2	Result . . . . .	66
8.3	GW emission effect . . . . .	67
8.3.1	Case of infinite cosmic string . . . . .	69
8.3.2	Case of infinite cosmic superstring . . . . .	73
8.3.3	Case A: GW background with $\mu_1 : \mu_2 : \mu_3 = 1 : 1 : 1$ and $n_p = 1$ . . . . .	73
8.3.4	Case B: GW background with $\mu_1 : \mu_2 : \mu_3 = 1 : 1 : 1$ and $n_p = \frac{1}{3}$ . . . . .	74
8.3.5	Case C: GW background with $\mu_1 : \mu_2 : \mu_3 = 1 : 10 : 10$ and $n_p = \frac{1}{3}$ . . . . .	74
8.4	Summary . . . . .	76
9	Summary	78
	Appendix	82
A	Conservation of the kinks number	82
B	Analytic solution of kinks distribution function	82
C	Strain amplitude of GW from one kink	84
D	Condition of sharpness mostly contributing to GW background of frequency $f$	85
E	Energy momentum tensor $T^{\mu\nu}$ of cusp and kink	90
E.1	$I^\mu$ for a discontinuity . . . . .	92
E.2	$I^\mu$ for a stationary point . . . . .	92

# 1 Introduction

At present, the standard big bang theory, which is considered as the most suitable cosmological model, describes that the Universe was born with a high temperature and cools down as the Universe itself expands. It is the ultimate aim of cosmology to understand the evolutionary history of the Universe from birth to the present. Using electromagnetic waves in a wide range of wavelength, the history of the Universe is revealed step by step. However, we are not able to observe the early Universe through electromagnetic waves. In the early Universe, the interaction between photons and baryons were very strong. As a result, photons cannot propagate freely in the Universe.

Gravitational waves (GWs) from the black-hole or neutron-star binary mergers were detected recently [1, 2, 3]. GWs are emitted not only from astrophysical phenomena but also from cosmological ones in the early Universe, where we can not observe directly by using electromagnetic waves. In the near future, various instruments will be operated, for example, Advanced LIGO [4], Advanced Virgo [5] and KAGRA [6]. Thus, we can use GWs as a new observational tool and it opens the new era not only in astrophysics but also in cosmology.

In this thesis, we focus on the one-dimension high energy region called "cosmic string" and "cosmic superstring" as gravitational wave sources in the early Universe. Cosmic strings are topological defects produced in spontaneous symmetry breaking. It is predicted that the symmetry breaks spontaneously in some models of the early universe. Therefore, we can reveal the high energy physics through probing cosmic strings.

It is proposed that the Universe has experienced various cosmological phase transitions. The phase transitions relate to the spontaneous symmetry breaking in particle physics. Therefore, during the phase transitions in the early universe, cosmic strings can be generated by the spontaneous symmetry breaking of phase transition [7, 8]. In particular, one possible candidate of the phase transitions produced the cosmic strings is the phase transition related to grand unified theories (GUTs) which are theoretical models to unify the strong, and weak and electromagnetic interactions into a single interaction. The energy scale of this phase transition is called grand unified theory scale. Probing GWs of cosmic strings provides us important information about this energy scale.

In addition, cosmic strings could be also produced at the end of inflation in the early universe. Inflation is a theoretical model in which the rapid expansion of the universe happens in the early universe and some problems in the standard big bang theory can be solved. Although Cosmological observations strongly support the existence of the inflationary expansion in the early universe, we do not know the detailed nature of inflation. Currently, many inflation models are suggested motivated by the particle physics theories. The hybrid inflation model is proposed from supersymmetric grand unified theory [9, 10]. This model predicts that cosmic strings are generated at the end of the inflation by the spontaneous symmetry breaking. Cosmic strings might be important relics related to inflation. If we can detect GWs from cosmic strings, we can probe the energy scale associated inflation model.

On the other hand, cosmic superstrings are proposed in the framework of superstring theory, which is known as a fundamental theory at present. Cosmic superstrings are classified into two types; fundamental strings (F-strings) and 1-dimensional Dirichlet branes (D-strings) which are produced at the end of brane inflation. It is predicted that these strings might be stretched to cosmological scales and play a role similar to cosmic strings [11, 12, 13, 14]. Therefore, it is expected that cosmic string observations could open new ways to access high energy physics such as string theory and brane inflation models.

Cosmic strings and cosmic superstrings are known to provide huge impacts on the evolution of the Universe. Using precise cosmological observations, we can constrain the nature of cosmic strings and cosmic superstrings. For example, cosmic strings might be the seeds of the large scale structure [15, 16, 17, 18]. However, CMB observation showed that cosmic strings can contribute to the CMB temperature anisotropies no more than 7 %, which corresponds to the bound on the tension of cosmic strings as  $G\mu < 1.8 \times 10^{-7}$  at 68 % confidence level, where  $\mu$ , called a tension, is the energy per unit length of the cosmic string and  $G$  is the gravitational constant [19, 20, 21, 22]. When we assume that such cosmic strings are generated at the end of inflation, we can obtain constraints on the parameters of the inflation model [23].

Furthermore, cosmic strings can induce gravitational lensing [24]. This lensing due to cosmic strings is extremely different from the lensing due to a point source; the two lensed images caused by a cosmic string is aligned axisymmetrically with respect to the cosmic string. Although there was a report that such lensed images of a galaxy have been observed, the following analysis concludes that these images are just two very similar elliptical galaxies [25, 26]. We have eagerly looked for observational signals of cosmic strings and cosmic superstrings, and continue trying to constrain the tension of strings. Although the constraints keep getting tighter, these strings have never been detected directly by observations with electromagnetic waves.

Cosmic strings and cosmic superstrings emit GWs continuously since their formation. In particular, burst-like GW emissions from these strings happens at the different epochs and the different positions of the Universe. Then, these GW bursts overlap each other and, finally, form a GW background over a broad frequency range. Since we can now use GWs as observational tools of the Universe, we can test the existence of cosmic strings and cosmic superstring by GW observations. Various experiments are available to probe the GW background at different frequencies: pulsar timing experiments [27, 28] measure GWs at  $\sim 10^{-8}\text{Hz}$ ; space missions such as LISA [29, 30] and DECIGO [31, 32] can explore  $10^{-3}\text{Hz}$  and  $0.1\text{Hz}$ , respectively; ground-based experiments such as Advanced-LIGO [33], Advanced-Virgo [34] and KAGRA [35] focus on  $\sim 100\text{Hz}$ . Now it is the best time to explore the cosmic strings and cosmic superstrings through GWs.

It is known that cosmic strings and cosmic superstrings form complex networks in the Universe. These strings have two configurations called loops and infinite strings. The length of infinite strings is larger than the Hubble horizon. Cosmic strings reconnect when they intersect each other. The reconnection between infinite strings forms loops. After the formation, loops shrink by emitting GWs and disappear in the end. In other words, cosmic strings can throw

away their energy into GWs by producing loops. As a result, the number of infinite strings in the horizon is always kept constant. This process is known as the scaling law. This scaling law ensures that, once the energy density of strings is subdominant, they do not modify the expansion history of the Universe. In the reconnections, sharp structures called kinks are also produced. Kinks can propagate on strings with the speed of light. They can emit GWs during the propagation [36, 37] as well as in their collisions [38]. On loops, singularity points, called cusps, arise on loops. They can also emit strong GW bursts. These GWs overlap each other and, then, form a GW background.

In addition to them, cosmic superstrings have unique features. First, as mentioned above, the cosmic string network can be composed of different string types, D-strings and F-strings, and they have different tensions. Their reconnection probability  $p$  could be much smaller than unity, while  $p \sim 1$  is expected for cosmic strings [39]. The reconnection probability is  $10^{-1} \lesssim p_D \lesssim 1$  for D-strings and  $10^{-3} \lesssim p_F \lesssim 1$  for F-strings, respectively [40]. D-strings and F-strings can form the bound state. As a result, the string network contains Y-junctions where two different strings join and separate. Interestingly, the number of kinks increases when they enter Y-junctions. Therefore, it is suggested that the existence of Y-junction could enhance the amplitude of the GW background [41].

The GW background from cusps on cosmic string loops has been studied in many literatures [42, 43, 44, 45, 46, 47, 48, 49, 50, 51, 52]. For cosmic superstrings, [53] studied the GW background from cusps on loops by taking into account the different tensions and reconnection probabilities, while [54] investigated GWs from kinks on loops with including the effect of Y-junctions which increase the number of kinks. Infinite strings can generate GWs over a wide range of frequencies from the cosmological scales to the interferometric scales. However the amplitude of produced GWs could be much smaller than the one generated by loops [55, 56, 57, 58, 59].

In this thesis, we investigate the GW background from kink propagations and kink-kink collisions on infinite strings. In particular, we focus on the impact of the characteristic natures of cosmic superstrings; two string types with different tensions, small reconnection probability and Y-junctions. First these effects appear in the evolution of the correlation length of infinite strings, which relates to the number of infinite strings in the horizon. In [61, 62], the authors provided the evolutionary equations of the correlation length, including these effects. We utilize and numerically solve these equations in the cosmological context in order to obtain the evolution of the superstring network. Next, we develop the evolutionary equation for the number distribution of kinks to include the effects on the kink evolution in cosmic superstrings. In the case of cosmic strings, the equations of the kink evolution was obtained in [63]. In order to modify this equation for cosmic superstrings, we incorporate the effect that a kink passing through a Y-junction transforms into three kinks: a reflected kink and two transmitted kinks [41]. By solving the equations numerically, we obtain the kink number density and calculate the amplitude of the GW background.

In Ref. [60], we showed that kink-kink collisions generate a large GW background. Thus, strings throw away their energy as GWs and modify the distribution of kinks. Therefore, it is

required to evaluate both the GW emissions and the kink distribution consistently. Otherwise, the obtained GW amplitude results in over-estimated. In order to avoid over-estimation of the GW amplitude, we improve the time evolution equations of the string energy density and the kink distribution taking into account the two factors: the energy loss of the string network through GW emissions and the GW backreaction on kinks. The former reduces the length of infinite strings while the later smoothes out kink sharpness. Using the modified evolution equations, we recalculate the kink distribution and the GW background amplitude.

In this thesis, we investigate the GW background from propagating kinks and kink-kink collisions on the cosmic string and cosmic superstring. In Sec.2, we briefly review the basics of cosmology. In Sec.3, we present the generation mechanisms and natures of cosmic strings and cosmic superstrings. In Sec.4, we describe the dynamics of these strings and the production of sharp structures on strings: kinks and cusps. In Sec.5, we discuss the dynamics of the networks formed by cosmic strings and cosmic superstrings. In Sec.6, we derive the number of kinks as a function of sharpness, called the distribution function of kinks. We also show the kink distribution as the results of our numerical calculations. In Sec.7, we calculate the power spectrum of the GW background from propagating kinks along these strings, using the distribution function of kinks obtained in the previous section. In Sec.8, we present the power spectrum of the GW background from kink-kink collisions. Finally, we summarize in Sec.9.

## 2 Basics of cosmology

We introduce the basics of cosmology briefly which is needed to describe the dynamics of cosmic strings. In the big bang theory which is the standard idea of cosmology, the Universe started with high temperature and high density and cooled down with expansion. The radiation at the big bang remains as the cosmic microwave background (CMB) which was discovered by Penzias and Wilson [64], and the temperature is  $2.726 \pm 0.010\text{K}$  [65]. The big bang theory is supported by observations.

### 2.1 Friedmann-Lemaître-Robertson-Walker(FLRW) metric

Observing the recession velocity of galaxies at long distances, Hubble discovered the relation between the recession velocity  $v$  and the distance  $r$  as

$$v = Hr. \quad (2.1.1)$$

This is called Hubble's law.  $H$  is the Hubble parameter and rewritten as

$$H = 100h \text{ [km/(s} \cdot \text{Mpc)]}, \quad (2.1.2)$$

where  $h$  is dimensionless and  $h = 0.6781 \pm 0.0092$  [66]. Since the universe is expanding, we use a convenient coordinate called comoving coordinate  $x$ . In the comoving coordinate, the galaxies are fixed. The physical coordinate  $r(t)$  can be written using the comoving coordinate and the scale factor  $a(t)$  which evolves with time as

$$r(t) = a(t)x. \quad (2.1.3)$$

Since Hubble's law is connected with the expansion of the universe, the Hubble parameter is defined as

$$H \equiv \frac{\dot{a}}{a}, \quad (2.1.4)$$

where the dot means the time derivative.

With the expansion of the universe, the wavelength of the light from the far galaxy is extended. It is called redshift. The redshift  $z$  is defined as

$$z \equiv \frac{\lambda_{\text{obs}} - \lambda_{\text{em}}}{\lambda_{\text{em}}}, \quad (2.1.5)$$

where  $\lambda_{\text{em}}$  is the wavelength of photons emitted from a long-distance galaxy and  $\lambda_{\text{obs}}$  is observed wavelength. The ratio  $\frac{\lambda_{\text{obs}}}{\lambda_{\text{em}}}$  is the same as the one of the scale factor. If  $t = t_0$ ,

$a(t_{\text{obs}}) = a(t_0)$ . Then, the redshift is

$$1 + z = \frac{a(t_0)}{a(t_{\text{em}})}. \quad (2.1.6)$$

Let us consider how the universe evolves. In the cosmological principle, the universe is homogeneous and isotropic at a large scale and they are confirmed by the observation [67]. The metric of the homogeneous and isotropic universe is written as

$$ds^2 = -dt^2 + a(t)^2(\gamma_{ij}dx^i dx^j), \quad (2.1.7)$$

where  $x^i$  is comoving coordinate and  $a(t)$  depends only on the time. In this paper, we define the speed of light  $c = 1$ . The discoverers of the specific metric formulation are Friedmann, Lemaître, Robertson and Walker [68, 69, 70]. So, it is called Friedmann-Lemaître-Robertson-Walker(FLRW) metric and written as

$$ds^2 = -dt^2 + a(t)^2 \left\{ \frac{dr^2}{1 - Kr^2} + r^2(d\theta^2 + \sin^2\theta d\phi^2) \right\} \quad (2.1.8)$$

using the polar coordinate.  $K$  is the curvature of the space. Depending on the sign of the curvature, the configuration of the universe is different respectively in the following way:

- $K > 0$  is open universe,
- $K = 0$  is flat universe,
- $K < 0$  is closed universe.

## 2.2 Friedmann equation

\*<sup>1</sup> In order to understand the dynamics of the universe, we must clarify the evolution of the scale factor. Therefore, let us derive the time evolution equation of the scale factor using the FLRW metric and the Einstein equation which connects the spacetime with the energy

$$R_{\mu\nu} - \frac{1}{2}g_{\mu\nu}R + \Lambda g_{\mu\nu} = 8\pi G T_{\mu\nu}, \quad (2.2.1)$$

where  $R_{\mu\nu}$ ,  $g_{\mu\nu}$ ,  $R$ ,  $\Lambda$ ,  $G$  and  $T_{\mu\nu}$  are a Ricci tensor, a metric, a Ricci scalar, a cosmological constant and an energy-momentum tensor, respectively. Considering the symmetries of the metric, the energy-momentum tensor must be symmetry, too. We assume that the universe is described as the perfect fluid

$$T_{\mu\nu} = \text{diag}(\rho, -p, -p, -p), \quad (2.2.2)$$

---

\*<sup>1</sup> We write this subsection referring to [71].

where the other components are 0 and the energy density  $\rho$  and pressure  $p$  have a time dependence. Using this energy-momentum tensor and the FLRW metric, Eq.(2.2.1) yields the two independent equations as

$$H^2 = \frac{8\pi G}{3}\rho - \frac{K}{a^2} + \frac{\Lambda}{3}, \quad (2.2.3)$$

$$\frac{\ddot{a}}{a} = -\frac{4\pi G}{3}(\rho + 3p) + \frac{\Lambda}{3}. \quad (2.2.4)$$

Eq.(2.2.3) is called the Friedmann equation and Eq.(2.2.4) is an acceleration equation. The Friedmann equation expresses the time evolution of the scale factor. By solving the equation, we get the evolution of the universe. Eq.(2.2.4) describes whether the velocity of the cosmic expansion has acceleration depending on the components of  $\rho$ ,  $p$  and  $\Lambda$ .

Imposing the energy conservation  $T_{\mu\nu}{}^{;\nu} = 0$  and using the  $\mu = 0$  component, we get the fluid equation

$$\dot{\rho} + 3\frac{\dot{a}}{a}(\rho + p) = 0. \quad (2.2.5)$$

We assume that the equation of state is defined as

$$p = w\rho \quad (2.2.6)$$

where  $w$  is a constant. Substituting Eq.(2.2.6) into Eq.(2.2.5), the energy density becomes

$$\rho \propto a^{-3(1+w)}. \quad (2.2.7)$$

The value of  $w$  is determined by the component of the universe.

### 2.3 Evolution of the homogeneous and isotropic universe

In order to solve the Friedmann equation, first, we must give the energy density evolution  $\rho(a)$  of each component (matter and radiation). In the case of the matter, the total number of the matter should conserve. When we define the total number as  $N_{\text{m, tot}} \equiv \frac{4\pi}{3}a(t)^3 n_{\text{m}}(t)$ , where  $n_{\text{m}}(t)$  is the number density, by considering the conservation of the total number, we find  $n_{\text{m}}(t)$  is proportional to  $a(t)^{-3}$ . Assuming that the average mass of the matter is given by  $m$ , the energy density is written as

$$\rho_{\text{m}}(t) \sim mn_{\text{m}}(t) \propto a(t)^{-3}. \quad (2.3.1)$$

Comparing with Eq.(2.2.7), we find the parameter is  $w = 0$  and  $p = 0$ . Let us consider the energy density of the radiation. The number density of the radiation  $n_{\text{r}}(t)$  is same as the matter. In addition to the number density, we must take into account the redshift. Since the radiation get redshift, the wavelength is proportional to  $a(t)$  and an energy of the redshift photon  $q(t)$  has the dependence of  $a(t)^{-1}$ . Then, the energy density of the radiation  $\rho_{\text{r}}(t)$  is

described as

$$\rho_r(t) \sim q(t)n_r(t) \propto a(t)^{-4}. \quad (2.3.2)$$

Using this result with Eq.(2.2.7), we obtain  $w = \frac{1}{3}$  and  $p = \frac{1}{3}\rho$ . In the case of the cosmological constant, the energy density is constant. Then, the parameter is  $w = -1$ .

We rewrite the Friedmann equation using the energy density at the present as

$$H^2 = \frac{8\pi G}{3} \left( \frac{\rho_{r,0}}{a^4} + \frac{\rho_{m,0}}{a^3} \right) - \frac{K}{a^2} + \frac{\Lambda}{3}, \quad (2.3.3)$$

where the suffix 0 denotes the present. Using the Hubble parameter today  $H_0$ , we define the critical energy density as

$$\rho_{c,0} \equiv \frac{3H_0^2}{8\pi G}. \quad (2.3.4)$$

We set the density parameters  $\Omega_{r,0}$  and  $\Omega_{m,0}$ , curvature parameter  $\Omega_{K,0}$  and cosmological constant parameter  $\Omega_{\Lambda,0}$  as

$$\Omega_{r,0} \equiv \frac{\rho_{r,0}}{\rho_{c,0}}, \quad \Omega_{m,0} \equiv \frac{\rho_{m,0}}{\rho_{c,0}}, \quad \Omega_{K,0} \equiv -\frac{3K}{8\pi G\rho_{c,0}}, \quad \Omega_{\Lambda,0} \equiv \frac{\Lambda}{8\pi G\rho_{c,0}}, \quad (2.3.5)$$

These parameters are constrained by the observation [66] as

$$\Omega_{r,0}h^2 = 4.31 \times 10^{-5}, \quad \Omega_{m,0} = 0.308, \quad \Omega_{K,0} = -0.005, \quad \Omega_{\Lambda,0} = 0.692. \quad (2.3.6)$$

The Friedmann equation is rewritten as

$$H = H_0 \sqrt{\frac{\Omega_{r,0}}{a^4} + \frac{\Omega_{m,0}}{a^3} + \frac{\Omega_{K,0}}{a^2} + \Omega_{\Lambda,0}}. \quad (2.3.7)$$

As the time passes, the scale factor varies from  $a = 0$  to  $a = 1$ . Since the dependence on  $a$  of each component is different, the dominant energy of the universe also changes. At the early stage of the universe when  $a$  is extremely small, the radiation is dominant (the RD era). Next, the matter dominates the universe (the MD era) and the cosmological constant is the main component of the universe (the  $\Lambda$ D era) at the present day. Using the relation between the Hubble parameter and the scale factor Eq.(2.1.4), we summarize the evolution of the universe for each different era respectively as

- at the RD era

$$H \simeq \sqrt{H_0^2 \frac{\Omega_{r,0}}{a^4}} \quad \Rightarrow \quad a(t) \propto t^{1/2}, \quad (2.3.8)$$

- at the MD era

$$H \simeq \sqrt{H_0^2 \frac{\Omega_{m,0}}{a^3}} \quad \Rightarrow \quad a(t) \propto t^{2/3}, \quad (2.3.9)$$

- at the curvature dominant era

$$H \simeq \sqrt{H_0^2 \frac{\Omega_{\text{K},0}}{a^2}} \quad \Rightarrow \quad a(t) \propto t, \quad (2.3.10)$$

- at the  $\Lambda$ D era

$$H \simeq \sqrt{H_0^2 \Omega_{\Lambda,0}} \quad \Rightarrow \quad a(t) \propto e^{\sqrt{\Lambda/3}t}. \quad (2.3.11)$$

### 3 Origin of cosmic string and cosmic superstring

It is suggested that the cosmic string and cosmic superstring in the early universe are generated. In this section, we describe how these strings are produced. First, we focus on cosmic strings production.

#### 3.1 Origin of cosmic string

It is proposed that there are two origins of cosmic strings; produced by the phase transition in the early universe and at the end of the inflation.

##### 3.1.1 From phase transition

The big bang takes place in the early Universe and the universe is cooled down with cosmic expansion. It is suggested that the fundamental interactions (strong, electromagnetic, weak and gravitational forces) are once unified at above the critical temperature where the symmetry is not broken yet. The unification of the electroweak interaction is succeeded by the Glashow-Weinberg-Salam theory over  $10^2\text{GeV}$ . At higher temperatures ( $10^{16}\text{GeV}$ ), the strong and electroweak interactions and the theory describing it is called the grand unified theory (GUT). The GUT model has not been confirmed yet.

In the early universe, the symmetry of the gauge theory restores [72], and the spontaneous symmetry breaking which happens by obtaining the vacuum expectation value of the scalar fields can play a role in making topological defects [73]. The configuration of the topological defects depends on the vacuum manifold and the production of defects is inevitable in the phase transition [7]. The temperature of the phase transition with the spontaneous symmetry breaking, for example, the GUT scale, is related to the features of the topological defects. Therefore, it is useful to probe the phase transition by considering topological defects. In the following, we focus on the cosmic string and introduce the features using some equations.

Using real  $n$ -plet scalar fields  $\phi \equiv (\phi_1, \phi_2, \dots, \phi_n)$ , the Lagrangian in Goldstone model [74] is written as

$$\mathcal{L} = \frac{1}{2}(\partial_\nu \phi)(\partial^\nu \phi) - \frac{\lambda}{4}(\phi^2 - \iota^2)^2, \quad (3.1.1)$$

where  $\lambda$  and  $\eta$  are positive constants. This also holds for complex scalar fields. For instance, the scalar field is  $\phi = \phi_1 + i\phi_2$  in the case of  $U(1)$  gauge theory, which yields cosmic strings. In the case of other topological defects such as domain wall, monopole, and texture, the type and number of the scalar fields are a real scalar ( $n = 1$ ), real triplet scalar ( $n = 3$ ) and real 4-plet scalar or doublet complex scalar field ( $n = 4$ ), respectively.

At extremely high temperatures, the symmetry is not broken, then, the scalar fields stay at  $\phi = 0$ . But the period of keeping the symmetry does not continue so long. As the universe gets cold, the phase transition occurs, where the symmetry is broken spontaneously. The scalar

fields change the value by moving to the potential minimum as

$$\phi^2 = (\phi_1)^2 + (\phi_2)^2 + \dots + (\phi_n)^2 = \iota^2. \quad (3.1.2)$$

The manifold  $\mathcal{M}$  where the vacuum forms are different structure with the number of scalar fields. In the case of cosmic strings ( $n = 2$ ), the values of the scalar fields satisfy  $(\phi_1)^2 + (\phi_2)^2 = \iota^2$ . Then, the vacuum region draw the circle like the bottom of the bottle and the vacuum manifold is a one-dimensional sphere  $S^1$ . In another case, for example, when we consider domain wall ( $n = 1$ ), the minimum energy state is  $\phi = \pm\iota$ . Therefore, the manifold is the zero-dimensional sphere  $S^0 = \{-1, +1\}$ . For monopole ( $n = 3$ ), the scalar fields are trapped in the sphere of  $(\phi_1)^2 + (\phi_2)^2 + (\phi_3)^2 = \iota^2$ , then, the manifold has the topology of the two-dimensional sphere  $S^2$ . Similarly, in the case of texture ( $n = 4$ ), the vacuum manifold forms  $S^3$ .

Solving the equation of the scalar field, we get a nontrivial solution, and these topological defects are the solitons. The configuration of these topological defects is determined by the vacuum manifold. In particular, the cosmic string forms a one-dimensional object. The details are the following.

Consider the cosmic string case ( $\phi = \phi_1 + i\phi_2$ ), where the potential looks like a wine bottle. When the spontaneous symmetry breaking happens, the vacuum manifold is written as

$$(\phi_1)^2 + (\phi_2)^2 = \iota^2. \quad (3.1.3)$$

This forms a circle. In order to see the formation of the cosmic string, let us imagine two regions A and B, which are not causally connected to each other. Let us assume that the expectation values of the scalar fields in the region A are  $\phi_{1,A} > 0$  and  $\phi_{2,A} > 0$ . Since there are no communications between regions A and B, there is the possibility that the expectation values in the region B are  $\phi_{1,B} < 0$  and  $\phi_{2,B} < 0$ . Because the value of the scalar field must be continuous in the space, there are areas satisfying  $\phi_1 = 0$  somewhere between regions A and B. Similarly in the case of  $\phi_2$ ,  $\phi_2$  becomes 0 in somewhere. When the areas of  $\phi_1 = 0$  and  $\phi_2 = 0$  cross, there is a one-dimensional space satisfying  $\phi_1 = \phi_2 = 0$  (Fig.3.1.1), where the false vacuum stays. In this way, the one-dimensional object called cosmic string is formed.

Let us estimate the cosmic string energy per unit length, called tension  $\mu$ . Here, we consider the straight global string, in other words, we assume no gauge field. The tension can be estimated by integrating  $(\partial_\nu\phi)(\partial^\nu\phi)$  over the volume. Using the dimension conversion,  $\partial_\nu\phi$  can be approximated as  $\frac{\eta}{r}$  at a distance  $r$  from cosmic string core. Then, the tension is written as

$$\mu \sim \int d^2x (\partial_\nu\phi)(\partial^\nu\phi) \sim \iota^2 \int dr 2\pi r \frac{1}{r^2}. \quad (3.1.4)$$

If we integrate the equation to  $r = \infty$ , the tension diverges logarithmically.

Next, we estimate the tension in the case of the local string with the local gauge invariance, known as the abelian-Higgs model [75]. In this case, the gradient term  $\partial_\nu\phi$  is displaced by

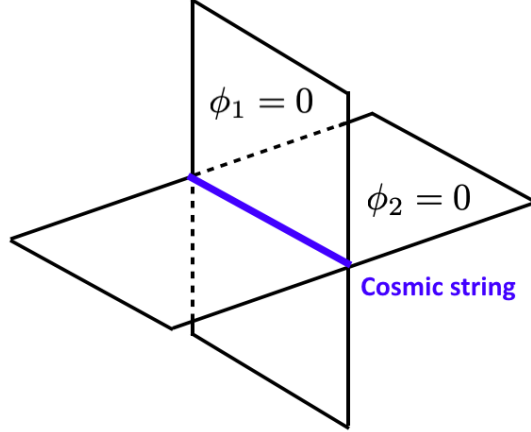


Fig. 3.1.1 The formation of a cosmic string at the false vacuum of the potential.

$\mathcal{D}_\nu\phi = \partial_\nu\phi + ieA_\nu\phi$ , where  $e$  is the gauge coupling and  $A_\nu$  is a gauge vector field. Using  $\mathcal{D}_\nu\phi$ , the Lagrangian of the scalar field is rewritten as

$$\mathcal{L} = \frac{1}{2}(\mathcal{D}_\nu\phi)(\mathcal{D}^\nu\phi)^\dagger - \frac{\lambda}{4}(\phi^2 - v^2)^2 - \frac{1}{4}F_{\mu\nu}F^{\mu\nu}, \quad (3.1.5)$$

where  $F_{\mu\nu} = \partial_\mu A_\nu - \partial_\nu A_\mu$ . When we apply the local gauge transformation

$$\phi(x) \rightarrow e^{i\chi(x)}\phi(x), \quad A_\nu(x) \rightarrow A_\nu(x) + \frac{1}{e}\partial_\nu\chi(x) \quad (3.1.6)$$

to this model, the Lagrangian is invariant. We assume that  $\partial_\nu\phi(x)$  damps faster than  $\frac{1}{r}$ . When the gauge vector field satisfies the relation

$$A_\nu(x) \rightarrow \frac{1}{e}\partial_\nu\chi(x), \quad (3.1.7)$$

as  $r \rightarrow \infty$ , this covariant derivative  $\mathcal{D}_\nu\phi$  becomes 0 far from the core of the string. Therefore, the tension does not diverge and has a finite value. In this case, there are a gauge vector field. Let us calculate the magnetic flux  $\Phi_B$  which flows along the string. We get  $\Phi_B$  to integrate the magnetic field  $\mathbf{B} = \nabla \times \mathbf{A}$  by the surface

$$\Phi_B = \int d^2x \mathbf{B} = \oint d_i x A_i = \frac{2\pi}{e}n, \quad (3.1.8)$$

where  $n$  is integer. Namely, the flux of the magnetic flux is quantized in the gauged  $U(1)$  theory.

A cosmic string has a thickness and lets us calculate it. The scalar and vector field in the universe drop in vacuum value exponentially and have masses  $m_\phi = \sqrt{2\lambda}v$  and  $m_A = e v$

respectively <sup>\*2</sup> after the spontaneous symmetry breaking. The thickness of the cosmic string can be estimated using the Compton wavelengths  $\delta_\phi \sim m_\phi^{-1}$  and  $\delta_A \sim m_A^{-1}$ . For  $m_\phi > m_A$ , the relation of the wavelength is  $\delta_\phi < \delta_A$ , then the scalar and vector fields have the same contributions on the tension;

$$\mu(\phi) \sim \lambda \iota^4 \delta_\phi^2 \sim \iota^2 \quad (3.1.9)$$

$$\mu(A) \sim B^2 \delta_A^2 \sim (e\delta_A^2)^{-2} \delta_A^2 \sim \iota^2 \quad (3.1.10)$$

where  $\lambda \iota^4$  is the potential at the cosmic string core ( $\phi = 0$ ). Then, at present, the string mass in the horizon is

$$\iota^2 t_0 \sim 10^{47} \left( \frac{\iota}{10^{16} \text{GeV}} \right)^2 [\text{kg}]. \quad (3.1.11)$$

Because the critical density of the universe is  $10^{52} \text{kg}$ , for the present, the observational conflict does not happen no matter how the spontaneous symmetry breaks at the GUT scale ( $10^{16} \text{GeV}$ ).

In this paper, we focus on cosmic strings with the local gauge invariance since the local strings do not have any divergence.

### 3.1.2 From inflation

The big bang theory explaining the history of the universe has problems such as flatness, horizon and monopole problems. In order to solve these problems, the inflation theory was suggested by Guth, Sato and so on in the first of the 1980s [76, 77]. There are a lot of models of inflation, and the slow-roll inflation which is one of the models and is driven by a scalar field rolls down on the potential. There are many kinds of potentials proposed to realize inflation. In these models, it is suggested that the hybrid inflation model, which has two scalar fields, makes cosmic strings at the end of the inflation [9]. Let us focus on this hybrid inflation.

To compare the hybrid inflation with the slow-roll inflation model of the single scalar field, first, we describe the later briefly. Single-field inflation continues while the scalar field, called inflaton  $\phi$ , rolls down on the potential, and inflation ends when the slow-roll ends or when the phase transition occurred. In the case of hybrid inflation, the end of inflation is different. The inflaton rolls down in the potential slowly and the second scalar field called the waterfall field  $\chi$  starts to roll down to the different direction of the potential rapidly, then, the inflation finishes. The merit of the hybrid inflation is that the model does not need fine-tuning of the parameters in the model. The hybrid inflation is described by the supersymmetry theory (SUSY) and the supergravity theory (SUGRA), which are suggested as high energy theory.

First, we explain the process of the formation of cosmic strings considering the simple potential. The potential of the two scalar fields inflaton  $\phi$  and waterfall field  $\chi$  is written as

---

<sup>\*2</sup> From the kinetic term of the Lagrangian, the term  $e^2 \phi^2 A_\nu A^\nu$  appears. At the vacuum, the value of the scalar field is  $\phi^2 = \eta^2$ , then, we define  $m_A$  as  $e^2 \eta^2 A_\nu A^\nu \equiv m_A^2 A_\nu A^\nu$ . On the other hand, we focus on the potential term of the Lagrangian and define  $m_\phi$  as  $\lambda \iota^2 \phi^2 / 2 \equiv m_\phi^2 \phi^2$ .

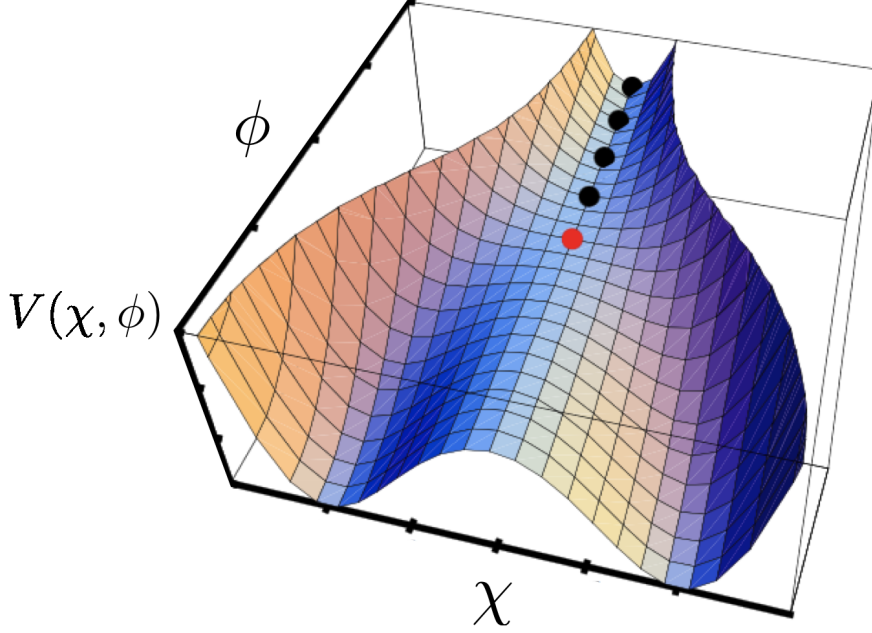


Fig. 3.1.2 The potential of the hybrid inflation [78], where we change the axes labels.

[9]

$$V(\chi, \phi) = \frac{1}{4\lambda}(M^2 - \lambda\chi^2)^2 + \frac{m^2}{2}\phi^2 + \frac{g^2}{2}\phi^2\chi^2, \quad (3.1.12)$$

where  $\lambda, M, m, g$  are constant. We assume the effective mass of  $\chi$  as

$$m_\chi^2 \equiv \frac{d^2V}{d\chi^2} = -M^2 + g^2\phi^2. \quad (3.1.13)$$

In the  $\phi > \phi_c = M/g$  region, the scalar field rolls down the bottom of the potential valley, where  $m_\chi^2 > 0$  at  $\chi = 0$ . After the symmetry breaks spontaneously at  $\phi = \phi_c$ , because in the  $\phi < \phi_c$  region, the mass of the scalar field at  $\chi = 0$  becomes negative  $m_\chi^2 < 0$ , the scalar field rolls down on the potential ridge. Then, it drops to the minimum of the potential at  $\chi \neq 0$  and the inflation ends. At the end of the inflation, high energy regions of  $\chi = 0$  remain, and the region becomes topological defects. Similarly to this case, when the scalar fields consist of two real scalar or one complex scalar, the topological defect becomes one-dimensional and cosmic strings.

Although there are numerous inflation models, we still do not know which model is appropriate as the real history of the universe. Constraining the inflation model is important in order to understand the early universe. For this purpose, it is very interesting to use cosmic

strings as a probe of the early universe.

### 3.2 Origin of cosmic superstring

In the first of the 2000s, cosmic superstrings are suggested as an early universe remnant having similar features of the cosmic string in the universe [11, 12, 13, 14, 79]. Cosmic superstrings originate from brane inflation based on the superstring theory. The superstring theory is one of the candidates, which has a possibility to unify the four fundamental interactions (strong, electromagnetic, weak and gravity) in the early universe. The string theory has been suggested to describe the behavior of the hadrons by describing it not as a point object but a string spreading object. The superstring theory is proposed [80, 81, 82] by adding supersymmetry to this string theory in order to treat fermions as well as bosons.

Since the superstring theory is known as the fundamental theory of elementary particles and high energy physics, we expect to be able to suggest inflation models independently of the initial condition, in the other words, they do not need fine-tuning. One such inflation model is called brane inflation and more generalized than the one from the common inflation introduced in the previous subsection. The outline of the brane inflation is the following. The superstring theory is the high dimensional theory. There are a three-dimensional membrane where we live, called a brane, and anti-brane in the high dimension space called a bulk. These branes are attracted by each other and the inflation occurs on the brane we are living as the distance between the brane and anti-brane becomes shorter. Finally, the inflation ends when the branes collide and annihilate. At the end of the inflation, the two type objects, fundamental string (F-string) and D-string are generated. They are the cosmological size and called cosmic superstring [83]. D-string is the one-dimensional remnant of the brane and expressed by the linear combination of  $U(1)$  gauge symmetry which exists in the brane and anti-brane. In the bulk, another linear combination of  $U(1)$  gauge symmetry is concentrated like a flux by the fundamental closed strings and it is called F-string [84].

The superstring theory is described at the extremely high energy, called the Planck scale ( $10^{19}\text{GeV}$ ), where the gravity interacts with the other three forces. Then, the tension is considered to be determined by the Planck scale corresponding to  $G\mu \sim 1$ , however, this is a serious conflict with today's observation such as CMB and pulsar timing arrays. Namely, cosmic superstrings which compose elementary particle should not exist. For one of the superstring theory suggesting the brane inflation, the type IIB string theory, the conflict is broken. In this model, the brane and anti-brane causing inflation exist at the bottom of the throat in the high dimensional manifold. Then, the throat is affected by the gravitational redshift expressed by the warp factor  $e^{2A(y)}$  and the metric is written as [85]

$$ds^2 = e^{2A(y)}\eta_{\mu\nu}dx^\mu dx^\nu + \dots, \quad (3.2.1)$$

where  $y$  is the coordinate of the co-dimension. Considering a string at  $y = y_0$  and using this metric, the action of the world sheet is rewritten by the warp factor. Therefore, the tension

of the string is expressed as

$$\mu = e^{2A(y_0)} \mu_{\text{no warp}}. \quad (3.2.2)$$

The warp factor  $e^{2A(y_0)}$  is smaller than 1 at the throat in this model, and the tension of the cosmic superstring is reduced. Therefore, this tension does not cause conflict with the observations.

## 4 Dynamics of cosmic string and cosmic superstring

This section explains the characteristics of cosmic strings and cosmic superstrings such as string dynamics, string reconnection, sharp structure on strings and the feature of the cosmic superstring.

### 4.1 Dynamics of strings

In the three dimensional space, cosmic strings and cosmic superstrings are the one-dimensional objects. These strings make a two-dimensional plane in the four dimensions, called "world sheet". From the action of these strings, the dynamics of the strings in the four dimension time-space can be derived using the parameter

$$x^\mu = x^\mu(\zeta^a), \quad (4.1.1)$$

where  $a = 0, 1$  and  $\zeta^0, \zeta^1$  is timelike and spacelike. The string action is required to follow three feature;

- unchangeable with general coordinate transformation,
- invariant under converting  $\zeta^a \rightarrow \tilde{\zeta}^a(\zeta)$ ,
- determined by  $x^\mu(\zeta^a)$  and string tension  $\mu$ .

Satisfying these characteristics, the action of strings is described by Nambu-Goto action [86, 87, 88] as

$$S[x^\mu] = -\mu \int d^2\zeta \sqrt{-\det(\gamma_{ab})}. \quad (4.1.2)$$

$\gamma_{ab}$  is the metric on the world sheet called induced metric and written as

$$\gamma_{ab} = \frac{\partial x^\mu}{\partial \zeta^a} \frac{\partial x^\nu}{\partial \zeta^b} g_{\mu\nu}. \quad (4.1.3)$$

#### 4.1.1 Dynamics of strings in Minkowski spacetime

In Minkowski spacetime, the metric is defined as

$$ds^2 = -dt^2 + dx^2 + dy^2 + dz^2. \quad (4.1.4)$$

$\det(\gamma_{ab})$  is given by

$$\det(\gamma_{ab}) = \dot{x}^2 x'^2 - (\dot{x} \cdot x')^2, \quad (4.1.5)$$

where the dot and the prime denote the derivative with respect to  $\zeta^0$  and  $\zeta^1$ ,  $a \cdot b = a^\mu b_\mu$ .

In order to understand the observable dynamics of strings, let us take the parameter as

$$\zeta^0 = t, \quad \zeta^1 = l, \quad (4.1.6)$$

where  $t$  is the time and  $l$  is the length along the string. The action is rewritten as [87]

$$S[x^\mu] = -\mu \int dt \int dl \sqrt{1 - \mathbf{v}_\perp^2}, \quad (4.1.7)$$

where  $\mathbf{v}_\perp$  is the transverse velocity defined as

$$\mathbf{v}_\perp = \frac{\partial \mathbf{x}}{\partial t} - \frac{\partial \mathbf{x}}{\partial l} \left( \frac{\partial \mathbf{x}}{\partial t} \cdot \frac{\partial \mathbf{x}}{\partial l} \right). \quad (4.1.8)$$

It is easy to understand the meaning of the action Eq.(4.1.7) since we use only the transverse motion along the string.

In general, the equation of motion of the string is [86, 88] given by

$$\frac{\partial}{\partial \zeta^a} \left( \frac{\partial L}{\partial x^\mu / \partial \zeta^a} \right) - \frac{\partial L}{\partial x^\mu} = 0 \quad (4.1.9)$$

where Lagrangian of the string is  $L = -\mu \sqrt{-\det(\gamma_{ab})}$ . Writing down concretely,

$$\frac{\partial}{\partial \zeta^0} \left\{ \frac{(\dot{x} \cdot x') x^{\mu'} - x'^2 \dot{x}^\mu}{\sqrt{(\dot{x} \cdot x')^2 - \dot{x}^2 x'^2}} \right\} + \frac{\partial}{\partial \zeta^1} \left\{ \frac{(\dot{x} \cdot x') \dot{x}^\mu - \dot{x}^2 x^{\mu'}}{\sqrt{(\dot{x} \cdot x')^2 - \dot{x}^2 x'^2}} \right\} = 0 \quad (4.1.10)$$

Since  $g_{\mu\nu}$  is independent of  $x^\mu$  in Minkowski spacetime, the last term of Eq.(4.1.9) is 0. The energy-momentum tensor is written as [89, 90]

$$T^{\mu\nu}(t, \mathbf{r}) = \mu \int d\zeta^0 \int d\zeta^1 (\dot{x}^\mu \dot{x}^\nu - x^{\mu'} x^{\nu'}) \delta^3(\mathbf{r} - \mathbf{x}(\zeta^0, \zeta^1)) \quad (4.1.11)$$

Simplifying the equation of motion, the parameters  $\zeta^0, \zeta^1$  are chosen as

$$\zeta^0 = t, \quad \zeta^1 = \sigma, \quad (4.1.12)$$

where  $\sigma$  is the length along the string. The trajectory of the string is written as  $\mathbf{x}(\sigma, t)$ . Imposing two gauge conditions

$$\dot{\mathbf{x}} \cdot \mathbf{x}' = 0, \quad (4.1.13)$$

$$\dot{\mathbf{x}}^2 + \mathbf{x}'^2 = 1, \quad (4.1.14)$$

the equation of motion is described as

$$\ddot{\mathbf{x}} - \mathbf{x}'' = 0. \quad (4.1.15)$$

This is the wave equation. It is easy to understand the physical meaning of the gauge conditions of Eqs. (4.1.13) and (4.1.14). From Eq.(4.1.13), we find  $\dot{\mathbf{x}}$  is perpendicular to the string. Namely,  $\dot{\mathbf{x}}$  is same as  $\mathbf{v}_\perp$  of Eq.(4.1.8) and it can be observe physically. Eq.(4.1.14) is related to the energy of string. It is rewritten as  $d\sigma = (1 - \dot{\mathbf{x}}^2)^{-\frac{1}{2}}|d\mathbf{x}|$  and this equation is integrated as

$$\mu \int d\sigma = \mu \int (1 - \dot{\mathbf{x}}^2)^{-\frac{1}{2}}|d\mathbf{x}| \equiv E, \quad (4.1.16)$$

where  $E$  is the energy of the string. Eq.(4.1.15) mentions the relation between the acceleration and the local curvature of the string. Using the local curvature of the string  $R \equiv \left| \frac{d^2\mathbf{x}}{dt^2} \right|^{-1}$  and Eq.(4.1.15), the acceleration of the string element is described as

$$\ddot{\mathbf{x}} = \frac{1}{R} \quad (4.1.17)$$

in the rest frame ( $\dot{\mathbf{x}} = 0$ ). The acceleration of string increases if the local curvature is small. The direction of the acceleration is the same as straightening the curved string. Generally, the solution of the wave equation (4.1.15) is given by

$$\mathbf{x}(t, \sigma) = \frac{1}{2} \{ \mathbf{a}(\sigma - t) + \mathbf{b}(\sigma + t) \}, \quad (4.1.18)$$

where the  $\mathbf{a}$ ,  $\mathbf{b}$  is arbitrary function satisfying the guage condition Eqs.(4.1.13) and (4.1.14),

$$|\mathbf{a}'|^2 = |\mathbf{b}'|^2 = 1. \quad (4.1.19)$$

This condition says that  $\mathbf{a}'$ ,  $\mathbf{b}'$  are the unit vector. However, the solution  $\mathbf{a}$ ,  $\mathbf{b}$  is propagating along the string at the speed of light, the velocity of string-self  $\dot{\mathbf{x}}$  is 70% of light speed [91] .  $\mathbf{a}$ ,  $\mathbf{b}$  are called "left-moving mode" and "right-moving mode".

#### 4.1.2 Dynamics of strings in Friedmann-Lemaître-Robertson-Walker spacetime

This universe is expanding. In this sub-sub-section, we describe the dynamics of cosmic strings and cosmic superstrings in FLRW spacetime [88] . Using the conformal time  $\tau$  defined as

$$\tau \equiv \int \frac{t}{a(t)}, \quad (4.1.20)$$

FLRW metric is rewritten as

$$ds^2 = a(\tau)^2 \left\{ -d\tau^2 + \frac{dr^2}{1 - Kr^2} + r^2(d\theta^2 + \sin^2\theta d\phi^2) \right\}. \quad (4.1.21)$$

First, a propagating mode on a string shows the gauge conditions are

$$\zeta^0 = \tau, \quad \zeta^1 = \sigma, \quad (4.1.22)$$

$$\dot{\mathbf{x}} \cdot \mathbf{x}' = 0. \quad (4.1.23)$$

Varying the action Eq.(4.1.2) by  $x^\mu$ , the equation of motion of the string is [86] given by

$$\ddot{\mathbf{x}} + 2\frac{\dot{a}}{a}\dot{\mathbf{x}}(1 - \dot{\mathbf{x}}^2) = \frac{1}{\epsilon} \left( \frac{\mathbf{x}'}{\epsilon} \right)', \quad (4.1.24)$$

where

$$\epsilon \equiv \sqrt{\frac{\mathbf{x}'^2}{1 - \dot{\mathbf{x}}^2}}. \quad (4.1.25)$$

The solution of Eq.(4.1.24) can be written using in the same way as left- and right-moving mode of Eq.(4.1.18). It is defined as  $\mathbf{p}_+(\tau, \sigma)$ ,  $\mathbf{p}_-(\tau, \sigma)$  where

$$\mathbf{p}_\pm \equiv \dot{\mathbf{x}} \mp \frac{1}{\epsilon} \mathbf{x}'. \quad (4.1.26)$$

$\mathbf{p}_\pm$  is similar to the tilt of the strings. The gauge condition gives the fact that  $\mathbf{p}_\pm$  are the unit vector

$$|\mathbf{p}_+|^2 = |\mathbf{p}_-|^2 = 1. \quad (4.1.27)$$

Using  $\mathbf{p}_\pm$ , the equation of motion Eq.(4.1.24) is rewritten as

$$\dot{\mathbf{p}}_\pm \pm \frac{\mathbf{p}'_\pm}{\epsilon} = -\frac{\dot{a}}{a} \{ \mathbf{p}_\mp - (\mathbf{p}_+ \cdot \mathbf{p}_-) \mathbf{p}_\pm \}. \quad (4.1.28)$$

By converting the variables  $\tau, \sigma$  to  $\epsilon\sigma + \tau, \epsilon\sigma - \tau$ , Eq.(4.1.28) becomes

$$\frac{\partial \mathbf{p}_+}{\partial(\epsilon\sigma + \tau)} \propto \frac{\dot{a}}{a}, \quad \frac{\partial \mathbf{p}_-}{\partial(\epsilon\sigma - \tau)} \propto \frac{\dot{a}}{a}. \quad (4.1.29)$$

Since the universe is flat and constant size ( $\dot{a} = 0, \epsilon = 1$ ) in Minkowski spacetime, under the condition,  $\mathbf{p}_\pm$  satisfies  $\frac{\partial \mathbf{p}_+}{\partial(\sigma + \tau)} = \frac{\partial \mathbf{p}_-}{\partial(\sigma - \tau)} = \mathbf{0}$ . Using  $\sigma + \tau, \sigma - \tau$ , the equation of motion in Minkowski spacetime, Eq.(4.1.15), is rewritten as

$$\frac{\partial}{\partial(\sigma + \tau)} \frac{\partial}{\partial(\sigma - \tau)} \mathbf{x} = \mathbf{0}. \quad (4.1.30)$$

Since the solutions of this equation are just  $\mathbf{a}$  and  $\mathbf{b}$ , they have the relation  $\frac{\partial \mathbf{a}'}{\partial(\sigma + \tau)} = \frac{\partial \mathbf{b}'}{\partial(\sigma - \tau)} = \mathbf{0}$ . This relation is same as  $\mathbf{p}_\pm$ , then, we regard  $\mathbf{p}_\pm$  is the solution in FLRW spacetime corresponding to  $\mathbf{a}'$  and  $\mathbf{b}'$  [92].

Using Eqs.(4.1.24), (4.1.22) and (4.1.23), the time evolution equation of coordinate energy per unit length [93] is derived as

$$\dot{\epsilon} = -2\frac{\dot{a}}{a}\epsilon\dot{\mathbf{x}}^2. \quad (4.1.31)$$

The energy-momentum tensor  $T^{\mu\nu}$  in FLRW spacetime is [94]

$$T^{\mu\nu}(y) = \frac{1}{\sqrt{-\det(g_{\mu\nu})}} \int d\tau \int d\sigma \sqrt{-\det(\gamma_{ab})} (U u^\mu u^\nu - T v^\mu v^\nu) \delta^4(y - x(\tau, \sigma)), \quad (4.1.32)$$

where  $U, T$  are the mass and the tension of string per unit length and  $u^\mu, v^\mu$  satisfy the following equation

$$u^\mu = \frac{\sqrt{\epsilon} \dot{x}^\mu}{(-\det(\gamma_{ab}))^{1/4}}, \quad v^\mu = \frac{x^{\mu'}}{\sqrt{\epsilon} (-\det(\gamma_{ab}))^{1/4}}. \quad (4.1.33)$$

However, usually,  $U = T = \mu$  is satisfied. If there are small ripples called wiggle on the strings,  $U > T$ . In this thesis, we assume that there are no wiggles. Using  $U = T = \mu$ ,  $T^{\mu\nu}$  is given as

$$T^{\mu\nu}(\tau, \mathbf{r}) = \frac{\mu}{a^4} \int d\sigma \left( \epsilon \dot{x}^\mu \dot{x}^\nu - \frac{x^{\mu'} x^{\nu'}}{\epsilon} \right) \delta^3(\mathbf{r} - \mathbf{x}(\tau, \sigma)). \quad (4.1.34)$$

The total string energy  $E(\tau)$  and momentum  $\mathbf{P}$  are written as [92]

$$E(\tau) \equiv \mu a(\tau) \int d\sigma \epsilon, \quad (4.1.35)$$

$$\mathbf{P} \equiv \mu a(\tau) \int d\sigma \epsilon \dot{\mathbf{x}}. \quad (4.1.36)$$

This total energy evolves with time. In the rest frame ( $\dot{\mathbf{x}} = \mathbf{0}$ ),  $\epsilon$  becomes constant, so the total energy grows with  $a(\tau)$ .

Second, dynamics of string-self is described as the following [88]. The gauge condition is

$$\zeta^0 = \tau, \quad \zeta^1 = x. \quad (4.1.37)$$

If the string is assumed moving only in the  $(x - y)$  plane, the Lagrangian in FLRW spacetime is described as

$$L = -\mu \sqrt{-\det(\gamma_{ab})} = -\mu a^2(\tau) \sqrt{1 + y'^2 - \dot{y}^2}. \quad (4.1.38)$$

Substituting this Lagrangian into Euler-Lagrange equation, Eq.(4.1.9), the equation of motion is obtained as

$$\left( \frac{\partial}{\partial \tau} + 2 \frac{\dot{a}}{a} \right) \left\{ \dot{y} (1 + y'^2 - \dot{y}^2)^{-1/2} \right\} = \frac{\partial}{\partial x} \left\{ y' (1 + y'^2 - \dot{y}^2)^{-1/2} \right\}. \quad (4.1.39)$$

If there is the straight string  $y = \text{Const.}$  in the universe, it is the solution of Eq.(4.1.39). The straight string does not change the configuration with time. Now, let us assume that there are small perturbations on the straight string. In the radiation-dominant era, the perturbation is defined as

$$y'^2, \dot{y}^2 \ll 1, \quad (4.1.40)$$

then the equation of motion is

$$\ddot{y} + 2\frac{\dot{y}}{\tau} - y'' = 0. \quad (4.1.41)$$

The solution of this equation is represented by the plane wave solution  $y(\tau)e^{ikx}$  [95], where  $\frac{2\pi}{k}$  is the conformal wavelength of string-self. The solution is written as

$$y(\tau) = A_1 \frac{\sin(k\tau)}{\tau}, \quad (4.1.42)$$

$$y(\tau) = A_2 \frac{\cos(k\tau)}{\tau}, \quad (4.1.43)$$

where  $A_1, A_2$  are constant.  $\lambda \equiv \frac{2\pi a(\tau)}{k}$  is the physical wavelength and  $\frac{t}{\lambda}$  is the rough ratio of the horizon size to the wavelength. Using the approximation  $k\tau \sim \frac{t}{\lambda}$ , the growth of the string is shown by comparing between the wavelength and the horizon as below, categorized into two cases:

- (i)  $k\tau \ll 1, \tau^2 \ll A$  (The wavelength and the amplitude are larger than the horizon.)

Because Eq.(4.1.40) is not satisfied in this case, the solution of the string's dynamics is just Eq.(4.1.42). When the limit is  $k\tau \rightarrow 0$  (the wavelength is much greater than the horizon), the solution Eq.(4.1.42) becomes constant. Namely, the string is fixed in the comoving coordinates and stretched by the expansion of the universe. The configuration of the string does not change and simply grows with  $a(\tau)$ .

- (ii)  $k\tau \gg 1, \tau^2 \gg A$  (The wavelength and the amplitude are shorter than the horizon.)

Although the physical wavelength of the string grows with  $a(\tau)$ , the string physical amplitude  $a(\tau)\frac{A}{\tau}$  stays constant because the scale factor is given by  $a(\tau) \propto \tau$  in the RD era. The ratio of the string amplitude to the wavelength becomes smaller with the time. Therefore, the amplitude is relatively smoothed out. It is also the same under the power-law expansion  $a(\tau) \propto \tau^\nu$ .

To summarize, when the string wavelength is bigger, the string grows conformally. On the other hand, the small scale wave is smoothed out by the expansion of the universe [16, 95]. The example of the string growth is shown as the following. When the loop initial size is larger than the horizon  $R = R_0 > t_0$  at  $t = t_0$ , the loop grows like  $a(t) \propto t^{\frac{1}{2}}$  in the RD era

$$R(t) = \left(\frac{t}{t_0}\right)^{\frac{1}{2}} R_0, \quad (4.1.44)$$

where  $R(t)$  is the loop size at  $t$ . The growth continues until the loop enters the horizon at  $t = t_{\text{enter}}$ . At that time, the loop size is approximately  $R(t_{\text{enter}}) \sim t_{\text{enter}}$  and  $t_{\text{enter}} \sim \frac{R_0^2}{t_0}$ . After this, the loop growth stops and separates from the expansion of the universe. The emission of GWs from loops through cusps is described later. The loop shrinks and vanishes by emitting GWs.

## 4.2 Reconnection of strings

Cosmic strings and cosmic superstrings intersect and reconnect each other in the universe [7]. Reconnection of strings plays an important role in the string network evolution. When the strings reconnect, loops are made from infinite strings whose length is longer than the horizon. The biggest difference between cosmic strings and cosmic superstrings in the formation of the network arise because of the reconnection probability  $p$ . It is determined by the intersection of the angle and velocity of the strings whether these strings reconnect. Usually, reconnection "probability" averaging of the angle and velocity is used. It is suggested that the reconnection probability of the cosmic string is close to 1 in the case of global string [39, 96, 97] and local string [98, 99] by simulations .

The reconnection probability of cosmic superstrings is smaller than the one of cosmic strings. There are two species in the cosmic superstrings; D-string, F-string [100, 11] . Because these strings are a high dimensional object, D-strings and F-strings pass through at high dimension, even though they look like intersecting in the four dimension [101]. The reconnection probability strongly depends on the models. Simulations [101, 40] show that the reconnection probability for the D-D collisions is  $10^{-1} < p_D < 1$  and for F-F collisions is  $10^{-3} < p_F < 1$ . For F-D collisions, the reconnection probability has not been understood.

Since the reconnection probability of the cosmic string and cosmic superstring is different, it affects various cosmological phenomena. Therefore, the investigation of the reconnection probability through these phenomena helps us to probe what strings exist. The relation of the reconnection probability and the string network is described in Sec.5.

## 4.3 Sharp structures

Sharp structures called "cusp" and "kink" form on the loops and infinite strings of both cosmic strings and cosmic superstrings.

### 4.3.1 Cusp

Because the loops are smaller than the horizon, they are not affected by the expansion of the universe. Then, their equation of motion and the solution are written in Minkowski spacetime by Eqs.(4.1.15), (4.1.18) and (4.1.19) [88, 102, 103] . Loops is closed, then the solution  $\mathbf{a}(\sigma - t)$ ,  $\mathbf{b}(\sigma + t)$  is periodic function

$$\mathbf{a}(\sigma - t + L_l) = \mathbf{a}(\sigma - t), \quad \mathbf{b}(\sigma - t + L_l) = \mathbf{b}(\sigma - t), \quad (4.3.1)$$

where  $L_l = \frac{M}{\mu}$  is the period of loops using the loop mass  $M$ . The period of the loop is  $T_l = \frac{L_l}{2}$ . We can confirm it to substitute  $t + \frac{L_l}{2}$ ,  $\sigma + \frac{L_l}{2}$  into  $t$ ,  $\sigma$  of  $\mathbf{x}(t, \sigma)$  as

$$\mathbf{x}\left(t + \frac{L_l}{2}, \sigma + \frac{L_l}{2}\right) = \mathbf{x}(t, \sigma + L_l) = \mathbf{x}(t, \sigma). \quad (4.3.2)$$

The loop has an interesting sharp structure moving at the speed of light. The velocity of the loops is described as

$$\dot{\mathbf{x}}^2(t, \sigma) = \frac{1}{4} \{ \mathbf{a}'(\sigma - t) - \mathbf{b}'(\sigma + t) \}^2, \quad (4.3.3)$$

where  $\dot{\mathbf{a}}(\sigma - t) = -\frac{\partial \mathbf{a}}{\partial(\sigma - t)} = -\mathbf{a}'$ ,  $\dot{\mathbf{b}}(\sigma - t) = -\frac{\partial \mathbf{b}}{\partial(\sigma - t)} = \mathbf{b}'$ . Because  $\mathbf{a}'$ ,  $\mathbf{b}'$  are the unit vector (Eq.(4.1.19)) and periodic function (Eq.(4.3.1)), we can consider the vectors  $\mathbf{a}'(\sigma - t)$ ,  $-\mathbf{b}'(\sigma + t)$  on the unit sphere for  $0 \leq \sigma \leq L$ . When the vectors are integrated by one period, the integration is

$$\int_0^{L_l} d\sigma \mathbf{a}' = \mathbf{a}(L_l) - \mathbf{a}(0) = 0, \quad \int_0^{L_l} d\sigma \mathbf{b}' = \mathbf{b}(L_l) - \mathbf{b}(0) = 0. \quad (4.3.4)$$

On the sphere, the vectors draw the closed curves respectively and the curves typically cross two or more (Fig. 4.3.1). When we assume that the intersection is  $\sigma = \sigma_0$ , namely  $\mathbf{a}'(\sigma_0 - t) =$

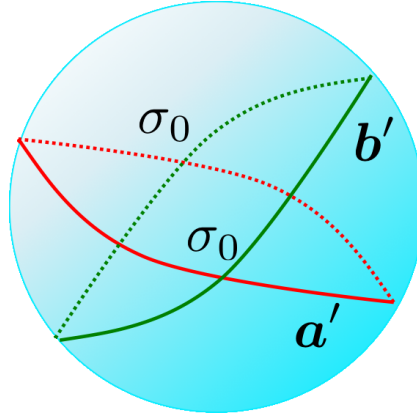


Fig. 4.3.1 The illustration of the unit sphere moving  $\mathbf{a}'$ ,  $\mathbf{b}'$ . The red and green curve lines represent the track and the coordinate of the intersection is  $\sigma_0$ .

$-\mathbf{b}'(\sigma_0 + t)$ , the velocity of the loop at the intersection point is

$$\dot{\mathbf{x}}^2(nL_l, \sigma_0) = \mathbf{1}, \quad (4.3.5)$$

where  $n$  is an integer. At the intersection of the unit sphere, the loop has the point whose velocity is the speed of light. It is called a "cusp".

Next, we describe the configuration of the cusp. The background is set at  $t = 0$  and  $\sigma = 0$ , and the coordinate at the cusp is put on the origin. Introducing the perturbation  $\sigma$ , the modes  $\mathbf{a}$ ,  $\mathbf{b}$  are expanded by Taylor expansion around the cusp to third order in  $\sigma$

$$\mathbf{a}(\sigma) = \mathbf{a}_0' \sigma + \mathbf{a}_0'' \frac{\sigma^2}{2} + \mathbf{a}_0''' \frac{\sigma^3}{6}, \quad (4.3.6)$$

$$\mathbf{b}(\sigma) = \mathbf{b}_0' \sigma + \mathbf{b}_0'' \frac{\sigma^2}{2} + \mathbf{b}_0''' \frac{\sigma^3}{6}, \quad (4.3.7)$$

where the subscript 0 symbolizes the position of the cusp. At the position, the modes satisfy

$$\mathbf{a}_0' = -\mathbf{b}_0'. \quad (4.3.8)$$

Using this equation and  $\dot{\mathbf{x}} = \frac{1}{2}(-\mathbf{a}' + \mathbf{b}')$ ,  $\mathbf{x}' = \frac{1}{2}(\mathbf{a}' + \mathbf{b}')$ , we obtain  $\dot{\mathbf{x}}_0 = \mathbf{b}_0'$ ,  $\mathbf{x}_0' = \mathbf{0}$ .  $\mathbf{x}_0$  is expanded in the similar way as  $\mathbf{a}$ ,  $\mathbf{b}$

$$\mathbf{x}(\sigma) = \mathbf{x}_0'' \frac{\sigma^2}{2} + \mathbf{x}_0''' \frac{\sigma^3}{6}. \quad (4.3.9)$$

Since  $|\mathbf{a}'(\sigma)| = 1$ ,  $|\mathbf{b}'(\sigma)| = 1$  must be satisfied, the following equations are required

$$\mathbf{a}'' \cdot \mathbf{a}' = 0 \quad (4.3.10)$$

$$\mathbf{a}''' \cdot \mathbf{a}' = -|\mathbf{a}''|^2. \quad (4.3.11)$$

These relations also apply to  $\mathbf{b}$ . From these equations and  $\mathbf{a}_0' = -\mathbf{b}_0'$ , the following equations are satisfied

$$\mathbf{x}_0'' \cdot \dot{\mathbf{x}}_0 = 0, \quad (4.3.12)$$

$$\mathbf{x}_0''' \cdot \dot{\mathbf{x}}_0 = \frac{1}{2}(|\mathbf{a}_0''|^2 - |\mathbf{b}_0''|^2). \quad (4.3.13)$$

From Eq.(4.3.12),  $\mathbf{x}_0''$  is perpendicular to  $\dot{\mathbf{x}}_0$ . With these information, we draw the cusp configuration in Fig.4.3.2. As seen in the figure, the cusp is characterized by  $\dot{\mathbf{x}}_0$ ,  $\mathbf{x}_0''$ ,  $\mathbf{x}_0'''$ .

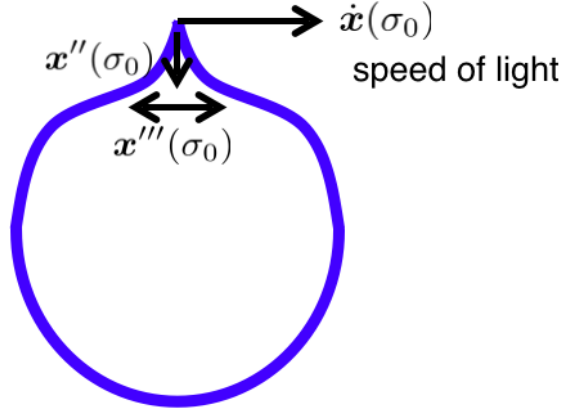


Fig. 4.3.2 The configuration of the cusp. The blue curve line is the cosmic string.

These vectors are described by the seven parameters;  $\mathbf{a}_0'$ ,  $\mathbf{b}_0'$ ,  $|\mathbf{a}_0''|$ ,  $|\mathbf{b}_0''|$ , the angle between  $\mathbf{a}_0''$  and  $\mathbf{b}_0''$ ,  $\mathbf{a}_0'''$  and  $\mathbf{b}_0'''$ .

Since  $\mathbf{a}$ ,  $\mathbf{b}$  are periodic function, many cusps appear on loops, but not on infinite strings. However, when there are "Y-junctions", described later, on the infinite strings made of the cosmic superstrings,  $\mathbf{a}$ ,  $\mathbf{b}$  becomes periodic function and infinite cosmic superstrings can have

cusps.

### 4.3.2 Kink

As mentioned in Sec.4.2, cosmic strings, and cosmic superstrings reconnect respectively and make a sharp structure called "kink". The kink is the discontinuity point of the left-moving mode  $\mathbf{a}$  or the right-moving mode  $\mathbf{b}$ . Since there are both moving modes on strings, two kinks move along the strings at the speed of light in the opposite direction after their formation by reconnection (Fig.4.3.3). If the string has a discontinuity in the left-moving mode  $\mathbf{a}$ , kink's

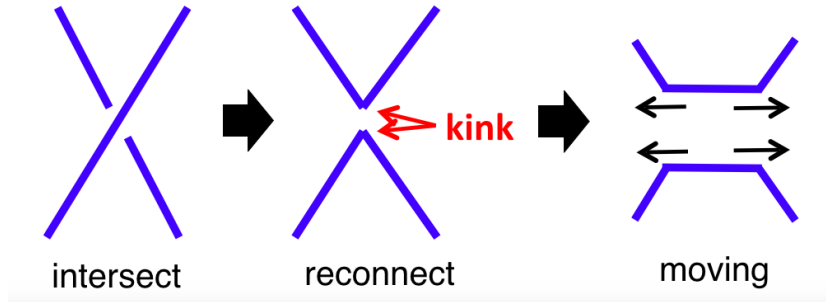


Fig. 4.3.3 The illustration of the kinks production. The blue lines are the cosmic string.

"sharpness" is defined as [63, 104]

$$\psi \equiv \frac{1}{2}(1 - \mathbf{a}'_+ \cdot \mathbf{a}'_-), \quad (4.3.14)$$

where  $\mathbf{a}'_{\pm}$  satisfies the following equation

$$\mathbf{a}'_{\pm}(\sigma_* - t_*) \equiv \lim_{\substack{t \rightarrow t_* \pm 0 \\ \sigma \rightarrow \sigma_* \pm 0}} \mathbf{a}'_{\pm}(\sigma - t). \quad (4.3.15)$$

$\sigma_*$ ,  $t_*$  denotes the point of the discontinuity. In the same way, when there is the discontinuity at  $\mathbf{b}$ , the sharpness is written as  $\psi \equiv \frac{1}{2}(1 - \mathbf{b}'_+ \cdot \mathbf{b}'_-)$ . Since  $\mathbf{a}'$ ,  $\mathbf{b}'$  is the unit vector, the sharpness is  $0 \leq \psi \leq 1$ . If  $\mathbf{a}'_+$  and  $\mathbf{a}'_-$  are in the opposite direction ( $\mathbf{a}'_+ = -\mathbf{a}'_-$ ), the sharpness becomes maximum  $\psi = 1$  and kink is the sharpest. On the other hand, if  $\mathbf{a}'_+$  and  $\mathbf{a}'_-$  are same direction ( $\mathbf{a}'_+ = \mathbf{a}'_-$ ), the sharpness is minimum  $\psi = 0$  (there is not kink on the string). Namely, when the vectors  $\mathbf{a}'_+$  and  $\mathbf{a}'_-$  are in the different direction, the sharpness becomes large.

There are kinks not only on infinite cosmic strings and cosmic superstrings but also on both loops. In this thesis, we focus on the kinks on infinite cosmic strings and cosmic superstrings.

## 4.4 Y-junction

There are two types of cosmic superstrings; F-string and D-string in the Universe.  $p$  F-strings and  $q$  D-string form a bound state [105, 106] as shown in Fig.4.4.1. The point where two different strings join and separate is called a "Y-junction".

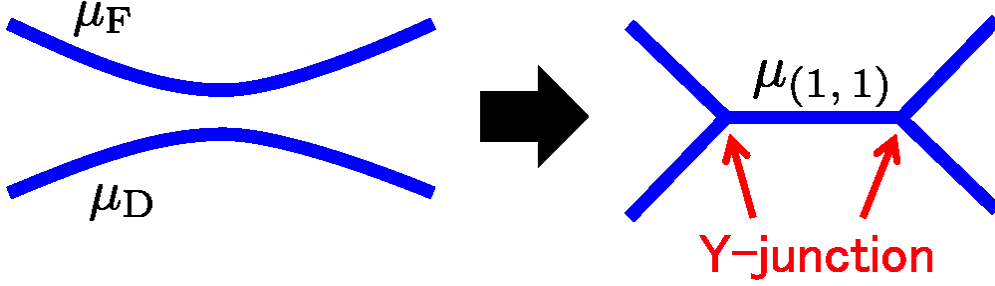


Fig. 4.4.1 The illustration of the Y-junction.

Even if the F-string and D-string intersect, they are not able to intercommunicate and do not reconnect. These strings carry the charge and the charge is conserved at the Y-junction. By taking the charge conservation into account and using the simplest model in the superstring theory, the tension of the bound strings  $\mu_{(p,q)}$  is defined as [105, 106, 107]

$$\mu_{(p,q)} = \mu_F \sqrt{p^2 + \frac{q^2}{g_s^2}}, \quad (4.4.1)$$

where  $\mu_F$  is the tension of the F-string and  $g_s$  is the string coupling constant. It is easy to verify that the bound state energy is lower than the unbound state using the relation  $\mu_F = g_s \mu_D$ . The tension binding 1 F-string and 1 D-string is defined as  $\mu_{(1,1)}$ , then it satisfies the relation

$$\mu_F + \mu_D > \mu_{(1,1)}, \quad (4.4.2)$$

assuming  $g_s = 0.1$  [107]. Therefore, strings prefer to stay in the bound state.

#### 4.4.1 Dynamics of cosmic superstring with Y-junction

Similarly to Sec.4.1, the dynamics of cosmic superstrings with Y-junctions is derived from the action to the equation of motion [108, 109]. In this section, we explain in Minkowski spacetime for simplicity. Choosing the coordinate of the world sheet as  $\mathbf{x}(t, \sigma)$ , the gauge conditions are

$$\dot{\mathbf{x}} \cdot \mathbf{x}' = 0, \quad (4.4.3)$$

$$\dot{\mathbf{x}}^2 + \mathbf{x}'^2 = 1. \quad (4.4.4)$$

The tensions of the strings connecting to a Y-junction is defined as  $\mu_j$  ( $j = 1, 2, 3$ ). Consider that a Y-junction is located at  $\sigma = s_j(t)$  on the world sheet and at  $\mathbf{X}(t) = \mathbf{x}(t, s_j(t))$  on the spatial coordinate. Then the action of the cosmic superstring with Y-junction is given as

$$S[x^\mu] = - \sum_j \mu_j \int dt \int d\sigma \Theta(s_j(t) - \sigma) \sqrt{-\det(\gamma_{ab}^j)} + \sum_j \int dt \mathbf{f}_j(t) \cdot \{\mathbf{x}_j(t, s_j(t)) - \mathbf{X}(t)\}, \quad (4.4.5)$$

where  $\Theta$  is the step function which imposes that there is no cosmic superstring outside of the Y-junction, and  $\mathbf{f}_j(t)$  are Lagrange multipliers. Using the gauge conditions, we can write as

$$\sqrt{-\det(\gamma_{ab}^j)} = \sqrt{\mathbf{x}_j'^2(1 - \dot{\mathbf{x}}_j^2)}. \quad (4.4.6)$$

When we vary the action in terms of  $\mathbf{x}_j$  and use the gauge conditions, the equation of motion is given by

$$\ddot{\mathbf{x}}_j - \mathbf{x}_j'' = \mathbf{0}. \quad (4.4.7)$$

This equation is same as Eq.(4.1.15), and the solution is

$$\mathbf{x}(t, \sigma) = \frac{1}{2}\{\mathbf{a}_j(\sigma - t) + \mathbf{b}_j(\sigma + t)\}. \quad (4.4.8)$$

Using this solution, the gauge condition is rewritten as  $\mathbf{a}_j'^2 = \mathbf{b}_j'^2 = 1$ . In the region where  $\sigma < s_j(0)$ , the functions  $\mathbf{a}_j(\sigma)$  and  $\mathbf{b}_j(\sigma)$  are determined by the initial conditions of  $\mathbf{x}_j, \dot{\mathbf{x}}_j$  at  $t = 0$ . Since we assume that Y-junctions are separated by large enough distance, we can consider the lower limit of  $\sigma$  as small enough.

#### 4.4.2 Energy conservation of cosmic superstring with Y-junction

The energy conservation of cosmic superstrings with Y-junctions is derived as the followings [108, 109]. Varying  $\mathbf{x}_j$ , the term proportional to  $\delta(s_j(t) - \sigma)$  is

$$\mu_j(\mathbf{x}_j' + \dot{s}_j \dot{\mathbf{x}}_j) = \mathbf{f}_j. \quad (4.4.9)$$

On the other hand, varying  $\mathbf{X}$ , we obtain

$$\sum_j \mathbf{f}_j = \mathbf{0}. \quad (4.4.10)$$

Combining these two equations and using the equation of motion solutions  $\mathbf{a}_j$  and  $\mathbf{b}_j$ , the Lagrange multipliers vanish as

$$\sum_j \mu_j \{(1 - \dot{s}_j)\mathbf{a}_j' + (1 + \dot{s}_j)\mathbf{b}_j'\} = \mathbf{0}, \quad (4.4.11)$$

where we apply  $\dot{\mathbf{a}}_j = -\mathbf{a}_j', \dot{\mathbf{b}}_j = \mathbf{b}_j'$ .  $\mathbf{a}_j$  is the injection wave and  $\mathbf{b}_j$  is an unknown outgoing wave. It is reasonable to use  $\mathbf{a}_j$  in order to describe the energy conservation. The boundary condition is

$$\frac{1}{2}\{\mathbf{a}_j(s_j(t) - t) + \mathbf{b}_j(s_j(t) + t)\} = \mathbf{X}(t). \quad (4.4.12)$$

The time derivative of this equation is described as

$$(1 - \dot{s}_j)\mathbf{a}_j' - (1 + \dot{s}_j)\mathbf{b}_j' = -2\dot{\mathbf{X}}. \quad (4.4.13)$$

Using Eqs.(4.4.11) and (4.4.13), we remove  $\mathbf{b}'_j$  from these equations as

$$\sum_j \mu_j (1 - \dot{s}_j) \mathbf{a}'_j = -(\mu_1 + \mu_2 + \mu_3) \dot{\mathbf{X}}. \quad (4.4.14)$$

Eliminating  $\mathbf{X}$  from Eqs.(4.4.13) and (4.4.14),  $\mathbf{b}'_j$  can be written by  $\mathbf{a}'_j$ ,  $\dot{s}_j$ . Using  $|\mathbf{b}'_j|^2 = 1$ ,  $\dot{s}_j$  is only related with  $\mathbf{a}'_j$ . Changing the notation from  $\mathbf{a}'_j$  to

$$c_{ij} = \mathbf{a}'_i(s_i - t) \cdot \mathbf{a}'_j(s_j - t) = c_{ji}, \quad (4.4.15)$$

$\dot{s}_j$  is rewritten as

$$\frac{\mu_1(1 - \dot{s}_j)}{\mu_1 + \mu_2 + \mu_3} = \frac{M_1(1 - c_{23})}{M_1(1 - c_{23}) + M_2(1 - c_{31}) + M_3(1 - c_{12})}, \quad (4.4.16)$$

where  $M_1 \equiv \mu_1^2 - (\mu_2 - \mu_3)^2$  and  $M_2, M_3$  is cyclic. Then, using the injection wave  $\mathbf{a}$  through the position of the Y-junction  $s_j$ , the energy conservation can be expressed as

$$\mu_1 \dot{s}_1 + \mu_2 \dot{s}_2 + \mu_3 \dot{s}_3 = 0. \quad (4.4.17)$$

## 5 String network dynamics

Cosmic strings and cosmic superstrings are moving in the universe with the speed of the light. Cosmic strings intersect and reconnect each other and cosmic superstrings also behave in the same manner. As a consequence of reconnections, a string network contains circular connected strings and strings as long as the horizon, called loops and infinite strings respectively. This section describes the complex network made of cosmic strings and cosmic superstrings.

First, let us derive the time evolution of the string energy density intuitively. The strings stretch and the interval extends with the cosmic expansion  $a(t)$ . In other words, the strings are fixed in the comoving frame. When one string energy and the physical volume are defined as  $\mu \frac{a(t)}{a_0} x_{\text{com}}$ ,  $\left(\frac{a(t)}{a_0} x_{\text{com}}\right)^3$  with the comoving coordinate  $x_{\text{com}}$ , the energy density of the string  $\rho_s$  is written as

$$\rho_s = \frac{\mu \frac{a(t)}{a_0} r}{\left(\frac{a(t)}{a_0} x_{\text{com}}\right)^3} = \frac{\mu}{\left(\frac{a(t)}{a_0} x_{\text{com}}\right)^2} \propto a^{-2}. \quad (5.0.1)$$

In the RD and MD era, the radiation and matter-energy densities are  $\rho \propto a^{-4}$  and  $a^{-3}$ , respectively. Compared with these energies density, the string energy density decreases slower. In this case, the universe would be dominated by the strings now [15], but it is not the case in reality. In order to solve this contradiction, we should consider the formation of loops from infinite strings. Cosmic strings and cosmic superstrings make loops by cutting off themselves. These loops shrink and vanish by emitting GWs. Because the string energy is thrown away through loops, the universe is never dominated by the string energy.

### 5.1 Network of cosmic string

Using the total energy and the average velocity of cosmic strings, the time evolution of the cosmic string energy density is described as the following [93]. The string average velocity  $v$  is defined as

$$v^2 \equiv \frac{\int d\sigma \dot{x}^2 \epsilon}{\int d\sigma \epsilon}, \quad (5.1.1)$$

where the dot denotes the derivative with respect to the conformal time. Substituting Eqs. (4.1.31) and (5.1.1) into the total string energy Eq.(4.1.35) differentiated by time, the physical time ( $t$ ) evolution equation of the cosmic string energy density  $\rho = \frac{E}{a^3}$  is represented by

$$\frac{d\rho}{dt} + 2H(1 + v^2)\rho = 0, \quad (5.1.2)$$

where  $H = \frac{da}{dt}/a$ . This equation includes the energy density of infinite strings and loops. We focus on the infinite strings network, then, we assume that Eq.(5.1.2) is able to be expressed by "correlation length"  $L$  meaning the interval and the curvature radius of the infinite string.

In [15, 16, 110], cosmic string network is described by a straight segment with the length  $L$  in the correlation volume  $L^3$  on average, then the network density of infinite strings  $\rho_{\text{inf}}$  is written as

$$\rho_{\text{inf}} \equiv \frac{\mu}{L^2}. \quad (5.1.3)$$

Infinite strings make loops. Let us estimate the probability of the collisions between the segment of the string  $L$  in  $L^3$  and the segment  $l$  which moves with the velocity  $v_{\text{inf}}$ . In the small-time  $\delta t$ , the collision probability is  $\frac{lv_{\text{inf}}\delta t L}{L^3}$ . With the assumption that the collision probability where loops are formed in the range of  $l \sim l + dl$  is expressed using the scale-invariant function  $W\left(\frac{l}{L}\right)$ , the string energy thrown away to loops is described as [110]

$$\left. \frac{d\rho_{\text{inf}}}{dt} \right|_{\text{loop}} = \rho_{\text{inf}} \frac{v_{\text{inf}}}{L} \int W\left(\frac{l}{L}\right) \frac{l}{L} \frac{dl}{L} \equiv cp^{n_p} v \frac{\rho_{\text{inf}}}{L}, \quad (5.1.4)$$

where  $p$  is the reconnection probability. In the cosmic string case, we expect  $p = 1$  and in the cosmic superstring case,  $p < 1$ .  $n_p$  is the power, in general  $n_p = 1, \frac{1}{3}$  [111, 112].  $c$  is the loop chopping efficiency and  $c \simeq 0.23$  from the simulation [113]. The first term of the left-hand side Eq.(5.1.2) means the time evolution of the string energy, then it is rewritten by  $\frac{d\rho_{\text{inf}}}{dt}$  and  $\left. \frac{d\rho_{\text{inf}}}{dt} \right|_{\text{loop}}$  like

$$\left( \frac{d\rho_{\text{inf}}}{dt} + \left. \frac{d\rho_{\text{inf}}}{dt} \right|_{\text{loop}} \right) + 2H(1+v^2)\rho_{\text{inf}} = 0. \quad (5.1.5)$$

Substituting Eqs. (5.1.3) and (5.1.4), the time evolution equation of the correlation length is given by

$$\frac{dL}{dt} = HL(1+v^2) + \frac{1}{2}cp^{n_p}v. \quad (5.1.6)$$

The first term stands for the effect of the cosmic expansion, and the second term represents the effect that infinite strings throw away the energy into loops. Differentiating Eq.(5.1.1) by time, the time evolution equation of the average velocity of cosmic strings is

$$\frac{dv}{dt} = (1-v^2) \left( \frac{k}{L} - 2Hv \right), \quad (5.1.7)$$

where  $k$  is the effective curvature [94] and it depends on  $v$  as [93]

$$k(v) \equiv \frac{1}{v(1-v^2)} \frac{\int d\sigma (1-\dot{\mathbf{x}}^2)(\dot{\mathbf{x}} \cdot \mathbf{u})\epsilon}{\int d\sigma \epsilon} \simeq \frac{2\sqrt{2}}{\pi} \frac{1-8v^6}{1+8v^6}, \quad (5.1.8)$$

where  $\dot{\mathbf{x}}$  is the velocity of the small scale structure on the infinite strings and  $\mathbf{u}$  is the unit vector along the curvature radius defined as  $\frac{a(\tau)}{L}\mathbf{u} \equiv \frac{d^2\mathbf{x}}{ds^2}$ . Here  $s$  is the physical length of the string written as  $ds = |\mathbf{x}'|d\sigma = \sqrt{1-\dot{\mathbf{x}}^2}\epsilon d\sigma$ . When there are no small structures on infinite strings,  $\dot{\mathbf{x}}$  is parallel to  $\mathbf{u}$  and  $k = 1$ . Then, the infinite strings accelerate. Namely,  $k$  works as the acceleration unless there are some structures on the infinite strings at the small

scale, while when there are small structures, we have  $k < 1$  and the acceleration is suppressed. When the infinite strings have a curvature  $L$  at the large scale, the strings accelerate by the factor  $\frac{1}{L}$  on the right-hand side of Eq.(5.1.7). In short, the numerator and denominator of  $\frac{k}{L}$  in Eq.(5.1.7) effectively describes how the acceleration by the small and large scale structure of the infinite strings. And the cosmic expansion term  $2Hv$  gives the deceleration.

We define the coefficient of the correlation length as  $\gamma \equiv \frac{L}{t}$ . We numerically calculate Eq.(5.1.6) and Eq.(5.1.7) with the evolution of the universe from the RD era to the MD era to the  $\Lambda$ D era. Fig.5.1.1 shows the time evolution of the correlation length and the average velocity of infinite strings. In the RD era,  $\gamma$  is constant, while we do not see it in the following

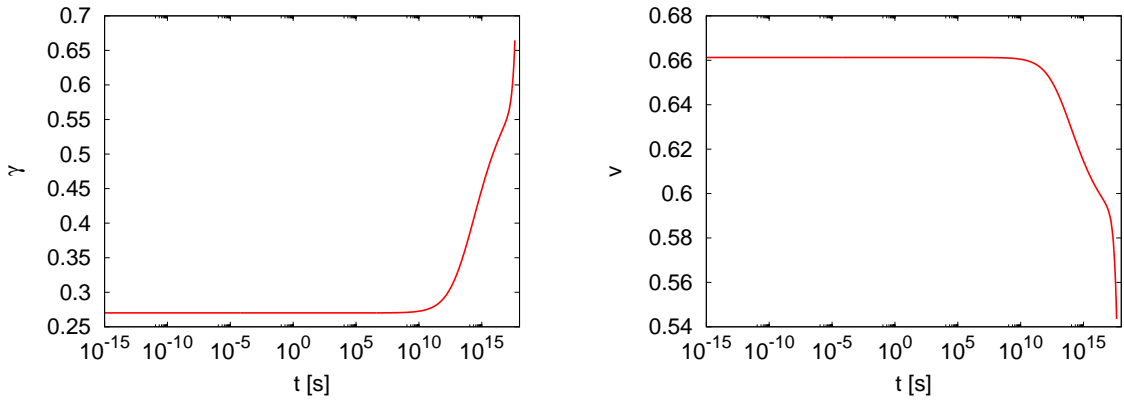


Fig. 5.1.1 The time evolution of  $\gamma$  and  $v$  of the cosmic string solving Eq.(5.1.6) and Eq.(5.1.7). The horizontal axis is time and the vertical axis is  $\gamma$  on the left panel and  $v$  on the right one. Both panels are calculated as  $p = 1$ , so the results using  $n_p = 1$  and  $n_p = 1/3$  are same. The constant region on the left side of each panel is in the RD, the transition around  $10^{12} < t < 10^{16}$  is the MD and the most right side corresponds to the  $\Lambda$ D era.

eras since it takes time to reach the scaling regime. During the RD era, the correlation length is proportional to  $t$  as

$$L \propto t \propto \text{horizon}. \quad (5.1.9)$$

In other words, the number of infinite strings in the horizon is constant. This is called "scaling law". In this case, the string network can be only parametrized  $L$  and  $v$ , so the model is called as "velocity-dependent one scale model (VOS model)" [93, 110].

We must confirm that the string energy in the horizon is less than the radiation and matter-energy. Using  $L \propto t$  and  $a \propto t^{\frac{1}{2}}, t^{\frac{2}{3}}$  in the RD, MD era, the time evolution of the string energy is

$$\rho_{\text{inf}} \propto \frac{\mu}{t^2} \propto \begin{cases} \mu a^{-4} & \text{for the RD era,} \\ \mu a^{-3} & \text{for the MD era.} \end{cases} \quad (5.1.10)$$

From this relation, the string energy has never been more than the other energy.

## 5.2 Network of cosmic superstring

Cosmic superstring also obeys the scaling law. One of the typical features of the cosmic superstring network is that the reconnection probability  $p$  is smaller than the one of the cosmic string. In addition, cosmic superstrings have Y-junctions [108] where three strings connect at one point on the strings. Y-junction is made when string 1 and string 2 collide and string 3 is formed by using their own length, called a zipper-type [61].

In order to formulate the time evolution equation of the correlation length with Y-junctions called extended VOS model, first, let us derive the time evolution of the energy density of cosmic superstring 1, 2 and 3. In general, these three strings can have different tension  $\mu_1, \mu_2, \mu_3$  and correlation length  $L_1, L_2, L_3$ , respectively. In the zipper-type, the length of cosmic superstring 1 and 2 converts to the length of cosmic superstring 3, then the time evolution equations are written as

$$\dot{\rho}_{\text{inf},i} = -2H(1 + v_i^2)\rho_{\text{inf},i} - \frac{c_i p_i^{n_p} v_i \rho_{\text{inf},i}}{L_i} - \dot{\rho}_{1,2 \rightarrow 3}, \quad (i = 1, 2) \quad (5.2.1)$$

$$\dot{\rho}_{\text{inf},3} = -2H(1 + v_3^2)\rho_{\text{inf},3} - \frac{c_3 p_3^{n_p} v_3 \rho_{\text{inf},3}}{L_3} + \dot{\rho}_{1,2 \rightarrow 3}, \quad (5.2.2)$$

where  $\dot{\rho}_{1,2 \rightarrow 3}$  is the energy made by binding cosmic superstring 1 and 2. By keeping the generality, we can set  $L_1 < L_2$ . Let us consider the probability of cosmic superstring 1 intersecting with 2. On average, we find one cosmic superstring 2 in the correlation volume  $L_2^3$ . The probability that cosmic superstring 1 moving at the velocity  $v_{12}$  intersects with cosmic superstring 2 in time  $\delta t$  is written as

$$\frac{v_{12} \delta t L_1}{L_2 L_2}. \quad (5.2.3)$$

The numerator of the first fraction expresses the distance cosmic superstring 1 can move in  $\delta t$ , and the second one means the amplification by the ratio  $L_1$  to  $L_2$ . We assume that the interval of Y-junctions has the distribution function and the peak is  $l(t)$ . We define an efficiency parameter  $\tilde{d}_{12}^3$  as integrating the distribution function in the same way as the loop chopping efficiency  $c_i$ . In the correlation volume  $L_2^3$ , the number of cosmic superstring 1 is given by  $\frac{\rho_1}{\mu_1 L_1} L_2^3 = \frac{L_2^3}{L_1^3}$ . Therefore, the energy density evolution is written as

$$\dot{\rho}_{1,2 \rightarrow 3} = \tilde{d}_{12}^3 \frac{v_{12}}{L_2} \frac{L_1}{L_2} \frac{\mu_3 l(t)}{L_2^3} \frac{L_2^3}{L_1^3} = \tilde{d}_{12}^3 \frac{v_{12} \mu_3 l(t)}{L_1^2 L_2^2} \quad (5.2.4)$$

When the cosmic superstring 1 and 2 collide and make cosmic superstring 3, in  $\delta t$ , the energy density

$$\delta \rho_{\text{inf}} = \tilde{d}_{12}^3 v_{12} (\mu_1 + \mu_2 - \mu_3) \frac{l(t)}{L_1^2 L_2^2} \delta t \quad (5.2.5)$$

remains because of  $\mu_1 + \mu_2 \neq \mu_3$  generally. Since the total energy of cosmic superstrings should

conserve, the remaining energy should be regarded as the kinetic energy of cosmic superstring  
 3. Then, let us add  $\frac{\delta \rho_{\text{inf}}}{\delta t}$  into the velocity evolution equation through the acceleration term

$$\dot{\rho}_{\text{acceleration}} = \frac{\partial \rho}{\partial v} \frac{dv}{dt} = \frac{v}{1-v^2} \rho \frac{dv}{dt}. \quad (5.2.6)$$

The acceleration term written by  $\left. \frac{dv_3}{dt} \right|_{\text{acceleration}}$  is

$$\left. \frac{dv_3}{dt} \right|_{\text{acceleration}} = (1-v_3^2) \tilde{d}_{12}^3 \frac{v_{12}}{v_3} \frac{\mu_1 + \mu_2 - \mu_3}{\mu_3} \frac{L_3^2}{L_1 L_2 (L_1 + L_2)}. \quad (5.2.7)$$

In summary, the evolution equations of correlation length and velocity are given by [61, 62, 112]

$$\frac{dL_1}{dt} = HL_1(1+v_1^2) + \frac{1}{2} c_1 p_1^{n_p} v_1 + \frac{1}{2} \frac{\tilde{d}_{12}^3 v_{12} L_1^2}{L_2 (L_1 + L_2)}, \quad (5.2.8)$$

$$\frac{dL_2}{dt} = HL_2(1+v_2^2) + \frac{1}{2} c_2 p_2^{n_p} v_2 + \frac{1}{2} \frac{\tilde{d}_{12}^3 v_{12} L_2^2}{L_1 (L_1 + L_2)}, \quad (5.2.9)$$

$$\frac{dL_3}{dt} = HL_3(1+v_3^2) + \frac{1}{2} c_3 p_3^{n_p} v_3 - \frac{1}{2} \frac{\tilde{d}_{12}^3 v_{12} L_3^3}{L_1 L_2 (L_1 + L_2)}, \quad (5.2.10)$$

$$\frac{dv_1}{dt} = (1-v_1^2) \left( \frac{k(v_1)}{L_1} - 2Hv_1 \right), \quad (5.2.11)$$

$$\frac{dv_2}{dt} = (1-v_2^2) \left( \frac{k(v_2)}{L_2} - 2Hv_2 \right), \quad (5.2.12)$$

$$\frac{dv_3}{dt} = (1-v_3^2) \left\{ \frac{k(v_3)}{L_3} - 2Hv_3 + \tilde{d}_{12}^3 \frac{v_{12}}{v_3} \frac{\mu_1 + \mu_2 - \mu_3}{\mu_3} \frac{L_3^2}{L_1 L_2 (L_1 + L_2)} \right\}, \quad (5.2.13)$$

where  $v_{12} \equiv \sqrt{v_1^2 + v_2^2}$ . The first terms of the correlation lengths are the same as the cosmic string case. In the second term, which describes the effect of loop production, we have an additional factor of  $p^{n_p}$ . For a simple one-scale model [93], one would expect  $n_p = 1$ . However, numerical simulations indicate that small-scale structure on strings increases the loop production efficiency and we can effectively include the effect by setting  $n_p = \frac{1}{3}$  [111], while another simulation indicates  $n_p = \frac{1}{2}$  [114]. In this paper, we set  $c_1 = c_2 = c_3 \simeq 0.23$  and investigate the two cases:  $n_p = 1$  and  $\frac{1}{3}$ .

The parameter  $\tilde{d}_{12}^3$  describes the efficiency of the process where strings of type 1 and 2 produce type 3 and is given by [40, 115, 116]

$$\tilde{d}_{12}^3 = \tilde{d}_{(p,q),(p',q')} P_{(p,q),(p',q')}^{\pm}, \quad (5.2.14)$$

where the probability of the Y-junction production which made by  $(p, q)$ -string and  $(p', q')$ -

string is

$$P_{(p,q),(p',q')}^{\pm} = \frac{1}{2} \left( 1 \mp \frac{pp'g_s^2 + qq'}{\sqrt{p^2g_s^2 + q^2}\sqrt{p'^2g_s^2 + q'^2}} \right). \quad (5.2.15)$$

and  $g_s$  is the string coupling. Typically,  $\tilde{d}_{(p,q),(p',q')}$  ranges as  $10^{-3} \leq \tilde{d}_{(p,q),(p',q')} \leq 1$  [62]. Following [62] in order to implement the kinematic constraint, we replace  $\tilde{d}_{12}^3$  with the suppression factor  $S_{12}^3$  as

$$\tilde{d}_{12}^3 \rightarrow \tilde{d}_{12}^3 = S_{12}^3 \tilde{d}_{(p,q),(p',q')} P_{(p,q),(p',q')}^{\pm}. \quad (5.2.16)$$

Using the velocity of collision string  $v$  and the angle  $\alpha_{\text{ang}}$ ,  $S_{12}^3$  is written by

$$S_{12}^3 = \frac{2}{\pi} \int_0^1 dv \int_0^{\frac{\pi}{2}} d\alpha_{\text{ang}} \Theta(-f(v, \alpha_{\text{ang}})) \exp\left(\frac{-(v - v_{12})^2}{\sigma_v^2}\right) < 1 \quad (5.2.17)$$

where  $\Theta$  is the Heaviside function imposing the kinematic constraints

$$f(v, \alpha_{\text{ang}}) \equiv A_1(1 - v^2)^2 + A_2(1 - v^2) + A_3 < 0, \quad (5.2.18)$$

where

$$A_1 = \bar{\mu}_+^2 \cos^2 \alpha_{\text{ang}} (\bar{\mu}_3^2 - \bar{\mu}_+^2 \sin^2 \alpha_{\text{ang}} - \bar{\mu}_-^2 \cos^2 \alpha_{\text{ang}}), \quad (5.2.19)$$

$$A_2 = 2\bar{\mu}_+^2 \bar{\mu}_-^2 \cos^2 \alpha_{\text{ang}} - \bar{\mu}_3^4 - (2\cos^2 \alpha_{\text{ang}} - 1)\bar{\mu}_+^2 \bar{\mu}_3^2, \quad (5.2.20)$$

$$A_3 = \bar{\mu}_3^4 - \bar{\mu}_+^2 \bar{\mu}_-^2, \quad (5.2.21)$$

with  $\bar{\mu}_{\pm} = \mu_1 \pm \mu_2$ . The string of type 3 is bound states of  $p$  F-strings and  $q$  D-strings and its tension  $\bar{\mu}_3$  is given by

$$\bar{\mu}_3 \equiv \frac{\mu_{\text{F}}}{g_s} \sqrt{p^2 g_s^2 + q^2}. \quad (5.2.22)$$

The tension of the type 3 string  $\bar{\mu}_3 = \mu_3$  would be roughly determined by heavier strings among type 1 and 2. For the variance, we take  $\sigma_v^2 = 0.25$ .

Moreover,  $\tilde{d}_{12}^3$  should include the reconnection probability and be modified as [112]

$$\tilde{d}_{12}^3 \rightarrow \tilde{d}_{12}^3 = S_{12}^3 \tilde{d}_{(p,q),(p',q')} P_{(p,q),(p',q')}^{\pm} p_3^{n_p}. \quad (5.2.23)$$

In this thesis, we consider the simple case where one D-string  $(p, q) = (0, 1)$  and one F-string  $(p', q') = (1, 0)$  make the bound state and form Y-junctions. Substituting  $(p, q), (p', q') = (0, 1), (1, 0)$  into Eq.(5.2.15), we get  $P_{(p,q),(p',q')}^{\pm} = \frac{1}{2}$ . Since we are interested in seeing the maximum effect of Y-junctions, we set  $\tilde{d}_{(p,q),(p',q')} = 1$ .

In Figures 5.2.1 and 5.2.2, we show the results of numerical calculations for the evolution of the correlation lengths and average velocities, obtained by simultaneously solving Eqs. (5.2.8) – (5.2.13). In the case of cosmic superstrings, there is a large variety of parameter

choice and it is difficult to present results of all the possible parameter space. Thus, we choose three example cases for string tensions and  $n_p$ , as a demonstration to obtain a rough idea of parameter dependence, which is listed below. We set that all string types have same reconnection probability  $p_1 = p_2 = p_3$  for simplicity. In Fig. 5.2.1, we show the results for  $p_1 = p_2 = p_3 = 1$ , and Fig. 5.2.2 shows the results for smaller reconnection probabilities. In both figures, the dimensionless string tension is set to  $G\mu = 10^{-11}$ , where  $G$  is the gravitational constant.

### 5.2.1 Case A: string network with $\mu_1 : \mu_2 : \mu_3 = 1 : 1 : 1$ and $n_p = 1$

First, we consider the strings of type 1, 2, and 3 all have the same tension  $\mu$  with low loop production efficiency  $n_p = 1$ . In Fig. 5.2.1, we find that  $\gamma_1$  and  $\gamma_2$  are larger than  $\gamma_3$ , because the third terms of Eqs. (5.2.8) and (5.2.9), which describes the formation of Y-junctions, increases the correlation length, while the third term of Eq. (5.2.10) makes  $\gamma_3$  small. In the right top panel, we find  $v_1$  and  $v_2$  are slower and  $v_3$  is faster than the case of ordinary cosmic strings. This is because the acceleration term of Eqs. (5.2.11) – (5.2.12) ( $k(v_1)/L_1$  and  $k(v_2)/L_2$ ) becomes smaller, while  $k(v_3)/L_3$  becomes larger.

In Fig. 5.2.2, we find that  $\gamma$  becomes smaller for smaller  $p$ . This is because the string network with small reconnection probability cannot produce loops efficiently and accumulate more infinite strings until it can sufficiently eventually enhance the loop production and leads to the scaling solution. From the figure, we find the relation between the correlation length  $\gamma$  and the reconnection probability  $p$  at the RD era is

$$\gamma \propto p^{0.975}. \quad (5.2.24)$$

In the case of ordinary cosmic strings, we do not have the third terms of Eqs. (5.2.8) – (5.2.10) and Eq. (5.2.13), and we find the relation is  $\gamma \propto p$  [49].

### 5.2.2 Case B: string network with $\mu_1 : \mu_2 : \mu_3 = 1 : 1 : 1$ and $n_p = \frac{1}{3}$

Next, we consider the strings of type 1, 2, and 3 all have the same tension  $\mu$  with high loop production efficiency  $n_p = \frac{1}{3}$ . The results in Fig. 5.2.1 are the same as Case A, since when  $p = 1$ , the result does not depend on the value of  $n_p$  since the loop production term is multiplied by  $p^{n_p}$ .

On the other hand, in Fig. 5.2.2, we find the asymptotic values of the scaling solution is different from Case A when reconnection probabilities are smaller than 1. This is because the loop production efficiency, determined by  $n_p$ , is higher in Case B and the number of strings inside the horizon is reduced compared to Case A, which gives the larger value of  $\gamma$ . We find the relation between  $\gamma$  and  $p$  in the RD era is given by

$$\gamma \propto p^{0.319}. \quad (5.2.25)$$

### 5.2.3 Case C: string network with $\mu_1 : \mu_2 : \mu_3 = 1 : 10 : 10$ and $n_p = \frac{1}{3}$

Lastly, we investigate the case where the D- and F-strings have different tension and we consider the case of  $\mu_1 : \mu_2 : \mu_3 = 1 : 10 : 10$  with  $n_p = \frac{1}{3}$ . We do not find any remarkable difference compared to Cases A and B in Fig. 5.2.1 because the effect of string tension arises only in the terms of  $\tilde{d}_{12}^3$  and the difference is small.

In Fig. 5.2.2, we find the asymptotic values of the scaling solution is almost the same as Case B and the dependence in the RD era is given by

$$\gamma \propto p^{0.318}. \quad (5.2.26)$$

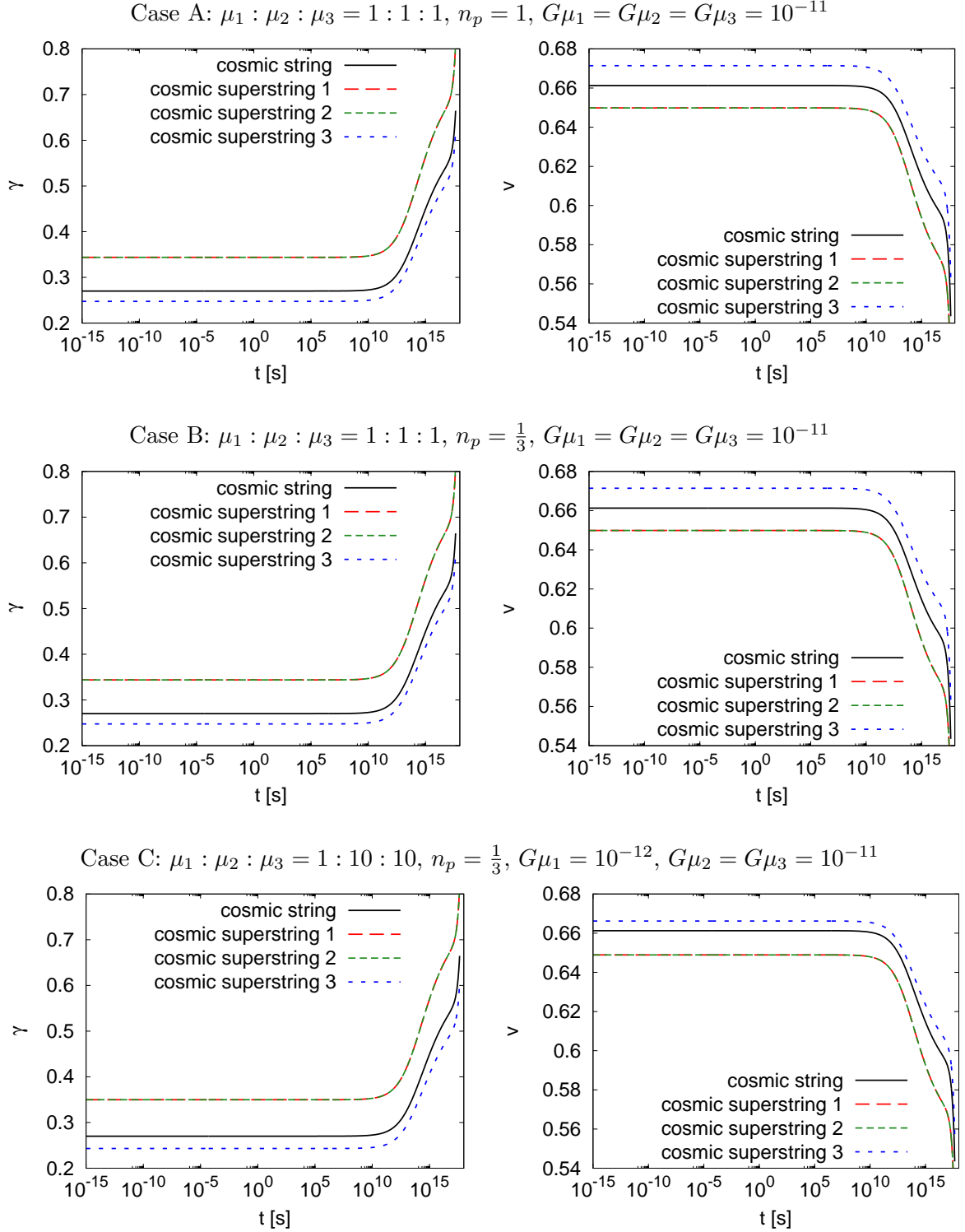


Fig. 5.2.1 The left and the right panels respectively show the evolution of the correlation length and average velocity of cosmic superstrings for different string types. The solid black line shows the case of ordinary cosmic strings presented in Sec. 5.1, and the red, green and blue broken lines correspond to the type of cosmic superstrings labeled 1, 2, and 3. The axes are the same as in Fig. 5.1.1. The top, middle, and bottom panels show a different choice of  $n_p$  and tensions, which corresponds to Case A, B, and C in the text. Here, the reconnection probability is fixed as  $p_1 = p_2 = p_3 = 1$ . The tension is assumed to be  $G\mu = 10^{-11}$  ( $G\mu_2 = G\mu_3 = 10^{-11}$  for Case C).

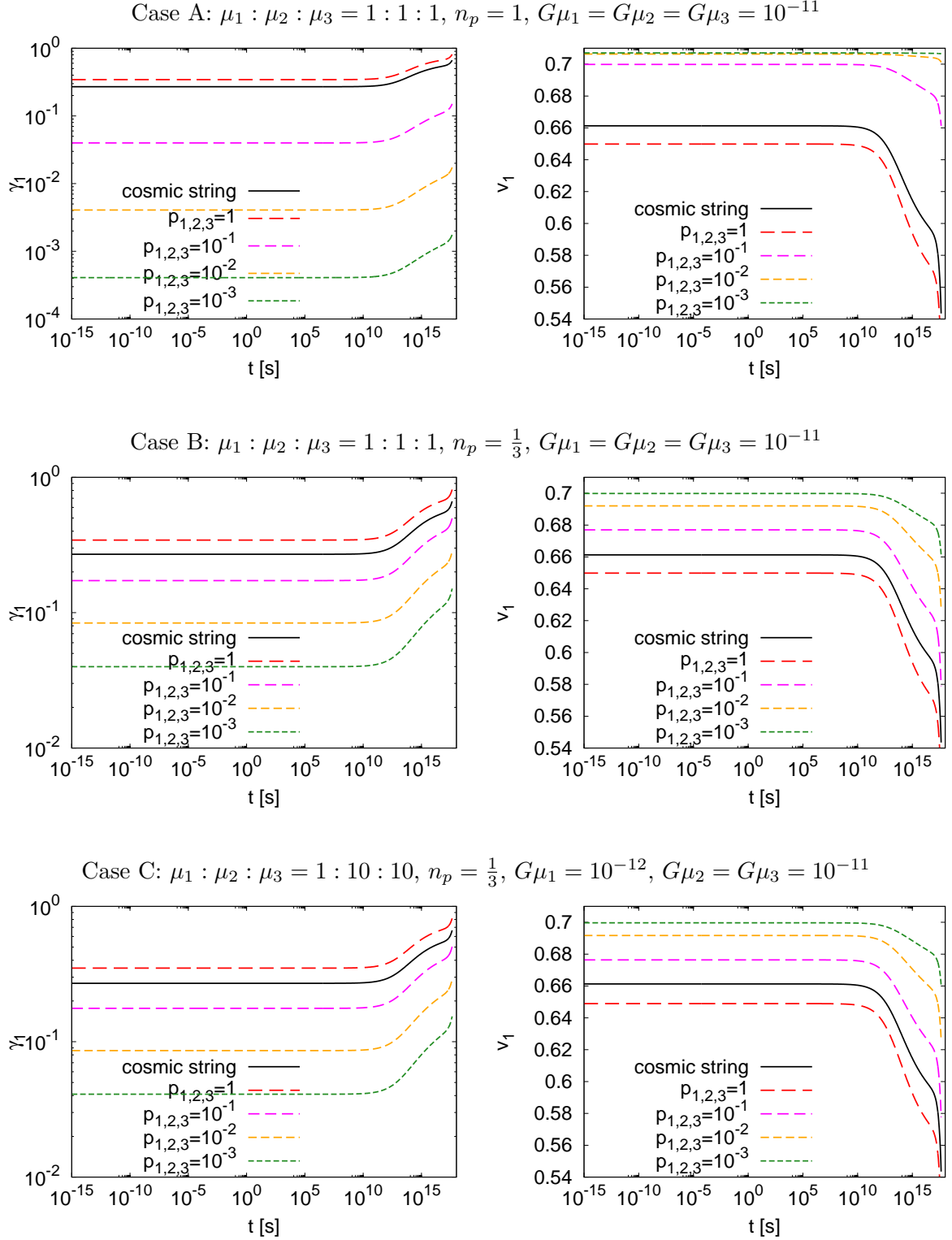


Fig. 5.2.2 The same plot as in Fig. 5.2.1 but for different reconnection probabilities (and the type of string is fixed to be 1). The solid black line shows the case of ordinary cosmic strings presented in Sec. 5.1, and the red, magenta, orange and green broken lines represent the cases of  $p_1 = p_2 = p_3 = 1, 10^{-1}, 10^{-2}, 10^{-3}$ , respectively.

## 6 Distribution of kinks

The sharp structures, cusps, and kinks, on cosmic strings and cosmic superstrings, emit GWs. These GWs overlap and form a GW background. The GW background from cusps has been investigated attentively because they are expected strong enough. On the other hand, the GW background from kinks on infinite strings of cosmic strings and cosmic superstrings, called "infinite cosmic strings" and "infinite cosmic superstrings" hereafter, have not been studied yet because it is considered that the amplitude is smaller than the one from cusps. However, previous works have not considered the time evolution of the number and the sharpness of kinks, described by the distribution function of kinks. There are kinks with various sharpness and they contribute to the GW background at a wide range of the frequency, unlike the cusp case. In order to calculate the power spectrum of the GW background from kinks, we should first derive the distribution of kinks on infinite cosmic strings and infinite cosmic superstrings.

### 6.1 Evolution of sharpness

The sharpness of a kink changes with the cosmic expansion in FLRW spacetime. We will derive the time evolution of the sharpness. In FLRW spacetime, the solution of the string dynamics is  $\mathbf{p}_{\pm}$  where  $\pm$  denote the left / right moving mode. When there is a kink of the left moving mode, using the solution, the sharpness is defined as [63]

$$\psi \equiv \frac{1}{2}(1 - \mathbf{p}_{+,I} \cdot \mathbf{p}_{+,II}), \quad (6.1.1)$$

where the subscripts I, II mean the left / right side solution at the kink (see Fig. 6.1.1). Using

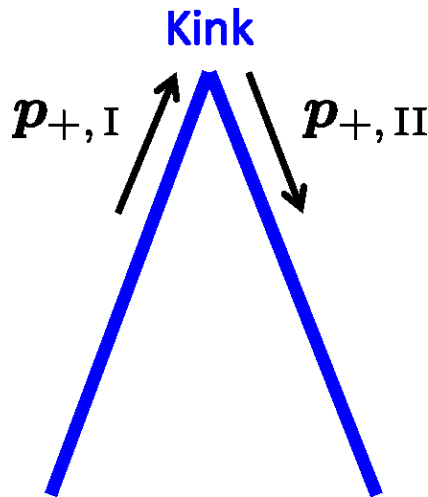


Fig. 6.1.1 The definition of sharpness. The solid blue line is the infinite string around the kink.

$\mathbf{p}_{\pm}$ , the string equation of motion Eq.(4.1.24) is rewritten as Eq.(4.1.28), where the dot and

the prime denote the derivative with respect to  $t$  and  $\sigma$  in this section. Applying the relation  $\frac{dt}{d\sigma} = 0$ , we get  $\mathbf{p}'_{\pm} = \frac{dt}{d\sigma} \frac{d\mathbf{p}_{\pm}}{dt} = 0$ . Then, the equation of motion with  $\mathbf{p}_{\pm}$ , Eq.(4.1.28) becomes

$$\dot{\mathbf{p}}_{\pm} = -H\{\mathbf{p}_{\mp} - (\mathbf{p}_{+} \cdot \mathbf{p}_{-})\mathbf{p}_{\pm}\}. \quad (6.1.2)$$

Substituting Eq.(6.1.1) into this equation, the time evolution equation of the sharpness is described as

$$\dot{\psi} = \frac{1}{2}H\{\mathbf{p}_{-} \cdot \mathbf{p}_{+, \text{II}} - (\mathbf{p}_{-} \cdot \mathbf{p}_{+, \text{I}})(\mathbf{p}_{+, \text{I}} \cdot \mathbf{p}_{+, \text{II}}) + \mathbf{p}_{+, \text{I}} \cdot \mathbf{p}_{-} - (\mathbf{p}_{+, \text{I}} \cdot \mathbf{p}_{+, \text{II}})(\mathbf{p}_{+, \text{II}} \cdot \mathbf{p}_{-})\}, \quad (6.1.3)$$

where  $\mathbf{p}_{-} = \mathbf{p}_{-}(t_{*}, \sigma_{*})$  is evaluated at the kink  $t = t_{*}$ ,  $\sigma = \sigma_{*}$ . This equation expresses that the sharpness changes with the Hubble time. We define the time average of  $\mathbf{p}_{\pm}$  as

$$\langle \mathbf{p}_{+} \cdot \mathbf{p}_{-} \rangle \equiv -\kappa = -(1 - 2\mathbf{v}^2), \quad (6.1.4)$$

and then the time evolution of the sharpness is rewritten as

$$\dot{\psi} = -2H\kappa\psi. \quad (6.1.5)$$

From the simulation [63], the value of the coefficient is estimated as  $\kappa_{\text{r}} \approx 0.18$  and  $\kappa_{\text{m}} \approx 0.3$ , where the suffixes "r" and "m" stand for the RD and MD era. We define the evolution of the scale factor as  $a \propto t^{\nu}$  ( $\nu_{\text{r}} = \frac{1}{2}$ ,  $\nu_{\text{m}} = \frac{2}{3}$ ) and  $\zeta \equiv \kappa\nu$ . Integrating Eq.(6.1.5), we get the time evolution of the sharpness as

$$\psi \propto t^{-2\zeta}, \quad (6.1.6)$$

where  $\zeta_{\text{r}} \approx 0.09$  and  $\zeta_{\text{m}} \approx 0.2$ .

## 6.2 On infinite cosmic strings

As seen in the previous subsection, the sharpness changes with time. We define "the distribution function of kinks"  $N(\psi, t)$ , the number of kinks as a function of sharpness [63, 117]. We derive the time evolution equation of kink distribution function considering these three factors;

- kink production by intersections of infinite strings,
- kinks blunted by the expansion of the universe,
- kinks are lost into loops by loop formation

First, we study the number of kink production. In order to count the number of infinite strings intersecting in the volume  $V$  and per time  $dt$ , we consider the small areas  $A_1, A_2$  in the world sheet made of infinite string 1 and 2. The world sheet coordinate is transformed as  $u \equiv \sigma - t$ ,  $v \equiv \sigma + t$ . Using this coordinate, the small areas of string 1, 2 are rewritten as  $u_1 \sim u_1 + du_1$ ,  $v_1 \sim v_1 + dv_1$  and  $u_2 \sim u_2 + du_2$ ,  $v_2 \sim v_2 + dv_2$ . When  $A_1$  and  $A_2$  intersect,

the infinite string 1, 2 also intersect. The probability of intersection between  $A_1$  and  $A_2$  is given by

$$\frac{\text{four-volume made of } A_1 \text{ and } A_2}{\text{four-volume at } V \text{ and } dt} \equiv \frac{d\Omega}{Vdt}, \quad (6.2.1)$$

where four-volume  $d\Omega$  is defined as

$$d\Omega = \left| \sqrt{-\det(g_{\mu\nu})} \epsilon_{\lambda\mu\nu\rho} \frac{\partial x_1^\lambda}{\partial u} \frac{\partial x_1^\mu}{\partial v} \frac{\partial x_2^\nu}{\partial u} \frac{\partial x_2^\rho}{\partial v} \right| du_1 dv_1 du_2 dv_2. \quad (6.2.2)$$

Because of  $A_1, A_2 \ll$  horizon and  $\frac{\partial t}{\partial u} = \frac{\partial t}{\partial v} = \frac{1}{2}$ , by imposing the gauge condition Eq.(4.1.13) and Eq.(4.1.14) in Minkowski spacetime,  $d\Omega$  is rewritten as

$$d\Omega = \frac{1}{4} \Delta du_1 dv_1 du_2 dv_2, \quad (6.2.3)$$

where

$$\begin{aligned} \Delta &= \frac{1}{4} \left\| \begin{array}{cccc} 1 & 1 & 1 & 1 \\ \mathbf{p}_{+,1} & \mathbf{p}_{-,1} & \mathbf{p}_{+,2} & \mathbf{p}_{-,2} \end{array} \right\| \\ &= \frac{1}{4} |(\mathbf{p}_{+,1} \times \mathbf{p}_{+,2}) \cdot (\mathbf{p}_{-,1} - \mathbf{p}_{-,2}) + (\mathbf{p}_{+,1} - \mathbf{p}_{+,2}) \cdot (\mathbf{p}_{-,1} \times \mathbf{p}_{-,2})|. \end{aligned} \quad (6.2.4)$$

The probability  $dp_1$  where the infinite string 1 intersects with the string 2 is described as the following equation

$$dp_1 = \frac{\int d\Omega}{Vdt} = \frac{\int du_2 dv_2 \frac{1}{4} \Delta du_1 dv_1}{Vdt}. \quad (6.2.5)$$

We define the total length  $L_{\text{total}}$  of infinite strings in the volume  $V$ ,  $L_{\text{total}} \equiv \frac{V}{L^2} = \int d\sigma$ . Using the relation  $dt d\sigma = \frac{1}{2} du dv$ , the integration is

$$\int du_2 dv_2 = \int d\sigma \cdot 2dt = \frac{2V}{L^2} dt. \quad (6.2.6)$$

We consider the average of  $\Delta$  and define  $\bar{\Delta}$  as the probability of intersecting string-selves as

$$\Delta \rightarrow \bar{\Delta} = \int \frac{d^2 \mathbf{p}_{+,1}}{4\pi} \frac{d^2 \mathbf{p}_{-,1}}{4\pi} \frac{d^2 \mathbf{p}_{+,2}}{4\pi} \frac{d^2 \mathbf{p}_{-,2}}{4\pi} \Delta, \quad (6.2.7)$$

and the probability is rewritten as

$$dp_1 = \frac{\bar{\Delta}}{2L^2} du_1 dv_1. \quad (6.2.8)$$

Obtaining the number of string intersections (same as kink production) within the time interval  $dt$ , we integrate  $dp_1$ . Then, we get

$$dN_{\text{intersect}} = \frac{\bar{\Delta} V dt}{2L^4}, \quad (6.2.9)$$

where, in order to avoid the double count, we multiply  $\frac{1}{2}$  by  $dp_1$ .

Moreover, we take account of the initial sharpness distribution when kinks are produced. For this purpose, we focus on  $\Delta$ . Eq.(6.2.7) is integrated by each  $d^2\mathbf{p}$  over unit sphere, and the value is [63, 117]

$$\bar{\Delta} = \frac{2\pi}{35} \approx 0.18. \quad (6.2.10)$$

Let us add the effect of the small anti-correlation between  $\mathbf{p}_+$  and  $\mathbf{p}_-$  verified by Eq.(6.1.4) into  $\bar{\Delta}$ . We assume that the distribution function  $f(\mathbf{p}_+, \mathbf{p}_-)$  is expressed by the linear function of  $\mathbf{p}_+ \cdot \mathbf{p}_-$  in the isotropic universe. Considering the anti-correlation of  $\mathbf{p}_\pm$ , the distribution function is assumed as

$$f(\mathbf{p}_+, \mathbf{p}_-) = 1 - 3\kappa\mathbf{p}_+ \cdot \mathbf{p}_-, \quad (6.2.11)$$

which satisfies the relation

$$\int \frac{d^2\mathbf{p}_+}{4\pi} \frac{d^2\mathbf{p}_-}{4\pi} f(\mathbf{p}_+, \mathbf{p}_-) = 1. \quad (6.2.12)$$

Inserting the distribution function into Eq.(6.2.7),  $\bar{\Delta}$  increases as

$$\bar{\Delta} = \frac{2\pi}{35} \left( 1 + \frac{2\kappa}{3} - \frac{\kappa^2}{11} \right). \quad (6.2.13)$$

Then, the asymptotic values in the RD and MD era are  $\bar{\Delta}_r \approx 0.20$ ,  $\bar{\Delta}_m \approx 0.21$  [63, 117]. Since we calculate the average of  $\Delta$  with the effect of the anti-correlation of  $\mathbf{p}_\pm$ , we will define the initial sharpness distribution  $g(\psi)$  without the anti-correlation as following. We assume that  $\mathbf{p}_{-,1}$  and  $\mathbf{p}_{-,2}$  are placed on the unit sphere homogeneously and the small anti-correlation  $\mathbf{p}_+$ ,  $\mathbf{p}_-$  does not affect the initial distribution for simplification, thus  $\langle \mathbf{p}_+ \cdot \mathbf{p}_- \rangle = 0$ . Integrating the right-hand side of Eq.(6.2.7) with respect to all direction of  $\mathbf{p}_{-,1}$ ,  $\mathbf{p}_{-,2}$ , we get the initial sharpness distribution as

$$\begin{aligned} \bar{\Delta} &= \int \frac{d^2\mathbf{p}_{+,1}}{4\pi} \frac{d^2\mathbf{p}_{-,1}}{4\pi} \frac{d^2\mathbf{p}_{+,2}}{4\pi} \frac{d^2\mathbf{p}_{-,2}}{4\pi}, \\ &\quad \times \frac{1}{4} |(\mathbf{p}_{+,1} \times \mathbf{p}_{+,2}) \cdot (\mathbf{p}_{-,1} - \mathbf{p}_{-,2}) + (\mathbf{p}_{+,1} - \mathbf{p}_{+,2}) \cdot (\mathbf{p}_{-,1} \times \mathbf{p}_{-,2})|, \\ &= \int \frac{d^2\mathbf{p}_{+,1}}{4\pi} \frac{d^2\mathbf{p}_{+,2}}{4\pi} \Delta(\mathbf{p}_{+,1}, \mathbf{p}_{+,2}), \\ &\equiv \bar{\Delta} \int d\psi g(\psi), \end{aligned} \quad (6.2.14)$$

$$g(\psi) = \frac{35}{256} \sqrt{\psi} (15 - 6\psi - \psi^2). \quad (6.2.15)$$

We set  $\int_0^1 d\psi g(\psi) = 1$  and  $g(\psi) = 0$  for  $\psi < 0$  or  $1 < \psi$ . The average of the produced sharpness  $\bar{\psi}$  is

$$\bar{\psi} = \int_0^1 d\psi \psi g(\psi) = \frac{5}{9}. \quad (6.2.16)$$

We see that sharp kinks are produced more. From Eq.(6.2.4), when  $\mathbf{p}_{+,1} = \mathbf{p}_{+,2}$ ,  $\Delta = 0$  and the intersection probability becomes 0. On the other hand, the probability has finite value with  $\mathbf{p}_{+,1} \neq \mathbf{p}_{+,2}$ . Therefore,  $g(\psi)$  is asymmetric function, whose average  $\bar{\psi}$  is bigger than  $\frac{1}{2}$ . To summarize, the number of kinks produced by string intersections in  $\psi \sim \psi + d\psi$  per the volume  $V$  and per unit time is

$$\left. \frac{\partial N}{\partial t}(\psi, t) \right|_{\text{production}} d\psi = \frac{\bar{\Delta}V}{\gamma^4 t^4} g(\psi) d\psi, \quad (6.2.17)$$

using  $L = \gamma t$ .

Second, we consider the effect that kinks are blunted by the expansion of the universe [63]. Although kink sharpness decreases, the total number of kinks conserves, so we have [59]

$$\frac{d}{dt} \left\{ \int^{\psi(t)} d\psi' N(\psi', t) \right\} = 0. \quad (6.2.18)$$

Using Eq.(6.1.6), this kink conservation is rewritten as

$$\frac{d}{dt} \left\{ \int^{\psi(t)} d\psi' N(\psi', t) \right\} = \int^{\psi(t)} d\psi' \left\{ \frac{\partial N}{\partial \psi}(\psi', t) - \frac{2\zeta}{t} \frac{\partial}{\partial \psi'}(\psi' N(\psi', t)) \right\} = 0 \quad (6.2.19)$$

In order to have this equation always satisfied, the integrand should be 0 at all the time. Then, we get the number of blunted kinks as

$$\left. \frac{\partial N}{\partial t}(\psi, t) \right|_{\text{blunted}} = \frac{\partial}{\partial \psi}(\psi N(\psi, t)) \frac{2\zeta}{t}. \quad (6.2.20)$$

Of course, this equation can be derived by considering the conservation of kinks at  $0 \leq \psi \leq 1$  (see appendix A).

Finally, we derive the number of kinks on infinite strings lost into loops. Loops are produced by string intersection and self-intersection. They shrink by emitting GWs and finally vanish. Therefore, kinks moved into loops disappear before long. We consider the length of infinite string  $d$  transformed from infinite strings to loops. The interval of infinite strings is the correlation length  $L$ , then the average of the initial loop size are also  $L$ . The time evolution of  $d$  is written as

$$\frac{dd}{dt} = -\eta \frac{V}{L^3}, \quad (6.2.21)$$

where  $\eta = \frac{1}{2} c p^{n_p} v$  [63, 104, 117] and this is the same as the second term of Eq.(5.1.6). It is rewritten as

$$\left. \frac{\dot{d}}{d} \right|_{\text{loop}} = -\frac{\eta}{L} = -\frac{\eta}{\gamma t}. \quad (6.2.22)$$

We assume that the fraction of kinks taken away to loops is proportional to the loss of the

length  $\frac{d}{d} \propto \frac{\dot{N}}{N}$ , then we get the term of kink lost by loops as

$$\left. \frac{\dot{N}}{N} \right|_{\text{loop}} = -\frac{\eta}{\gamma t}. \quad (6.2.23)$$

Combining these three terms Eqs.(6.2.17), (6.2.20) and (6.2.23), we get the time evolution equation of the kink distribution function as

$$\frac{\partial N}{\partial t}(\psi, t) = \frac{\bar{\Delta} V}{\gamma^4 t^4} g(\psi) + \frac{2\zeta}{t} \frac{\partial}{\partial \psi}(\psi N(\psi, t)) - \frac{\eta}{\gamma t} N(\psi, t). \quad (6.2.24)$$

In order to solve this evolution equation, we need the initial condition. We assume that the time of kink production is the same as strings are made. The time when the cosmic strings are produced is defined as  $t_*$  and the initial condition is

$$N(\psi, t_*) = 0. \quad (6.2.25)$$

The time of string production has been discussed and several scenarios are proposed. Here we describe two scenarios. First, cosmic strings are produced at the spontaneous symmetry breaking in the RD era and they survive with the interaction between the particles in the thermal bath and strings. The interaction works as friction. The second scenario is that the cosmic strings or cosmic superstrings are formed at the end of the inflation, where the scalar field oscillates and behaves as a matter. In the first case, we should consider the friction effect. In the second scenario, we have to calculate the kink distribution since this matter dominant era. Because the evolution of the universe at this time depends on the models, in this paper for simplicity, we assume that the strings are produced in the RD era using the standard cosmology (Sec.2).

When the parameters  $\gamma$ ,  $\bar{\Delta}$ ,  $\eta$ ,  $\zeta$  are constant, we can solve the distribution function of kinks analytically. If we assume that the parameter is constant in the RD and the MD respectively. Then, the analytic solution of kinks distribution is given by

$$\frac{N(\psi, t)}{V(t)/(\gamma t)^2} \sim \begin{cases} \psi^{-\beta_m/2\zeta_m} t^{-1} & \text{for } \psi > \left(\frac{t_{\text{eq}}}{t}\right)^{2\zeta_m}, \\ \left(\frac{t}{t_{\text{eq}}}\right)^{-B/\zeta_r} \psi^{-\beta_r/2\zeta_r} t^{-1} & \text{for } \psi < \left(\frac{t_{\text{eq}}}{t}\right)^{2\zeta_m}, \end{cases} \quad (6.2.26)$$

where

$$\beta \equiv 3 - 3\nu - \frac{\eta}{\gamma} + 2\zeta, \quad (6.2.27)$$

$$\beta_r \approx 1.1, \quad \beta_m \approx 1.2, \quad (6.2.28)$$

$$B \equiv \beta_r \zeta_m - \beta_m \zeta_r \approx 0.11. \quad (6.2.29)$$

and  $t_{\text{eq}}$  is the time of radiation-matter equality. The detailed derivation process is written

in Appendix B. The left-hand side of the solution Eq.(6.2.26) corresponds to the number of kinks per unit length.

In order to get the exact solution, simultaneously, we numerically solve the evolution equation Eq. (6.2.24) using the scaling law Eqs.(5.1.6) and (5.1.7) and the following equations

$$\bar{\Delta} = \frac{2\pi}{35} \left\{ 1 + \frac{2}{3}(1 - 2v^2) - \frac{1}{11}(1 - 2v^2)^2 \right\}, \quad (6.2.30)$$

$$\zeta = (1 - 2v^2) \left\{ \frac{\ln(a/a_{\text{ini}})}{\ln(t/t_{\text{ini}})} \right\}, \quad (6.2.31)$$

$$\eta = \frac{1}{2} c p^{n_p} v, \quad (6.2.32)$$

where  $p = 1$ ,  $n_p = \frac{1}{3}$  and  $a_{\text{ini}}$ ,  $t_{\text{ini}}$  are an initial scale factor and an initial time. Furthermore at the same time, we solve the Hubble parameter Eq.(2.3.7) with  $\Omega_r h^2 = 4.31 \times 10^{-5}$ ,  $h = 0.678$ ,  $\Omega_m = 0.308$ ,  $\Omega_\Lambda = 0.692$  [66] and  $\Omega_K = 0$ .

Fig.6.2.1 shows the distribution function of kinks on infinite strings at the present. Since the sharpness of kinks decreases with time by the cosmic expansion and the initial sharpness distribution  $g(\psi)$  tells that newly produced kinks are mostly sharp, the most blunted kinks are made in the past. The number of old blunted kinks with small sharpness is larger than new ones because  $\mathcal{O}(1 - 10)$  of kinks are produced per horizon and the number of newly produced kinks per comoving length decreases as the horizon grows. Therefore, kinks at the left side of Fig.6.2.1 ( $\psi < 7 \times 10^{-2}$ ) are made during the RD era and at right side ( $\psi > 7 \times 10^{-2}$ ) are done during the MD and the  $\Lambda$ D era [59]. The kinks at  $\psi \sim 7 \times 10^{-2}$  are produced at the matter-radiation equality.

### 6.3 On infinite cosmic superstrings

Cosmic superstrings have Y-junctions in the network, where F and D strings meet and form the bound state. When a kink enters a Y-junction, two transmitted kinks and one reflected kink appear and the sharpness of these kinks differs from the original incoming kink depending on the tensions of cosmic superstrings and angles of three strings. Here, we define the transmission coefficient

$$C_{ij} = \frac{\psi_j^{(\text{out})}}{\psi_i^{(\text{in})}}, \quad (6.3.1)$$

where  $i, j = 1, 2, 3$  is the label of different strings connecting to the Y-junction, and (in) and (out) denote incoming and outgoing kinks. For example,  $C_{12}$  describes how much sharpness of the outgoing kink on string 2 is reduced or enhanced compared to the incoming kink when a kink entered from string 1, while  $C_{11}$  gives the sharpness of the kink reflected to string 1. Reference [41] has provided a detailed study on how the sharpness of the incoming kink is transmitted to the three daughter kinks using numerical simulation. Although the transmission coefficient was found to be distributed over a wide range of values depending on

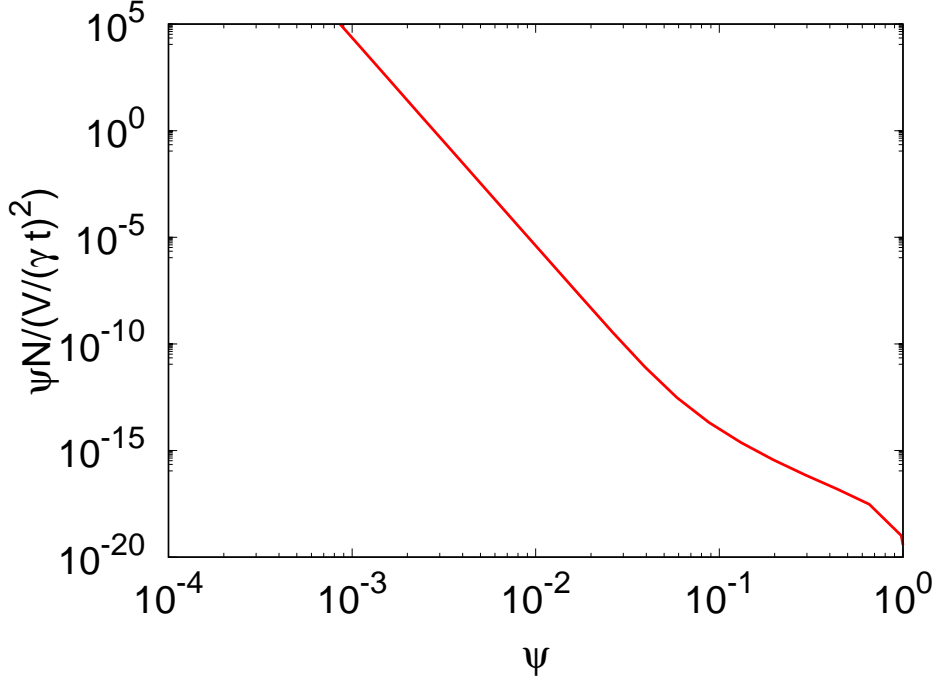


Fig. 6.2.1 The distribution function of kinks on infinite cosmic strings. The vertical axis is the number of kinks per unit length and the horizontal axis is the sharpness of kinks. We calculate it for  $G\mu = 10^{-11}$ , however, this distribution function of kink independent on the tension.

the configuration of three strings, we adopt the average value of the coefficient. For the choice of tensions, we investigate the two cases:  $\mu_1 : \mu_2 : \mu_3 = 1 : 1 : 1$  and  $\mu_1 : \mu_2 : \mu_3 = 1 : 10 : 10$ .

In the case of equal tensions, the sharpness of the reflected and transmitted kinks are  $0.49^2$  and  $0.72^2$  times smaller than the incoming kink in average, respectively (the value is taken from Fig. 3 of [41]).<sup>\*3</sup> The picture is given in Fig. 6.3.1. In summary, the transmission coefficient is given by

$$C_{ij} = \begin{pmatrix} C_{11} & C_{12} & C_{13} \\ C_{21} & C_{22} & C_{23} \\ C_{31} & C_{32} & C_{33} \end{pmatrix} = \begin{pmatrix} 0.49^2 & 0.72^2 & 0.72^2 \\ 0.72^2 & 0.49^2 & 0.72^2 \\ 0.72^2 & 0.72^2 & 0.49^2 \end{pmatrix}. \quad (6.3.2)$$

We also consider non-equal tensions with the ratio of  $\mu_1 : \mu_2 : \mu_3 = 1 : 10 : 10$ . When the incoming kink comes from the light string, the sharpness of the kinks transmitted to the other two heavy strings is  $0.09^2$  times smaller, while the reflected kink becomes  $0.49^2$  times. When the incoming kink is from the heavy string, the sharpness changes depending on the tension of the transmitted strings. The transmission coefficient is  $0.72^2$  for the light string and  $0.99^2$  for

<sup>\*3</sup> Note that the definition of the sharpness in [41] is  $|\sin(\theta/2)|$ , where  $\theta$  is the kink angle, while our definition of  $\psi$ , Eq. (6.1.1), is transformed to  $\sin^2(\theta/2)$  [63]. Thus, the values of the transmission coefficient obtained in [41] are squared in this paper.

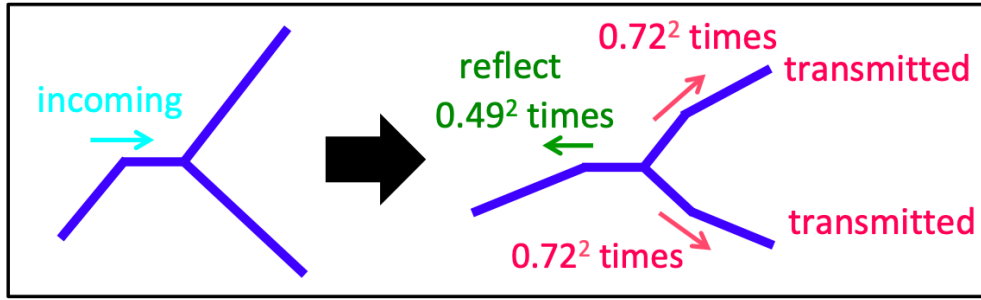


Fig. 6.3.1 The changes of sharpness for  $\mu_1 : \mu_2 : \mu_3 = 1 : 1 : 1$ .

the heavy string. The reflected kink becomes  $0.09^2$  times smaller. See Appendix A.1 and A.2 of [41] for the details. The values are summarized in Fig. 6.3.2. The transmission coefficient is

$$C_{ij} = \begin{pmatrix} 0.49^2 & 0.09^2 & 0.09^2 \\ 0.72^2 & 0.09^2 & 0.99^2 \\ 0.72^2 & 0.99^2 & 0.09^2 \end{pmatrix}. \tag{6.3.3}$$

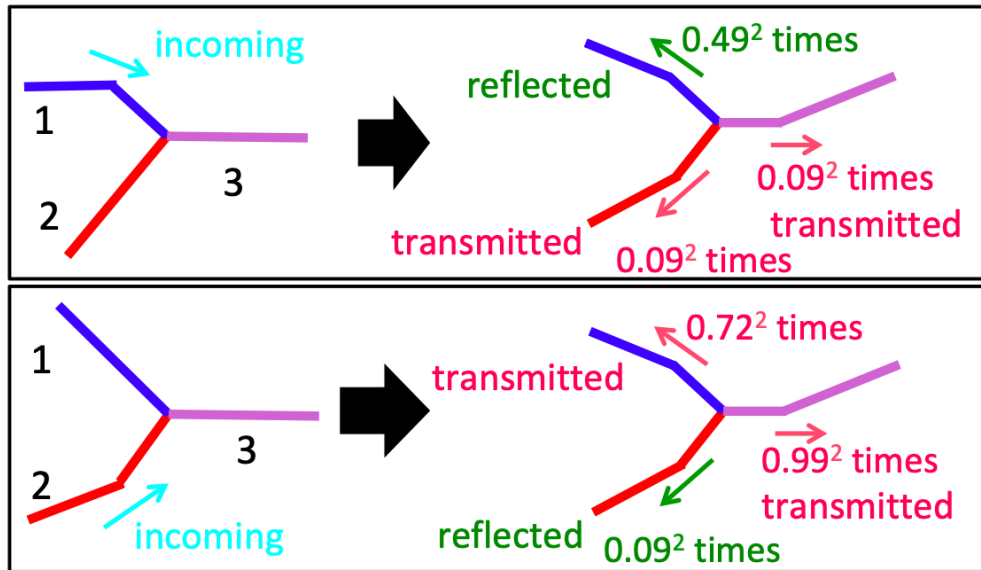


Fig. 6.3.2 The changes of sharpness for  $\mu_1 : \mu_2 : \mu_3 = 1 : 10 : 10$ .

Then, we find the evolution equations of the distribution function of kinks for string types

1, 2 and 3 are given as the following,

$$\begin{aligned} \frac{\partial N_1}{\partial t}(\psi, t) = & \frac{p_1 \bar{\Delta}_1 V}{\gamma_1^4 t^4} g(\psi) + \frac{2\zeta_1}{t} \frac{\partial}{\partial \psi} (\psi N_1(\psi, t)) - \frac{\eta_1}{\gamma_1 t} N_1(\psi, t) \\ & + \frac{\alpha}{t} N_2 \left( \frac{\psi}{C_{21}}, t \right) + \frac{\alpha}{t} N_3 \left( \frac{\psi}{C_{31}}, t \right) + \frac{\alpha}{t} N_1 \left( \frac{\psi}{C_{11}}, t \right) - \frac{\alpha}{t} N_1(\psi, t), \end{aligned} \quad (6.3.4)$$

$$\begin{aligned} \frac{\partial N_2}{\partial t}(\psi, t) = & \frac{p_2 \bar{\Delta}_2 V}{\gamma_2^4 t^4} g(\psi) + \frac{2\zeta_2}{t} \frac{\partial}{\partial \psi} (\psi N_2(\psi, t)) - \frac{\eta_2}{\gamma_2 t} N_2(\psi, t) \\ & + \frac{\alpha}{t} N_1 \left( \frac{\psi}{C_{12}}, t \right) + \frac{\alpha}{t} N_3 \left( \frac{\psi}{C_{32}}, t \right) + \frac{\alpha}{t} N_2 \left( \frac{\psi}{C_{22}}, t \right) - \frac{\alpha}{t} N_2(\psi, t), \end{aligned} \quad (6.3.5)$$

$$\begin{aligned} \frac{\partial N_3}{\partial t}(\psi, t) = & \frac{p_3 \bar{\Delta}_3 V}{\gamma_3^4 t^4} g(\psi) + \frac{2\zeta_3}{t} \frac{\partial}{\partial \psi} (\psi N_3(\psi, t)) - \frac{\eta_3}{\gamma_3 t} N_3(\psi, t) \\ & + \frac{\alpha}{t} N_1 \left( \frac{\psi}{C_{13}}, t \right) + \frac{\alpha}{t} N_2 \left( \frac{\psi}{C_{23}}, t \right) + \frac{\alpha}{t} N_3 \left( \frac{\psi}{C_{33}}, t \right) - \frac{\alpha}{t} N_3(\psi, t). \end{aligned} \quad (6.3.6)$$

The parameters  $\bar{\Delta}_i$ ,  $\zeta_i$  and  $\eta_i$  are given by the average velocity of each string  $v_i$  as

$$\bar{\Delta}_i = \frac{2\pi}{35} \left\{ 1 + \frac{2}{3} (1 - 2v_i^2) - \frac{1}{11} (1 - 2v_i^2)^2 \right\} \quad (6.3.7)$$

$$\zeta_i = (1 - 2v_i^2) \left\{ \frac{\ln(a/a_{\text{ini}})}{\ln(t/t_{\text{ini}})} \right\}, \quad (6.3.8)$$

$$\eta_i = \frac{1}{2} c_i p_i^{n_p} v_i. \quad (6.3.9)$$

Compared to the ordinary cosmic string case described in Eq. (6.2.24), we added two effects associating with the characteristics of the superstring network. First, the kink production term is multiplied by  $p$  as kinks are generated by the intersection of strings and the number of intersections is reduced linearly by the reconnection probability. Second, the new terms are added in order to include the effect of kinks entering Y-junction. The fourth and fifth terms describe kinks coming from different types of strings by changing their sharpness. The sixth term corresponds to reflected kinks. These terms describe that kinks, whose sharpness was  $\psi_i^{(\text{in})} = \psi_j^{(\text{out})}/C_{ij}$ , transmit to different or the same string with the rate of  $\alpha$  times per horizon time. The seventh term describes the disappearance of incoming kinks.

For the value of  $\alpha$ , we use the following estimation. Since kinks move with the speed of light, kinks move  $\sim t$  in a Hubble time, while the average distance between Y-junction would be roughly given by the correlation length of three strings as  $\sim \frac{1}{3}(\gamma_1 + \gamma_2 + \gamma_3)t$ . Thus, the number of kinks encountering Y-junctions in a Hubble time is roughly given by

$$\alpha = \frac{3}{\gamma_1 + \gamma_2 + \gamma_3}. \quad (6.3.10)$$

In Fig. 6.3.4, we show the distribution function of kinks obtained by numerically calculating Eqs.(6.3.4) – (6.3.6) and Eq. (5.2.8) – Eq. (5.2.13). From the top to the bottom, we show

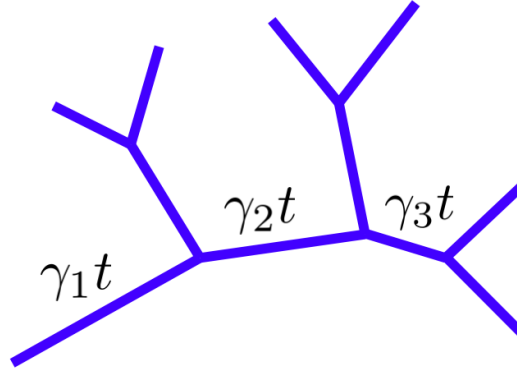


Fig. 6.3.3 The cosmic superstring network with Y-junctions and the interval between the Y-junctions.

Case A, B, and C. For the transmission coefficient, we use Eq.(6.3.2) for Cases A and B, and Eq.(6.3.3) for Case C. The left panels show results for different string types 1, 2 and 3 with  $p_1 = p_2 = p_3 = 1$ . In the right panels, we show how different reconnection probabilities affect the results. The lines represent the sum of the kink numbers of different string types for  $p_1 = p_2 = p_3 = 1, 10^{-1}, 10^{-2}$  and  $10^{-3}$ . For comparison, we also plot the result of ordinary cosmic strings (same as Fig. 6.2.1).

### 6.3.1 Case A: kink distribution with $\mu_1 : \mu_2 : \mu_3 = 1 : 1 : 1$ and $n_p = 1$

In the left panels, the reconnection probabilities are all set to unity, so that we can simply see the effects of Y-junctions by comparing with the ordinary cosmic string case, which should be identical when we set  $p_1 = p_2 = p_3 = 1$  and remove the Y-junction terms. In all cases, we find that the number of distribution is flatter when we include the effect of Y-junctions. This is because, when a kink enters a Y-junction, three transmitted kinks typically have smaller sharpness than the original one. Thus, the Y-junctions increase the number of kinks with small sharpness, while they decrease the number of kinks with large sharpness, which flattens the distribution and extends the cutoff to a much lower sharpness <sup>\*4</sup>.

In the right panels, we find that smaller reconnection probability tends to flatten the distribution more. This is the result of two combined effects. First, small  $p$  decreases the correlation length and increases the number of strings inside the horizon. This enhances the kink production term, as it is proportional to  $p/\gamma^4$  and  $\gamma \propto p$  for Case A, and increase the overall number of kinks. On the other hand, the small correlation length increases the number of kinks encountering Y-junctions  $\alpha$  and makes the effect of Y-junction terms stronger. In Case A, we find that the latter effect is always stronger than the former, and we find that the

<sup>\*4</sup> Note that, although the figures may give the impression that the total number of kinks decreases when we include the effect of Y-junctions, this is not true since there are a huge number of kinks at much smaller sharpness beyond the plot range of the figure. In fact, Y-junctions increase the total number of kinks. However, the increased kinks have very small sharpness and they do not increase the GW background amplitude, as we will see in the next sections.

distribution is more flattened for smaller  $p$ .

### 6.3.2 Case B: kink distribution with $\mu_1 : \mu_2 : \mu_3 = 1 : 1 : 1$ and $n_p = \frac{1}{3}$

In Case B, the kink distribution looks similar to Case A. The only difference arises in the right panel, where we find a number of kinks are smaller than Case A when the reconnection probability is small. This is because the loop production is more efficient in the case of  $n_p = \frac{1}{3}$ , and the decrease of correlation length  $\gamma$  is milder for smaller reconnection probability as shown in the right panels of Fig. 5.2.2 and found  $\gamma \propto p^{0.32}$ . Since  $\gamma$  has a larger value, the kink production term  $\propto p/\gamma^4$  is suppressed, which is the reason that we find less number of kinks.

### 6.3.3 Case C: kink distribution with $\mu_1 : \mu_2 : \mu_3 = 1 : 10 : 10$ and $n_p = \frac{1}{3}$

In the left panel of Case C, we find the slope of the distribution function is more flattened compared to the cosmic string case because of the existence of Y-junctions, but not as much as Cases A and B. This is because kinks are smoothed out efficiently with the coefficient  $0.49^2$  and  $0.72^2$  in Cases A and B, while we have the coefficient of  $C_{32} = C_{23} = 0.99^2$  in Case C, which means that one of the three kinks stays with the original sharpness when a kink enters from type 3 and 2, which is  $2/3$  of the collisions. Thus, the effect of Y-junctions to smooth out kinks is weaker in Case C. We also find the number of kinks on string 1 is smaller than types 2 and 3. This is because the kinks with the original sharpness (with the coefficient of  $0.99^2$ ) are transmitted to string 2 or 3, and the sharpness of kinks going to string 1 is always multiplied by  $0.49^2$  or  $0.72^2$ . Thus, kinks on string 1 tend to get flat more compared to the ones for strings 2 and 3.

In the right panel, we find an interesting behavior that the kink number slightly increases for  $p = 10^{-1}$ , compared to the case of  $p = 1$ , because the effect of small reconnection probability to enhance the kink production term with smaller  $\gamma$  dominates the effect of Y-junctions to smooth out the sharpness of kinks. When the value of  $p$  decreases to  $10^{-2}$  and  $10^{-3}$ , the latter effect becomes stronger and the distribution gets flat.

## 6.4 Summary

The distribution function of kinks is determined by the balance of the effect of producing kinks and blunting by Y-junctions. In the case  $1 : 1 : 1$ , when the reconnection probability becomes small, the kink distribution gets flat. In other words, kinks with small sharpness increase because of the number of Y-junctions increases for smaller the reconnection probability. In the case of  $1 : 10 : 10$ , the kink number grows because the kink generation term affects the distribution strongly.

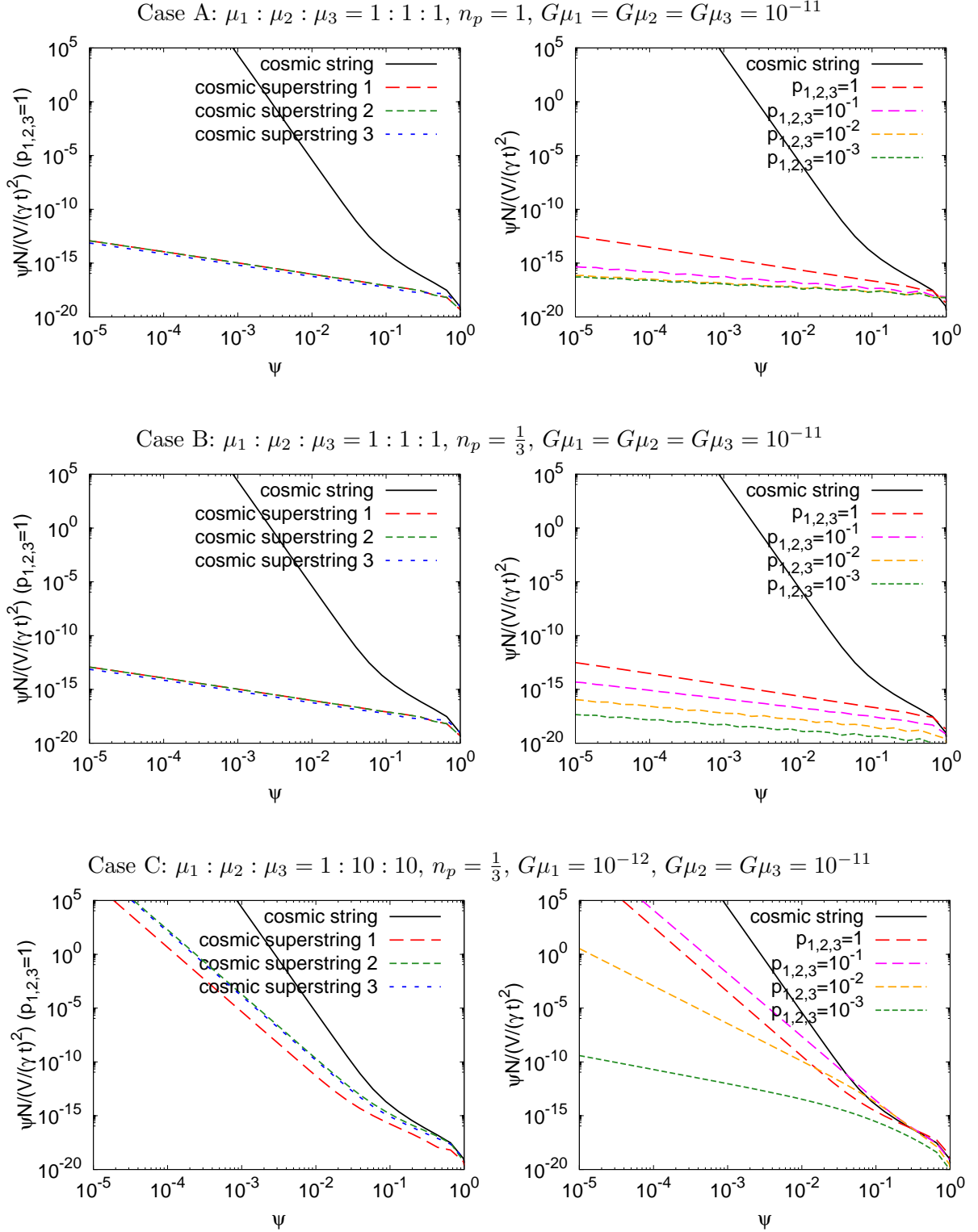


Fig. 6.3.4 The distribution function of kinks on infinite cosmic superstrings. The axes are the same as in Fig. 6.2.1. In the left panels, we show results for different string types 1, 2 and 3 (red, green and blue broken lines) for  $p_1 = p_2 = p_3 = 1$ . The right panels show results for different reconnection probabilities. The red, magenta, orange and green broken lines corresponds to the cases of  $p_1 = p_2 = p_3 = 1, 10^{-1}, 10^{-2}$  and  $10^{-3}$ , respectively. The lines represent the total kink number of string types 1, 2 and 3. In all panels, for comparison, we plot the case of ordinary cosmic strings with the black solid line ( $G\mu = 10^{-11}$ ).

## 7 Gravitational wave background from propagating kinks

In the previous work, it is expected that the GW background from loops is larger than the one from kinks. Because of this, the estimation of the GW background from kinks has not been intensively developed. However, we can hope that the GW background from kinks are emitted at the low frequency because loops cannot emit GWs whose wavelength is longer than the loop size. In our previous work [59], considering the evolution of the distribution function of kinks, we estimated the power spectrum of the GW background from propagating kinks on infinite strings. Then, it is compared with the one from loops. In this section, first, we describe the strain amplitude and the rate of GWs from propagating kinks and formulate the power spectrum of the GW background from propagating kinks. Then, using the distribution function of kinks obtained in the previous section and the evolution equation of the string network, we calculate the power spectrum of the GW background numerically.

### 7.1 Formulation

Because kinks move along the curved strings, in other words, they have the radial acceleration of the strings, they emit GWs vertically to the moving direction of the kink. In addition, kinks move with the speed of light, then GWs are beamed in the direction of the movement of kinks. Fig.7.1.1 shows the illustration of GW emission from a propagating kink. When the direction of the GW emission is parallel to the line of sight to the kink, we can detect the GW. Then, we observe the GW from the propagating kink as a burst event.

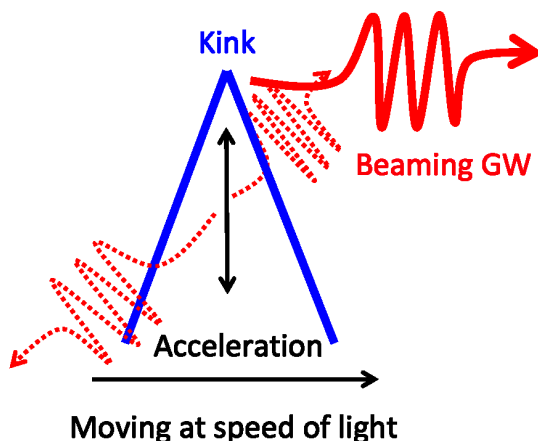


Fig. 7.1.1 The illustration of the GW direction from a propagating kink. The solid blue line is the kink moving with the speed of light toward the right side. The broken red waves toward us and to the opposite side mean the GW from the kink if the kink moves at a slower speed than the speed of light, and the solid red wave is the beamed GW by the relativistic motion.

The power spectrum of the GW background depends on the strain amplitude of each event and the number of GWs. First, we describe the relationship between the energy-momentum

tensor of the source  $T_{\mu\nu}(x^\lambda)$  and the GW strain amplitude  $h$ . We consider the GW strain amplitude at the distance  $r$  from the source and assume that  $r$  is much larger than the GW wavelength, while much smaller than the Hubble radius. Considering a perturbation of the metric created by the source

$$g_{\mu\nu}(x^\lambda) = \eta_{\mu\nu} + h_{\mu\nu}(x^\lambda), \quad (7.1.1)$$

and using the trace-reversed metric perturbation

$$\bar{h}_{\mu\nu} \equiv h_{\mu\nu} - \frac{1}{2}\eta_{\mu\nu}h, \quad h \equiv h^\rho{}_\rho, \quad (7.1.2)$$

where we impose the harmonic condition  $\frac{\partial \bar{h}_{\mu\nu}}{\partial x_\nu} = 0$ , we get the linearized Einstein equations

$$\square \bar{h}_{\mu\nu}(x^\lambda) = -16\pi G T_{\mu\nu}(x^\lambda). \quad (7.1.3)$$

Let us replace  $\phi \rightarrow \bar{h}_{\mu\nu}(x^\lambda)$  and  $S \rightarrow 4GT_{\mu\nu}(x^\lambda)$  in the general formulas [37] described in detail in appendix C. Focusing on the leading term, we get

$$\bar{h}_{\mu\nu}(\mathbf{x}, t) \simeq \frac{4G}{r} \sum_{\omega_m} e^{-i\omega_m(t-r)} T_{\mu\nu}(\mathbf{k}, \omega), \quad (7.1.4)$$

$$T_{\mu\nu}(\mathbf{k}, \omega) = \frac{1}{T_l} \int_0^{T_l} dt \int d^3 e^{i(\omega t - \mathbf{k} \cdot \mathbf{x})} T_{\mu\nu}(\mathbf{x}, t), \quad (7.1.5)$$

where  $\omega_m = \pm m\omega_l$  with  $m$  being a natural number. We have  $\omega_l \equiv \frac{2\pi}{T_l}$  and  $T_l = \frac{L_l}{2} = \frac{L}{2}$ , where the period is written by the typical length of the infinite string; the curvature radius, namely, the correlation length  $L = \gamma t$  in the kink case.  $\mathbf{k}$  is parallel to the line of sight to the source. Because the sum in terms of  $\omega_m$  is up to  $m \rightarrow \infty$ , we can transform from the sum to Fourier integration as  $\sum_{\omega_m} = \sum_m \simeq \int dm = \frac{\gamma t}{2} \int \frac{d\omega}{2\pi} = \frac{\gamma t}{2} \int df$ , thus we get

$$\bar{h}_{\mu\nu}(\mathbf{x}, t) \simeq \frac{2G\gamma t}{r} \int \frac{d\omega}{2\pi} e^{-i\omega(t-r)} T_{\mu\nu}(\mathbf{k}, \omega). \quad (7.1.6)$$

We introduce the logarithmic Fourier transformation as

$$F(f) \equiv |f| \int dt e^{2\pi i f t} F(t), \quad (7.1.7)$$

where  $F(t)$  is a time-varying arbitrary continuous function. The advantage of this transformation is that  $F(t)$  and  $F(f)$  are the same dimension. Using the transformation, the trace-reversed metric perturbation is

$$\bar{h}_{\mu\nu}(\mathbf{n}, f) \simeq \frac{2G\gamma t f T_{\mu\nu}(\mathbf{k}, \omega)}{r}, \quad (7.1.8)$$

where  $\mathbf{n} = \frac{\mathbf{k}}{\omega}$  and  $f$  is the frequency of the GW from one kink. We should consider that the

distance from the source is affected by the cosmic expansion and the GW is redshift in FLRW spacetime  $g_{\mu\nu} = \bar{g}_{\mu\nu} + h_{\mu\nu}$  where  $\bar{g}_{\mu\nu}$  is FLRW metric. Thus, we get

$$\bar{h}_{\mu\nu}(f) = \frac{2G\gamma t(1+z)fT_{\mu\nu}((1+z)f\mathbf{n}, (1+z)f)}{r(z)}, \quad (7.1.9)$$

where  $f$  is the conformal frequency and  $\omega \sim (1+z)f$  and

$$r(z) = \int_0^z \frac{dz'}{H(z')}. \quad (7.1.10)$$

Then, the strain amplitude of the GW  $h(f)$  is

$$\bar{h}(f) \equiv \sqrt{\bar{h}_{\mu\nu}(f)\bar{h}^{\mu\nu}(f)} = \frac{2G\gamma t(1+z)f}{r(z)} \sqrt{T_{\mu\nu}T^{\mu\nu}}. \quad (7.1.11)$$

Since the strain amplitude depends on  $T_{\mu\nu}$ , it is different between a propagating kink and a kink-kink collision.

Second, we introduce the rate of the GW for  $\ln \psi \sim \ln \psi + d\psi$ ,  $n(f, z)$  and define as

$$n(f, z) = \frac{1}{f} \times (\text{rate of GW bursts per kink}) \\ \times \left( \# \text{ of kinks per unit volume: } \psi \frac{N(\psi, t)}{V} \right) \times \frac{dV(z)}{d \ln z}, \quad (7.1.12)$$

where

$$\frac{dV}{dz} = \frac{1}{z} \frac{dV}{d \ln z} = \frac{4\pi r^2(z)}{(1+z)^3 H(z)} \quad (7.1.13)$$

is the volume between  $z$  and  $z + dz$ . It depends on the case of the propagating kinks and kink-kink collisions.

Let us formulate the GW background power spectrum. One kink emits GWs at various frequencies. The GWs and the ones from other kinks overlap and interfere. When the interval of the kinks is equal to the wavelength of the GW background (we define the frequency as  $f_{\text{GW background}}$ ), the GWs from one kink whose frequency is  $f = f_{\text{GW background}}$  do not just cancel out (see Fig.7.1.2). Then, we can regard  $f$  in the strain amplitude as  $f_{\text{GW background}}$  and the frequency  $f$  satisfies this relation [58]

$$\left\{ \psi \frac{N(\psi, t)}{V(t)/(\gamma t)^2} \right\}^{-1} \sim \{2\pi f(1+z)\}^{-1}, \quad (7.1.14)$$

where the left-hand side is the interval of the kinks and the right one is the wavelength of the GW background. The sharpness satisfying Eq.(7.1.14) contributes most to the GW amplitude (see appendix D). We define this sharpness as  $\psi = \psi_{\text{max}}$ . We explain  $\psi_{\text{max}}$  using the distribution function of the kinks. Because the inverse of the left-hand side of Eq.(7.1.14) is

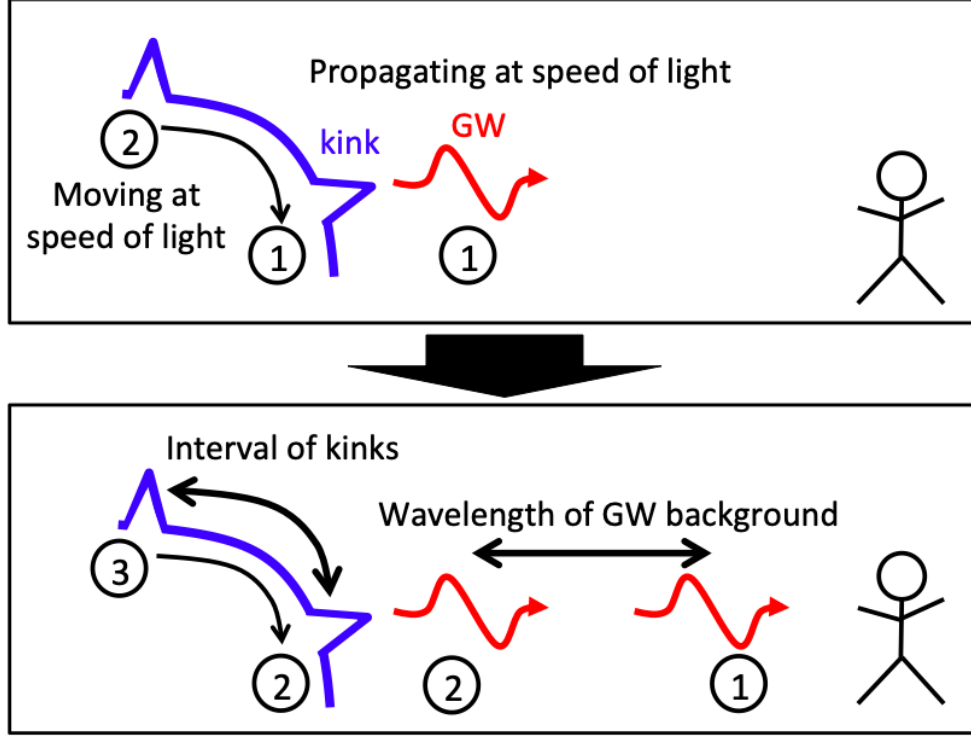


Fig. 7.1.2 The illustration of the GW from one kink, the interval of the kinks and the wavelength of the GW background. The illustration of the wavelength of GWs from one kink and interval of kinks. The GWs survive and propagate to us only when the wavelength is equal to the interval.

same as the vertical axis of the kinks distribution, the intersection where the kink distribution crosses with the line of  $2\pi f(1+z)$  parallel to the horizontal axis determines  $\psi_{\max}$ .

Since the GW background is formed by overlapped GWs from kinks, we define the total energy of the GW integrating with respect to  $z$  as

$$h_{\text{tot}}^2(f) = \int \frac{dz}{z} \Theta(n(f, z) - 1) n(f, z) h^2(f, z), \quad (7.1.15)$$

where  $\Theta$  is a step function introduced to remove rare bursts. We also define the energy density of the GW per the logarithmic frequency as

$$\frac{d\rho_{\text{GW}}}{d \ln f} \equiv \frac{(2\pi f h_{\text{tot}}(f))^2}{16\pi G} = \frac{\pi}{4G} f^2 h_{\text{tot}}^2(f), \quad (7.1.16)$$

then, the density parameter  $\Omega_{\text{GW}}$  is expressed as

$$\Omega_{\text{GW}}(f) \equiv \frac{1}{\rho_c} \frac{d\rho_{\text{GW}}}{d \ln f} \equiv \frac{2\pi^2 f^2}{3H_0^2} \int \frac{dz}{z} \Theta(n(f, z) - 1) n(f, z) h^2(f, z), \quad (7.1.17)$$

$h(f, z)$  and  $n(f, z)$  are different between propagating kinks and kink-kink collisions.

Now, we introduce the power spectrum of the GW background from propagating kinks on infinite cosmic strings and infinite cosmic superstrings. Because kinks are the small scale structure, the energy-momentum tensor of the kinks can be expressed by  $\mathbf{a}(u)$  and  $\mathbf{b}(v)$  which are the solution of the string dynamics in the Minkowski spacetime. If there are a discontinuity or a stationary point on the phase of the energy-momentum tensor, represented as  $\mathbf{a}'(u_*)$  and  $\mathbf{b}(v_s)$  respectively, from Appendix E, the energy-momentum tensor is expressed as [37]

$$T^{\mu\nu}(\omega, \omega \mathbf{n}) \simeq -\frac{\mu}{\omega^{\frac{5}{3}}} \left( \frac{a_+^{\mu'}}{1 + \mathbf{n} \cdot \mathbf{a}'_+} - \frac{a_-^{\mu'}}{1 + \mathbf{n} \cdot \mathbf{a}'_-} \right) \times b_s^{\nu} \left( \frac{12}{|\mathbf{n} \cdot \mathbf{b}_s''|} \right)^{2/3} \frac{\Gamma(\frac{2}{3})}{2\sqrt{3}} e^{\frac{i}{2}\omega(v_s - u_* - \mathbf{n} \cdot \mathbf{a}(u_*) - \mathbf{n} \cdot \mathbf{b}_s)} + (\mu \leftrightarrow \nu), \quad (7.1.18)$$

where  $\mathbf{a}'_{\pm} \equiv \mathbf{a}'(u_*)$  whose suffix  $\pm$  represents the left and right at the kink,  $\mathbf{b}_s \equiv \mathbf{b}(v_s)$ ,  $\mathbf{n} = \mathbf{b}'_s$  and  $\int_{-\infty}^{\infty} dw w e^{-iw^3} = -\frac{i}{\sqrt{3}} \Gamma(\frac{2}{3})$ . Using Eq.(7.1.18), we derive the strain amplitude of GWs from one propagating kink. We approximate the inner product of  $\mathbf{a}'_{\pm}$  and  $\mathbf{b}'_s$  as [58]

$$\left\langle \frac{1}{(1 + \mathbf{b}'_s \cdot \mathbf{a}'_+)^2} \right\rangle \sim \left\langle \frac{1}{(1 + \mathbf{b}'_s \cdot \mathbf{a}'_-)^2} \right\rangle \sim \left\langle \frac{1}{(1 + \mathbf{b}'_s \cdot \mathbf{a}'_+)(1 + \mathbf{b}'_s \cdot \mathbf{a}'_-)} \right\rangle \sim \mathcal{O}(1) \sim 1. \quad (7.1.19)$$

Since  $\mathbf{a}'$ ,  $\mathbf{b}'$  is unit vectors, the vectors  $\mathbf{b}'_s$ ,  $\mathbf{b}_s''$ ,  $\mathbf{b}_s'''$  are assumed as

$$|\mathbf{b}_s''| \sim (\gamma t)^{-1}, \quad |\mathbf{b}_s'''| \sim (\gamma t)^{-2}, \quad |\mathbf{b}'_s \cdot \mathbf{b}_s'''| \sim |\mathbf{b}'_s| |\mathbf{b}_s'''| \sim (\gamma t)^{-2}, \quad (7.1.20)$$

and  $\mathbf{a}'$  satisfies

$$|a_+^{\mu'}|^2 \sim |a_-^{\mu'}|^2 \sim 1, \quad 1 - \mathbf{a}'_+ \cdot \mathbf{a}'_- = 2\psi. \quad (7.1.21)$$

Then, by omitting numerical factors, the strain amplitude of GWs from one propagating kink is

$$h_k(f, z) \sim \frac{G\mu\sqrt{\psi_{\max}}\gamma t}{\{(1+z)f\gamma t\}^{2/3} r(z)} \Theta(1 - \theta_m), \quad (7.1.22)$$

where  $\theta_m = \{(1+z)f\gamma t\}^{-1/3}$  and we add the step function  $\Theta$  to cutoff the low-frequency GWs because kinks cannot emit GWs whose wavelength is longer than the curvature radius  $\gamma t$ .

In order to obtain the rate of the GW  $n(f, z)$ , let us consider the rate of the GW bursts per kink. Since GWs emitted from a propagating kink is beamed towards the moving direction, the emitted GWs has a cone shape. Therefore, the rate of GW bursts per kink can be estimated by the solid angle made by the radiation cone of the GW per kink per unit time divided by all solid angles. We assume that the moving kink on the curved infinite string  $\gamma t$  can be regarded as the moving kink on a loop with the circumference  $\gamma t$  [45]. Because the angle of the radiation cone is  $2\theta_m$  and the average length of the kink motion is  $\pi$ , the solid angle of the radiation cone of the GW emitted from the kink is  $2\theta_m \times \pi$ . Then, it is written as  $\frac{2\theta_m \pi}{\gamma t}$  per unit time.

Adding the effect of redshifting, the rate of the GW bursts per kink per unit time is

$$\frac{2\theta_m\pi/\gamma t(1+z)}{4\pi} = \frac{1}{2}\theta_m\gamma t^{-1}(1+z)^{-1}. \quad (7.1.23)$$

Then, the rate of the GW is written as

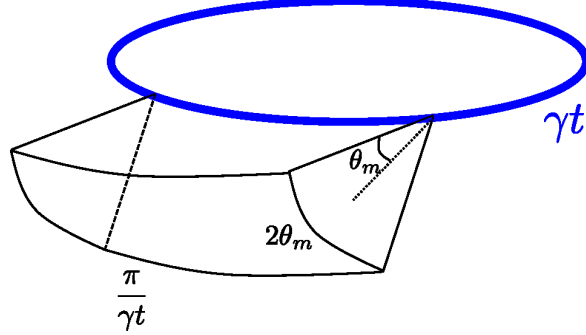


Fig. 7.1.3 The radiation cone of the GW from a kink (black solid angle).

$$n_k(f, z) = \frac{1}{f} \frac{\theta_m}{2} \frac{z}{1+z} \frac{1}{\gamma t} \frac{\psi_{\max} N(\psi_{\max}, t)}{V} \frac{dV(z)}{dz}. \quad (7.1.24)$$

Using Eqs.(7.1.22), (8.1.3) and (7.1.14), we can find  $\Omega_{\text{GW}}(f)$  has the dependence of  $\psi_{\max}\gamma^{-8/3}$ . Therefore, the power spectrum becomes stronger with shorter correlation length.

## 7.2 Result

### 7.2.1 Case of infinite cosmic string

Using the kinks distribution function, we numerically calculate the power spectrum of the GW background from propagating kinks on infinite strings by solving Eqs.(7.1.17), (7.1.22), (8.1.3) and (7.1.14) simultaneously. The result is in Fig.7.2.1. From Eq.(7.1.14) and the distribution function of kinks, the numerous kinks with small sharpness contribute to the high-frequency GW background, which are made during the RD era. The power spectrum is simply written as  $\Omega_{\text{GW}} \propto \int dV \frac{\psi_{\max} N(\psi_{\max}, t)}{V/(\gamma t)^2}$ . In other words, if there are many kinks in the horizon, the power spectrum is strong. Because there are a lot of kinks with small sharpness contributing to the high-frequency GW background in the horizon, the power spectrum becomes strong at the high frequency.

### 7.2.2 Case of infinite cosmic superstring

Next, we calculate the power spectrum of the GW background from propagating kinks on infinite superstrings. The results are shown in Fig. 7.2.2. The left panels of Fig. 7.2.2 are calculated assuming  $p_1 = p_2 = p_3 = 1$  for different string types 1, 2, and 3. The right panels show the results for different reconnection probabilities. From the top to the bottom, we show Case A, B, and C.

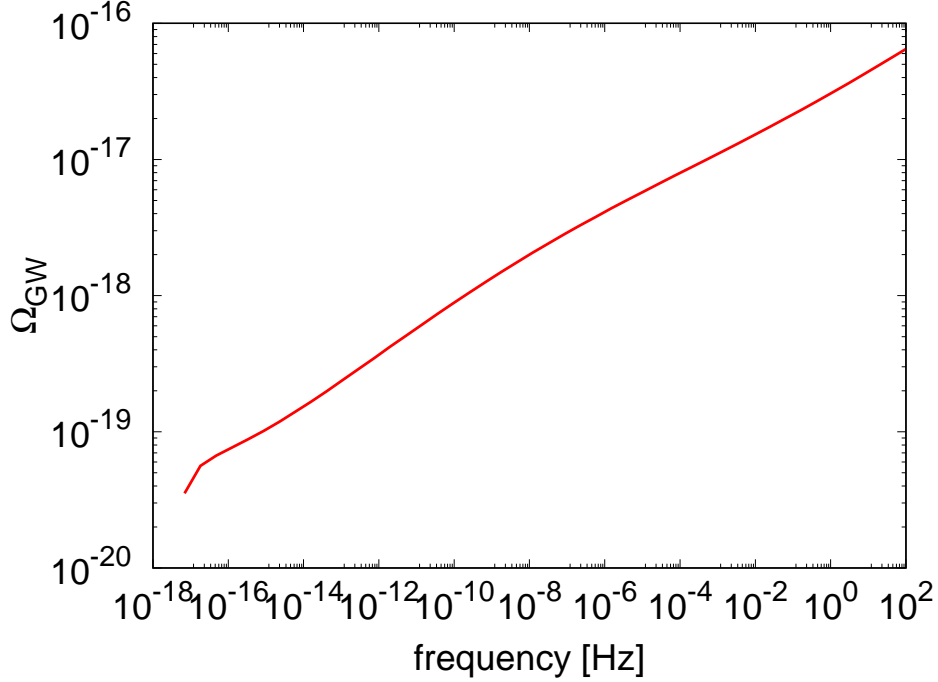


Fig. 7.2.1 The power spectra of the GW background from propagating kinks on the infinite cosmic string for  $G\mu = 10^{-11}$ . The vertical axis is the spectral amplitude of the GW background  $\Omega_{\text{GW}}$  and the horizontal axis is the frequency.

### 7.2.3 Case A: GW background with $\mu_1 : \mu_2 : \mu_3 = 1 : 1 : 1$ and $n_p = 1$

Let us first see the left panel, which is helpful to see the pure effect of Y-junctions. We see the power spectrum of ordinary cosmic strings, which is shown for comparison, increases gradually towards high frequencies. The GW background is mainly formed by GWs emitted from kinks existing today and today's kink distribution determines the spectral shape. For detailed explanations, see [59]. On the other hand, in Case A, we see the spectra of cosmic superstrings are constant at high frequency and the amplitude is lower than the cosmic string case. The differences arise because the dominant contribution to the GW amplitude comes from GWs emitted from kinks in the old-time just after formation when they are  $\psi \sim 1$ . As we have seen in the previous section, sharp kinks are smoothed out rapidly because of Y-junctions, and since the GW strain amplitude depends on  $\propto \psi^{1/2}$ , kinks today with very small sharpness no longer contribute to the GW background.

Since kinks are formed by collisions of infinite strings, when a new kink with  $\psi \sim 1$  is formed, the GWs emitted soon after the kink formation have a wavelength of  $\sim \gamma t$  and thus we have the relation of  $(1+z)f\gamma t \sim 1$ . From this, we see that higher frequency GWs are produced by kinks in earlier times of the Universe. Since a number of infinite strings in the Hubble horizon are always the same because of the scaling law, the number of newly formed kinks inside the horizon is also the same. This means that, if we only consider GWs emitted from new kinks, the energy ratio  $\rho_{\text{GW}}/\rho_c$  is constant in time, which is the reason for the flat

shape of the spectrum.

The flat spectrum can be also explained by using equations. Let us describe the steepness of kink distribution is given by the power-law as  $\propto \psi^{-l}$ . In [58], it has been shown that the kink number decreases as  $\propto t^{-1}$  in the RD era. Thus we can write the number distribution in the RD era as  $\psi \frac{N(\psi, t)}{V(t)/(\gamma t)^2} \propto \psi^{-l} t^{-1}$ . Substituting this into Eq. (7.1.14), we find  $\psi_{\max}$  can be described as

$$\psi_{\max} \propto [(1+z)ft]^{-1/l}. \quad (7.2.1)$$

Considering that the GW mode contributing to the background amplitude satisfies  $(1+z)f\gamma t \sim 1$  and  $\gamma$  is constant because of the scaling law, we find  $\psi_{\max}$  is determined independently of the frequency and time. Using Eq. (7.1.14) and  $\psi_{\max} = \text{const.}$ , we find  $\Omega_{\text{GW}} \propto f^0$ . The flat spectrum is produced by GWs from the RD era while the increase of GW amplitude at low frequencies corresponds to GWs generated in the MD era.

The right panel of the figure shows the effect of reconnection probability. We find that the power spectrum becomes smaller for smaller reconnection probability. This can be explained by the balance between the correlation length and  $\psi_{\max}$ . As one can see from Eq. (7.2.1), when the slope of the kink distribution is flattened and  $l$  is small, the value of  $\psi_{\max}$  becomes very small. This means that kinks contributing to the GW background have very small sharpness, and since  $\Omega_{\text{GW}}$  has the dependence of  $h^2 \propto \psi_{\max}$ , the amplitude of GWs drops. As shown in Fig. 6.3.4, the slope of the distribution function get gentler for smaller reconnection probability in Case A, which leads to smaller GW amplitude. At the same time, the power spectrum has the dependence of  $\gamma^{-8/3}$  and smaller reconnection probability decreases the value of  $\gamma$ , but the effect of  $\psi_{\max}$  dominates in Case A.

In the figure, we find that the low-frequency cutoff moves towards high frequency. This is because of the cutoff  $\Theta(1-\theta_m)$ , which prohibits the emission of GWs with a wavelength longer than the curvature radius of strings. Small reconnection probability makes the correlation length short and curvature of strings small so that we do not find GWs at low frequency.

#### 7.2.4 Case B: GW background with $\mu_1 : \mu_2 : \mu_3 = 1 : 1 : 1$ and $n_p = \frac{1}{3}$

In Case B, the power spectrum looks similar to Case A and the reasons are the same as explained for Case A. In the right panel, we find that the GW amplitude decreases more for small reconnection probability compared to Case A. This is because, loop production is more efficient in the case of  $n_p = \frac{1}{3}$ , and the decrease of correlation length  $\gamma$  is milder compared to Case A as shown in the right panels of Fig. 5.2.2. Since the value of  $\gamma$  does not decrease, a more prominent effect of  $\psi_{\max}$  is seen, which turns into a smaller amplitude of the GW background.

#### 7.2.5 Case C: GW background with $\mu_1 : \mu_2 : \mu_3 = 1 : 10 : 10$ and $n_p = \frac{1}{3}$

In the left panel of Case C, the shape of the power spectrum looks similar to the ordinary cosmic strings. This because the effect of Y-junction to smooth out the sharpness is gentler in Case C, and the dominant contribution to the GW power is made by kinks existing today.

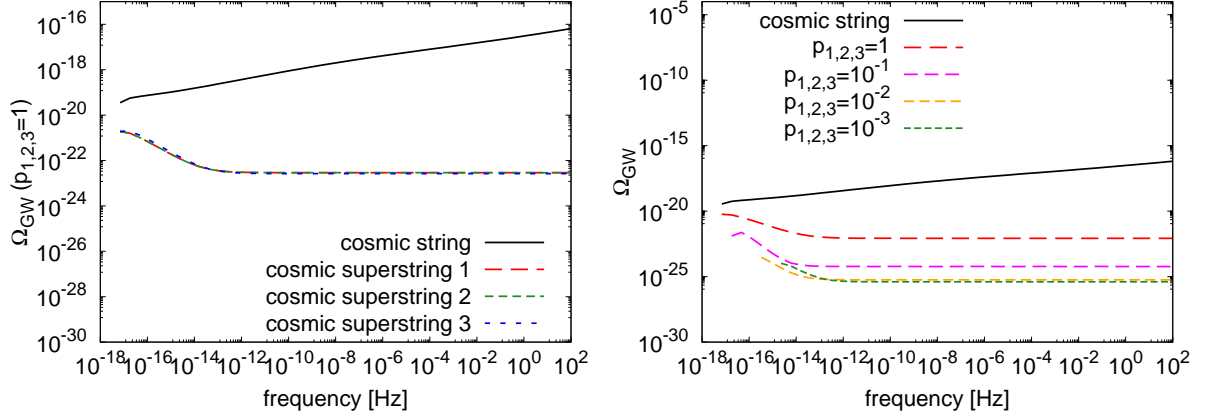
We find that strings 2 and 3 generate the larger GW amplitude than string 1 since they have larger string tension and the power spectrum has the dependence of  $\propto (G\mu)^2$ . We also find string 3 has a slightly larger amplitude compared to string 2 because the correlation length of string 3 is smaller than the others and the power spectrum has the dependence of  $\propto \gamma^{-8/3}$ .

In the right panel, we find the cases where the power spectrum is slightly larger than the ordinary cosmic string case. This is because the slope of the kink distribution is not entirely flattened compared to Cases A and B as shown in Fig. 6.3.4 and the value of  $\psi_{\max}$  is relatively large. We find that the effect of small correlation length dominates the effect of small  $\psi_{\max}$  in case of  $p = 10^{-1}$  and  $10^{-2}$ , while the kink distribution becomes too gentle when  $p = 10^{-3}$  and the latter effect dominates the former.

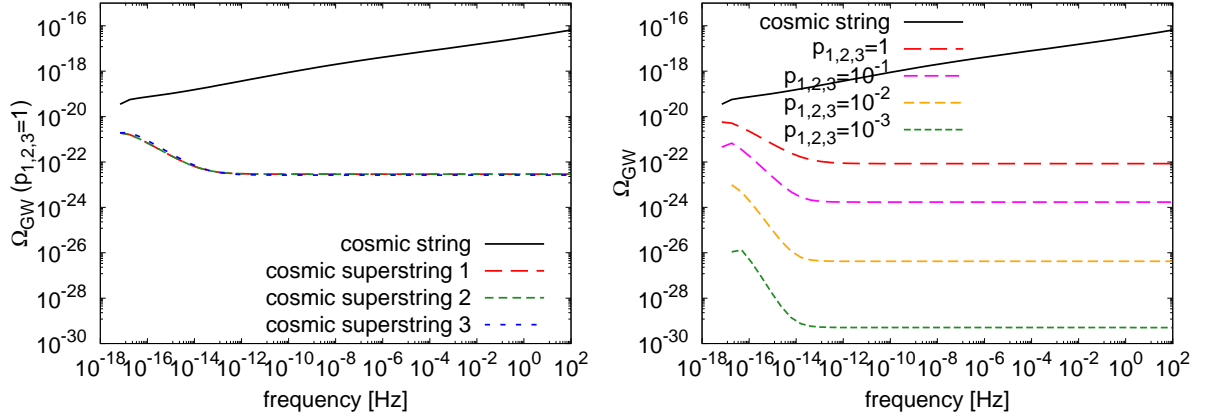
### 7.3 Summary

Using the kink distribution function, we investigate the power spectrum of the GW background from propagating kinks on infinite cosmic strings and superstrings. The sharpness of kinks contributing to the GW background mainly corresponds to the one frequency of the GW background. When the distribution function of kinks is flatter, the sharpness contributing to the GW background becomes smaller. Then, in the case of 1 : 1 : 1, the GW amplitude becomes smaller with smaller reconnection probability. In the case of 1 : 10 : 10, when the reconnection probability is relatively large, the kink distribution is steeper. In this case, the GW amplitude from infinite cosmic superstrings is enhanced and is larger than the one from infinite cosmic strings.

Case A:  $\mu_1 : \mu_2 : \mu_3 = 1 : 1 : 1$ ,  $n_p = 1$ ,  $G\mu_1 = G\mu_2 = G\mu_3 = 10^{-11}$



Case B:  $\mu_1 : \mu_2 : \mu_3 = 1 : 1 : 1$ ,  $n_p = \frac{1}{3}$ ,  $G\mu_1 = G\mu_2 = G\mu_3 = 10^{-11}$



Case C:  $\mu_1 : \mu_2 : \mu_3 = 1 : 10 : 10$ ,  $n_p = \frac{1}{3}$ ,  $G\mu_1 = 10^{-12}$ ,  $G\mu_2 = G\mu_3 = 10^{-11}$

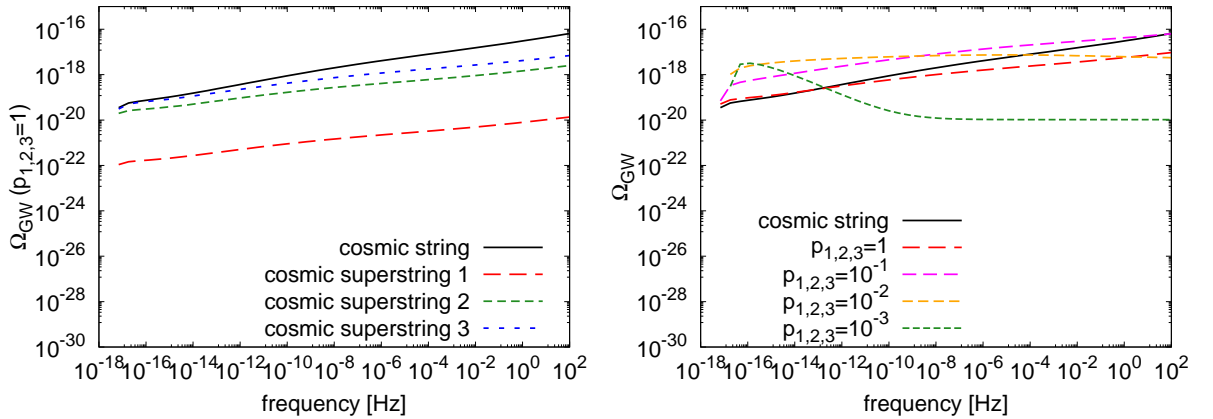


Fig. 7.2.2 The power spectrum of the GW background from propagating kinks on infinite cosmic superstrings. The vertical axis is the spectral amplitude of the GW background  $\Omega_{\text{GW}}$  and the horizontal axis is the frequency. Left panels show the case of  $p_1 = p_2 = p_3 = 1$  for different string types. The red, green and blue broken lines represent string types 1, 2, and 3, respectively. The right panels are the power spectrum of the GW background for different reconnection probabilities. The red, magenta, orange and green broken lines represent  $p = 1, 10^{-1}, 10^{-2}$  and  $10^{-3}$ , respectively. In all panels, for comparison, we plot the case of ordinary cosmic strings with the black solid line ( $G\mu = 10^{-11}$ ).

## 8 Gravitational wave background from kink-kink collisions

Although the power spectrum of the GW from kink-kink collisions is formulated and calculated [41] in the previous work, the evolution of the kink distribution function is not considered. Since the number and sharpness of kinks contributing to the GW background changes with time, we should also consider the evolution of the distribution function of kinks in order to estimate the power spectrum of the GW background from kink-kink collisions more precisely. In this section, similar to the previous section, we formulate the power spectrum of the GW background from kink-kink collisions and calculate numerically. Furthermore, we consider the effect of the GW emission, which is energy loss by the strong GW emission, and estimate the distribution function of the kinks and the power spectrum.

### 8.1 Formulation

Similar to the previous section, first, we describe the strain amplitude of GWs from kink-kink collisions. In Ref.[118], if there are discontinuities on the phase of the energy-momentum tensor, expressed as  $\mathbf{a}'(u_*)$  and  $\mathbf{b}'(v_*)$ , the energy-momentum tensor is described as

$$\begin{aligned}
 T^{\mu\nu}(\omega, \omega \mathbf{n}) \simeq & -\frac{\mu}{\omega^2} \left( \frac{a_+^{\mu'}}{1 + \mathbf{n} \cdot \mathbf{a}'_+} - \frac{a_-^{\mu'}}{1 + \mathbf{n} \cdot \mathbf{a}'_-} \right) \\
 & \times \left( \frac{b_+^{\nu'}}{1 - \mathbf{n} \cdot \mathbf{b}'_+} - \frac{b_-^{\nu'}}{1 - \mathbf{n} \cdot \mathbf{b}'_-} \right) e^{\frac{i\omega}{2} \{v_* - u_* - \mathbf{n} \cdot (\mathbf{a}(u_*) + \mathbf{b}(v_*))\}} \\
 & + (\mu \leftrightarrow \nu), \tag{8.1.1}
 \end{aligned}$$

where  $\mathbf{a}_\pm^{\mu'} \equiv \mathbf{a}'(u_*)$  and  $\mathbf{b}_\pm^{\mu'} \equiv \mathbf{b}'(v_*)$  in the same way as the previous section. We assume that the sharpness of two colliding kinks contributing to the GW background is the same, namely we assume  $1 - \mathbf{a}'_+ \cdot \mathbf{a}'_- = 1 - \mathbf{b}'_+ \cdot \mathbf{b}'_- = 2\psi$ . Using Eqs.(7.1.19) and (7.1.19) and  $|b_+^{\nu'}|^2 \sim |b_-^{\nu'}|^2 \sim 1$ , we express the strain amplitude of a kink-kink collision as

$$h_{\text{kk}}(f, z) = \frac{\psi_{\text{max}} G \mu}{(1+z)f} \frac{1}{r(z)} \Theta(1 - \theta_m). \tag{8.1.2}$$

Comparing with Eq.(7.1.22), the strain amplitude of the GW, in this case, depends on  $\psi_{\text{max}}$  strongly.

Next, let us describe the rate of GW. For kink-kink collisions, the number of kinks coming into one kink per time is given by  $\frac{\psi_{\text{max}} N(\psi_{\text{max}}, t)}{V/(\gamma t)^2}$ . By multiplying  $\frac{1}{2}$  to avoid double counting and taking into account the redshift, the rate of GW bursts per kink is given by  $\frac{(\gamma t)^2}{2(1+z)} \frac{\psi_{\text{max}} N(\psi_{\text{max}}, t)}{V}$ . Note that a kink-kink collision emits GWs in all directions so that we do not multiply a

beaming angle. Then, the rate of the GW is represented as

$$n_{\text{kk}}(, f, z) = \frac{1}{f} \frac{(\gamma t)^2}{2(1+z)} \left\{ \frac{\psi_{\text{max}} N(\psi_{\text{max}}, t)}{V} \right\}^2 \frac{dV(z)}{d \ln z}. \quad (8.1.3)$$

Unlike the rate of GWs from propagating kinks, it depends on the square of the kinks number. It is an important point to understand how the rate of GWs contributes to the GW background. By substituting Eqs. (8.1.2) and (8.1.3) into Eq. (7.1.17), we obtain the GW background spectrum for kink-kink collisions. Using (7.1.14), we can estimate that  $\Omega_{\text{GW}}(f)$  is proportional to  $\gamma^{-2} \psi_{\text{max}}^2$ . Therefore, the power spectrum becomes stronger with shorter correlation length and sharper kinks satisfy Eq.(7.1.14).

## 8.2 Result

We calculate the power spectrum of the GW background from kink-kink collisions on infinite cosmic strings by solving the VOS equation Eqs.(5.1.6) and (5.1.7) and the condition of sharpness most contributing the GW background Eq.(7.1.14) simultaneously. In Fig. 8.2.1, we compare the power spectrum of the GW background from propagating kinks and kink-kink collisions.

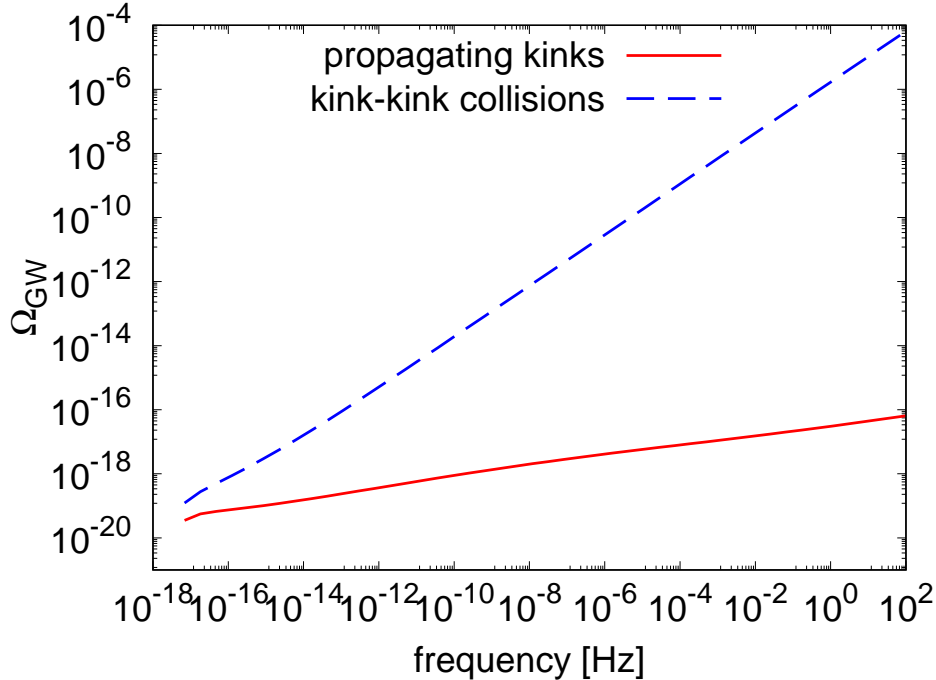


Fig. 8.2.1 The power spectrum of the GW background from propagating kinks (red solid) and kink-kink collisions (blue dashed) on the infinite cosmic strings. For both lines, we assume  $G\mu = 10^{-11}$ .

With the fact that  $\psi \frac{N(\psi, t)}{V(t)/(\gamma t)^2}$  is a decreasing function of  $\psi$ , Eq. (7.1.14) indicates that the high frequency GWs are produced by kinks with small sharpness, which has high event rate.

The large amplitude difference at high-frequencies between the two cases arises because the event rate of kink-kink collisions increases in proportion to the square of the kink number, while the dependence is linear in the case of propagating kinks. From Fig. 8.2.1, the GW spectrum from kink-kink collisions scales as  $\Omega_{\text{GW}} \propto f^{0.77}$ . This dependence is explained as follows. Substituting Eqs. (8.1.2) and (8.1.3) into Eq. (7.1.17), replacing the number of kinks with  $f$  using Eq. (7.1.14), and leaving only the frequency and the time dependence, we obtain

$$\Omega_{\text{GW}} \propto \int d(\ln t) \frac{\psi_{\text{max}}^2}{t(1+z)^3} f. \quad (8.2.1)$$

In our numerical calculation without GW backreaction, we find that the contribution to the integration of  $\Omega_{\text{GW}}$  gets larger as the time increases for all the frequencies. Thus, the shape of the GW spectrum is determined by the kink distribution today. From Fig. 6.2.1, we find  $\psi \frac{N(\psi, t)}{V(t)/(\gamma t)^2} \propto \psi^{-8.8}$ , and we get  $\psi_{\text{max}} \propto f^{-1/8.8}$  using Eq. (7.1.14). Substituting this into Eq. (8.2.1), we get  $\Omega_{\text{GW}} \propto f^{0.77}$ . This frequency dependence continues until the frequency where the oldest kinks, having the smallest sharpness, can generate GWs. Higher frequency GWs are generated by kinks with smaller sharpness and the amplitude of the GW background starts to decrease at the frequency corresponding to the smallest kinks. This frequency is determined by the time of the cosmic string generation, which strongly depends on the generation model. Thus, in this paper, we do not discuss the high-frequency behavior around the cutoff frequency.

One may find the overproduction of GWs at high frequencies violating the constraint by the Big Bang nucleosynthesis or the cosmic microwave background,  $\Omega_{\text{GW}} \lesssim 2 \times 10^{-6}$  [119]. However, this is not the final result and, in fact, it will be solved in the next subsection.

### 8.3 GW emission effect

As shown in the previous subsection, the power spectrum increases dramatically towards high frequencies in the case of kink-kink collisions. One may be concerned that a large amount of GW emissions could change the number of infinite strings since the energy of the string network is transferred to GWs. In addition, the backreaction of GW emission could smooth out the sharpness of kinks and reduce the power of GW emission. In this section, we take into account these two effects by modifying the VOS equation, Eq. (5.1.6), and the evolution equation of kink distribution, Eq. (6.2.24), and recalculate the GW power spectrum.

Let us first consider the effect of GW radiation on the VOS equation [117, 120]. The energy of GW emission from one kink-kink collision is estimated as  $E_{\text{GW}} \sim 2\pi^3 \psi^2 G\mu^2 \omega^{-1}$  [118]. Here, the factor  $2\pi^3$  is put to make  $E_{\text{GW}}$  consistent with the expression of  $\Omega_{\text{GW}}$ , in other words, with the choice of the factor in front of  $h_{\text{kk}}$  in Eq. (8.1.2). Considering the energy conservation law for the string network density  $\rho_\infty = \frac{\mu}{L^2}$  [113], the loss of energy density into

GW radiation is given by

$$\begin{aligned}\frac{d\rho_\infty}{dt} &= - \int_0^1 d\psi_{\max} E_{\text{GW}} \times (\# \text{ of GWs per unit volume, time, } d\psi_{\max}), \\ &= - \int_0^1 d\psi_{\max} 2\pi^3 \psi_{\max}^2 G\mu^2 \omega^{-1} \frac{\psi_{\max}}{2} \left\{ \frac{N(\psi_{\max}, t)}{V/(\gamma t)^2} \right\}^2 \frac{1}{(\gamma t)^2}.\end{aligned}\quad (8.3.1)$$

Here, the integral in terms of  $d\psi_{\max}$  corresponds to taking into account GWs of all the frequencies. By rewriting  $\rho_\infty$  in terms of  $L$  and adding it to Eq. (5.1.6), we get

$$\frac{dL}{dt} = HL(1+v^2) + \frac{1}{2}cpv + \frac{\pi^3 G\mu}{2} \gamma t \int_0^1 d\psi_{\max} \frac{N(\psi_{\max}, t)}{V/(\gamma t)^2} \psi_{\max}^2, \quad (8.3.2)$$

where we have used Eq. (7.1.14) to replace  $\omega = 2\pi f(1+z)$ .

Next, we consider the GW backreaction on kinks and estimate the effect on the kink distribution. Before presenting the equations, let us compare the energy of one kink and GW energy at one collision. When we treat a kink as a small perturbation  $\delta\mathbf{p}_\pm$  [121, 109], the energy of kink is estimated as  $E_{\text{kink}} = \mu(\delta\mathbf{p}_\pm)^2 \Delta\ell \sim \mu\psi\Delta\ell$  for a given length  $\Delta\ell$ , where we have used Eq. (6.1.1) in the second step. From Eq. (7.1.14), we expect that kinks contributing to the GW background distribute with the average interval of  $\omega^{-1}$ , so let us take  $\Delta\ell \sim \omega^{-1}$ . By taking the ratio  $E_{\text{GW}}/E_{\text{kink}} = 2\pi^3\psi G\mu$ , we find that the fraction of energy going to GW emission is initially as small as  $\sim G\mu$  for newly formed kinks  $\psi \sim 1$ , and the fraction gets even smaller when the kink sharpness becomes smaller by the expansion of the Universe. Thus, when we consider the GW energy at one collision, the GW backreaction seems to be negligible.

However, the accumulation of small GW backreaction through a huge number of collisions could change the kink distribution. This can be implemented as a modification of Eq. (6.2.24). By considering the energy fraction going to GWs, the backreaction term can be written as

$$\begin{aligned}& (\# \text{ of kinks lost by GW emission per } V, \text{ time, } d\psi_m) \\ & \sim \frac{E_{\text{GW}} \times (\# \text{ of GWs per } V, \text{ time, } d\psi_m)}{E_{\text{kink}} \times (\# \text{ of kinks per } V)} \times (\# \text{ of kinks per } V) \\ & \sim (2\pi^3\psi G\mu) \frac{\frac{1}{2}\psi \left\{ \frac{N(\psi)}{V/(\gamma t)^2} \right\}^2 \frac{V}{(\gamma t)^2}}{N(\psi, t)} N(\psi, t).\end{aligned}\quad (8.3.3)$$

By adding this term, Eq. (6.2.24) becomes

$$\frac{\partial N}{\partial t}(\psi, t) = \frac{\bar{\Delta}V}{\gamma^4 t^4} g(\psi) + \frac{2\zeta}{t} \frac{\partial}{\partial \psi} (\psi N(\psi, t)) - \frac{\eta}{\gamma t} N(\psi, t) - \frac{\pi^3 G\mu \psi^2 (\gamma t)^2}{V} N^2(\psi, t). \quad (8.3.4)$$

## 8.3.1 Case of infinite cosmic string

In Fig. 8.3.1 and 8.3.2, we show the time evolution of  $\gamma$  and the kink distribution, respectively, calculated by simultaneously solving the VOS equations with GW radiation, Eqs. (8.3.2) and (5.1.7), and the equation for kink distribution with GW backreaction, Eq. (8.3.4). From Fig. 8.3.1, we see that the correlation length does not change at first, but starts to increase when the GW radiation term becomes non-negligible compared to the Hubble term.

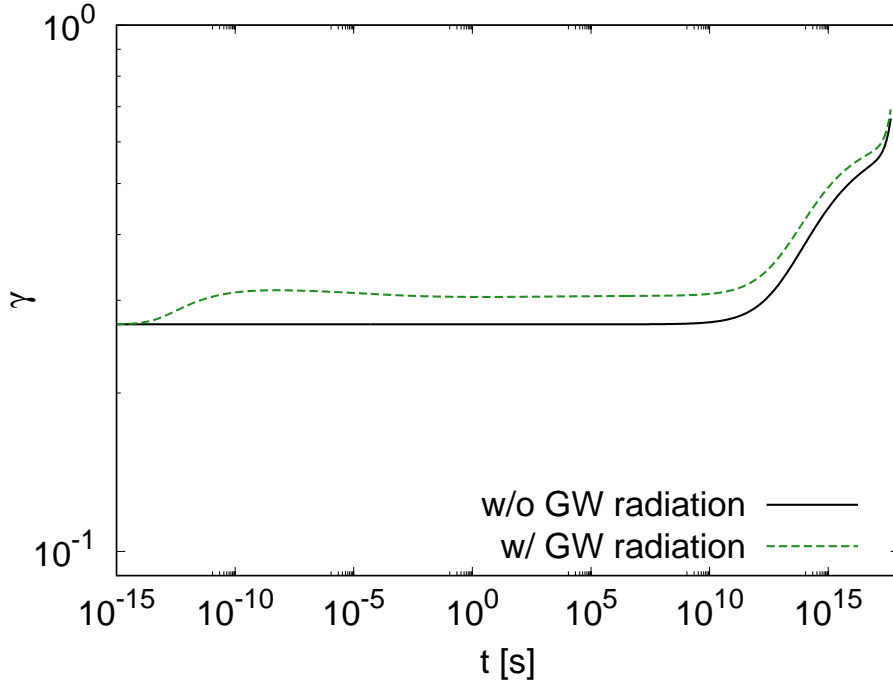


Fig. 8.3.1 The time evolution of  $\gamma$  calculated using Eqs. (8.3.2) and (8.3.4) for  $10^{-11}$ . For comparison, we also show the line calculated without the GW radiation term.

In Fig. 8.3.2, we find that the number of kinks with small sharpness is suppressed, since the backreaction term in Eq. (8.3.4) affects the distribution when  $N$  is large as it has the  $\propto N^2$  dependence. We also see that the effect extends to larger sharpness when  $G\mu$  is larger. The slope of the distribution function gets gentler for large  $G\mu$  because the value of  $\gamma$  is larger due to the modification in Eq. (8.3.2).

Fig.8.3.3 shows the power spectra of the GW background from kink-kink collisions with the effect of the GW emission. We see that high-frequency GWs get suppressed when we use the kink distribution with the GW modification. This is mainly because the number of small kinks is suppressed by the GW backreaction term in Eq. (8.3.4). We find that the suppression takes place at late times and it comes earlier for smaller sharpness, which corresponds to high-frequency GWs. As a result, GWs of the high-frequency plateau is dominantly produced kink-kink collisions in the RD era, while ones in the small bump are produced in the MD era and ones in the low-frequency slope are generated today without being affected by the

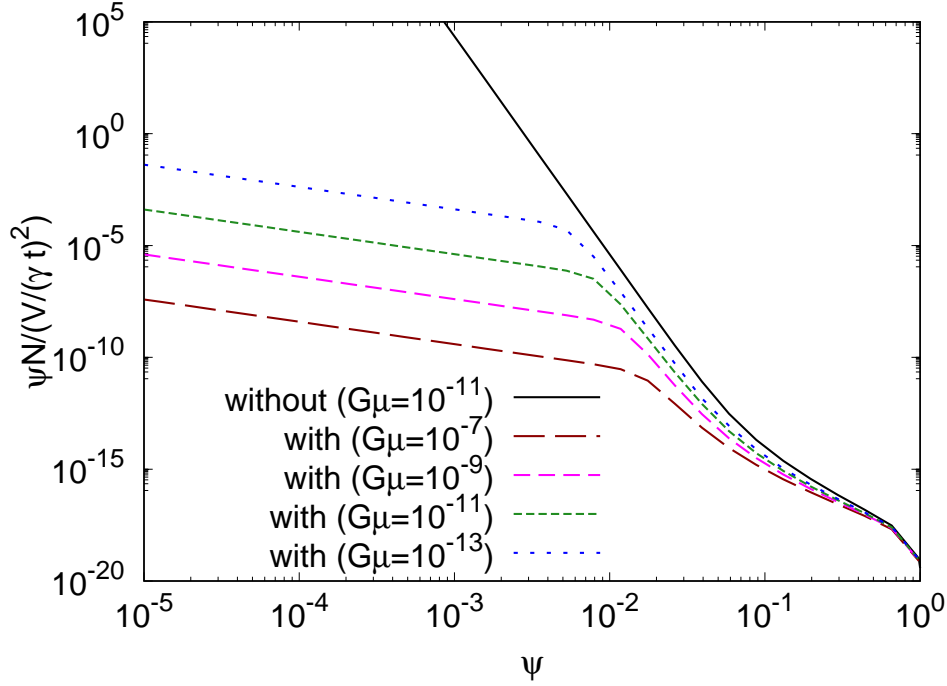


Fig. 8.3.2 The distribution function of kinks on the infinite cosmic strings, calculated using Eqs. (8.3.2) and (8.3.4) (colored broken lines). The number of kinks per unit length per logarithmic sharpness is shown as a function of sharpness. Each line represents different tension, from  $G\mu = 10^{-7}$  to  $10^{-13}$ . For comparison, we also show the line calculated using Eqs. (5.1.6) and (6.2.24) (black solid line).

suppression.

Let us explain the flat spectrum in detail with some equations. The GW backreaction starts to affect kinks with small sharpness first, and the effect gradually extends to larger sharpness. Let us define the transition sharpness as  $\psi_{\max, \text{cut}}(t)$ , below which kinks are affected by the GW backreaction at time  $t$ . In the numerical calculation, we find that the contribution to the integration of  $\Omega_{\text{GW}}$  peaks when the backreaction starts to affect, namely when  $\psi_{\max}(t) = \psi_{\max, \text{cut}}(t)$ . So let us evaluate Eq. (8.2.1) at the time  $t_c$  which satisfies  $\psi_{\max}(t_c) = \psi_{\max, \text{cut}}(t_c)$ . Here we focus on the radiation-dominated era since  $t_c$  is typically before the radiation-matter equality for high-frequency GWs. Using  $t \propto \frac{1}{(1+z)^2}$  and taking out only the contribution at  $t_c$ , Eq. (8.2.1) becomes

$$\Omega_{\text{GW}} \propto \frac{\psi_{\max, \text{cut}}^2(t_c)}{1+z_c} f. \quad (8.3.5)$$

Here,  $z_c$  is the redshift at  $t = t_c$ , which depends on the frequency of interest  $f$ . Let us first see the time dependence of  $\psi_{\text{m, cut}}$ . The GW backreaction starts to affect when the fourth term becomes larger than the second and third terms in Eq. (8.3.4). Thus we have

$$\left(\frac{\eta}{\gamma} - 2\zeta\right) \frac{N}{t_c} = \pi^3 G\mu \psi_{\max, \text{cut}} \left\{ \psi_{\max, \text{cut}} \frac{N}{V / (\gamma t_c)^2} \right\} N. \quad (8.3.6)$$

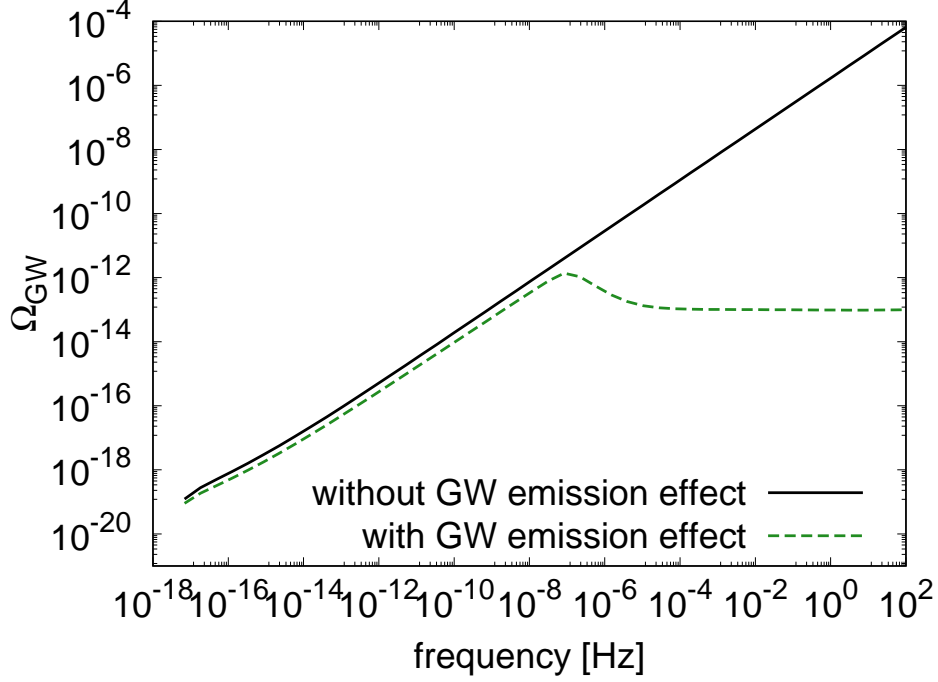


Fig. 8.3.3 The power spectra of the GW background from kink-kink collisions on the infinite cosmic strings with the GW emission effect (green broken line). For comparison, we also show the power spectrum without the effect. For both lines, we assume  $G\mu = 10^{-11}$ .

At early times, the backreaction term is negligible and the kink number evolves as  $\psi \frac{N(\psi)}{V/(\gamma t)^2} \propto t^{-1}$ , which is the analytic solution of Eq. (6.2.24) detailed in [63]. By substituting this, we find that  $\psi_{\max, \text{cut}}$  does not depend on time in the radiation-dominated era. The relation between  $z_c$  and  $f$  can be obtained using Eq. (7.1.14) as  $2\pi f = \psi \frac{N(\psi, t)}{V(t)/(\gamma t)^2} \frac{1}{1+z} \propto (1+z)$ . Applying this relation to Eq. (8.3.5), we get  $\Omega_{\text{GW}} \propto f^0$ .

Next, let us see how the energy of the GW is balanced in the string network. We define the energy density parameter of kinks as

$$\begin{aligned} \Omega_{\text{kink}}(t, \psi_{\max}) &= \frac{E_{\text{kink}} \times (\# \text{ of kinks per unit volume})}{\rho_c} \\ &\sim \frac{\mu \psi_{\max} \omega^{-1} \cdot \psi_{\max} \frac{N}{V/(\gamma t)^2} / (\gamma t)^2}{3H^2 / (8\pi G)} \end{aligned} \quad (8.3.7)$$

$$\sim \frac{8\pi G\mu}{3\gamma^2 t^2 H^2} \psi_{\max}. \quad (8.3.8)$$

In the second step, we have used the relation of Eq. (7.1.14). Note that this can be written as  $\Omega_{\text{kink}} = \psi_m \Omega_{\text{infinite}}$ , where  $\Omega_{\text{infinite}} \equiv \frac{\rho_\infty}{\rho_c}$ . This indicates that the kink energy is always smaller than the total energy density of infinite strings by the order of the sharpness  $\psi_{\max}$ . In Fig. 8.3.4, we plot the time evolution of the infinite string energy density, the kink energy density, and the GW energy density produced at time  $t$  (integrand of Eq. (7.1.17) before redshifting).

Two panels show different GW frequencies  $f = 10^{-2}\text{Hz}$  and  $10^2\text{Hz}$ , which correspond to different values of  $\psi_{\text{max}}$ . As one can see, the energy of GWs increases at the beginning, and when it becomes comparable to the kink energy, both kink and GW energies start to decrease and evolve along with each other. This behavior happens exactly because the GW energy is balanced by the kink energy thanks to the GW terms added to the VOS equation, Eq. (8.3.2), and to the evolution equation for kink number density, Eq. (8.3.4). In summary, one can find that the kink and GW energies become the same order when the GW terms turn on, and they always stay below the total energy of the scaling string network by the order of  $\psi_{\text{max}}$ .

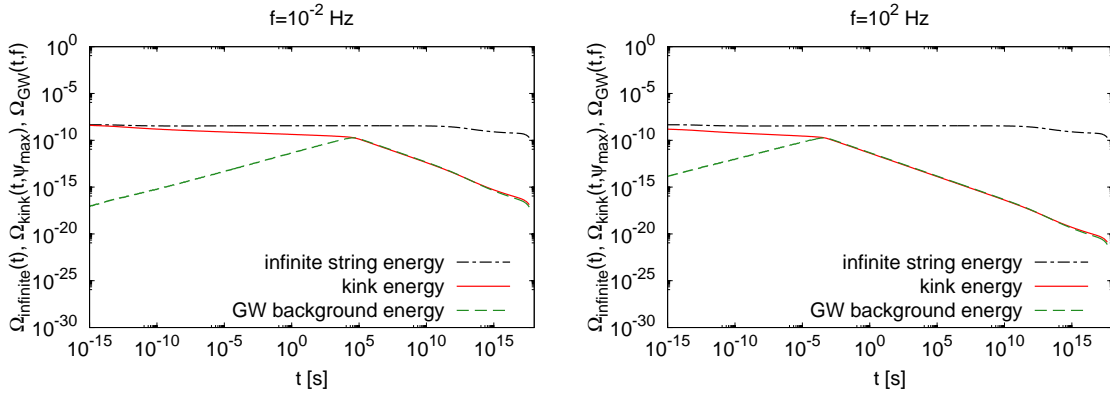


Fig. 8.3.4 The time evolution of the infinite string energy density, the kink energy density and the GW energy density produced at time  $t$ . The left panel is for kinks contributing to GW frequency  $f = 10^{-2}\text{Hz}$  and the right panel is for  $10^2\text{Hz}$ .

In Fig. 8.3.5, we plot the power spectra of the GW background from kink-kink collisions for different  $G\mu$ . We compare the spectra with sensitivity curves of various future GW experiments, such as SKA, LISA, DECIGO, and Advanced-LIGO in Fig.8.3.5. We also plot the current upper limit on the GW background amplitude by first observing run of Advanced-LIGO,  $\Omega_{\text{GW}} < 1.7 \times 10^{-7}$  at  $20 - 86 \text{ Hz}$  [122], and 11-year dataset of NANOGrav,  $\Omega_{\text{GW}} h^2 < 3.4 \times 10^{-10}$  at  $3.2 \times 10^{-8} \text{ Hz}$  [123]. We find that the current Advanced-LIGO upper limit gives the constraint on the string tension as  $G\mu \lesssim 10^{-5}$ , and the NANOGrav constraint gives  $G\mu \lesssim 4 \times 10^{-8}$ . In the future, Advanced-LIGO with full design sensitivity would provide  $G\mu \lesssim 10^{-7}$ , and pulsar timing with SKA would reach  $G\mu \sim 10^{-11}$ . With satellite experiments, we would be able to reach  $G\mu \sim 10^{-11}$  by LISA and  $G\mu \sim 10^{-13}$  by DECIGO. If cosmic strings are generated at the phase transition, the tension is expressed  $\mu \sim M_{\text{PT}}^2$  where  $M_{\text{PT}}$  denotes the energy of the phase transition. Thus,  $G\mu \sim \frac{M_{\text{PT}}^2}{M_{\text{Pl}}^2}$  where  $M_{\text{Pl}}$  means the Planck mass. Using the constraints  $G\mu \lesssim 10^{-5}$  and  $G\mu \lesssim 4 \times 10^{-8}$  from the current observation, we get  $M_{\text{PT}} \lesssim 3.2 \times 10^{16} \text{ GeV}$  and  $M_{\text{PT}} \lesssim 2 \times 10^{15} \text{ GeV}$ . If cosmic strings are formed at the end of the inflation, using its energy scale  $M_{\text{inflation end}}$ , we can express the tension  $\mu \sim M_{\text{inflation end}}^2$ . From this, we can provide a constraint on the energy scale of the inflation end.

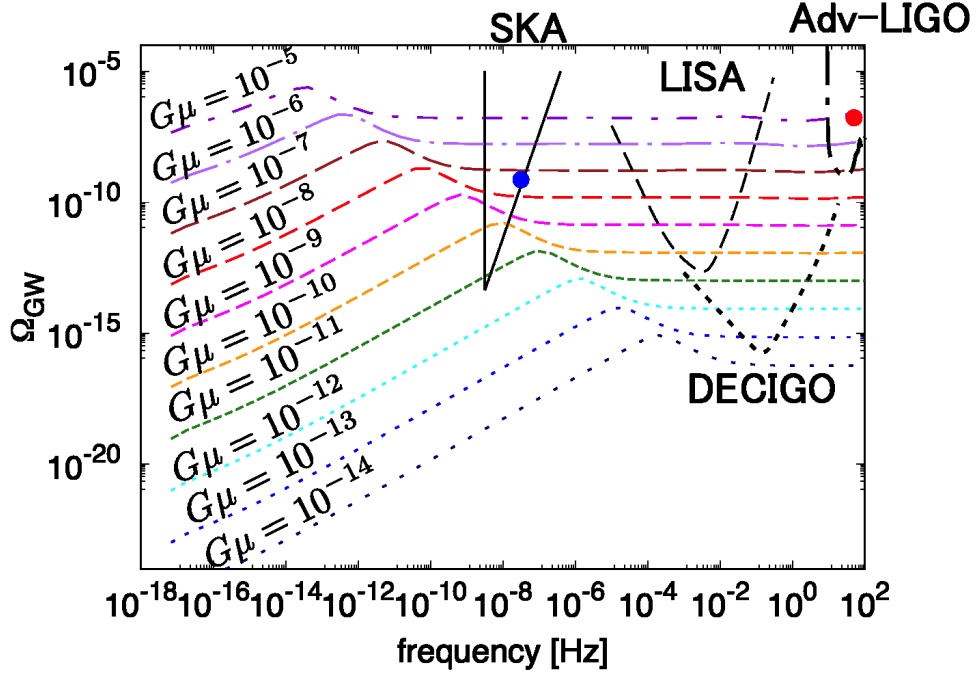


Fig. 8.3.5 The power spectra of the GW background from kink-kink collisions on infinite cosmic strings for different string tension, from  $G\mu = 10^{-5}$  to  $10^{-14}$ . We also show the sensitivities of the future observational instruments: SKA, LISA, DECIGO, and Advanced-LIGO. The red and blue circles represent the current upper limit on GW amplitude by Advanced-LIGO and NANOGrav.

### 8.3.2 Case of infinite cosmic superstring

We numerically calculate the power spectrum using Eqs. (8.1.2) and (8.1.3) by taking account of the backreaction effect of GW emission using Eqs. (8.3.2) and (8.3.4). In Fig. 8.3.6, we show the kink distribution on the left panels. The settings are the same as the right panels of Fig. 6.3.4 except here we include the backreaction effects of the GW emission by kink-kink collisions. The right panels show the power spectrum of the GW background from kink-kink collisions.

### 8.3.3 Case A: GW background with $\mu_1 : \mu_2 : \mu_3 = 1 : 1 : 1$ and $n_p = 1$

Let us first see the kink distribution function, shown in the left panel. Compared to Fig. 6.3.4, we find that the number of kinks with small sharpness is suppressed only in the case of ordinary cosmic string. The suppression occurs because kinks with small sharpness are numerous and a large number of their collisions generate the GW backreaction effect through Eq. (8.3.4). The correlation length also becomes large because of Eq. (8.3.2) and the slope of the distribution function gets slightly gentler. On the other hand, the suppression by the GW backreaction is not seen in the case of cosmic superstrings, since the number of kinks is reduced by Y-junctions and the effect of GW emission is too small.

In the right panel, in the case of cosmic strings, we find that the GW spectrum increases towards high frequency and the spectrum becomes flat at around  $10^{-7}$  Hz. See [60], for details. The flat behavior at a high frequency is because of the GW backreaction. In the case of cosmic superstrings, we find the spectral amplitude is low and it has an almost flat-spectrum since Y-junctions smooth out kink sharpness and the value of  $\psi_{\max}$  becomes very small. We also find that the overall GW power decreases with smaller reconnection probability. The reason is similar to the case of propagating kinks, explained in Sec. 7.2.3. In the case of kink-kink collisions, the correlation length and  $\psi_{\max}$  affects the GW spectrum as  $\Omega_{\text{GW}} \propto \gamma^{-2} \psi_{\max}^2$ . In Case A, the effect of  $\psi_{\max}$  dominates the one of  $\gamma$  for small reconnection probability.

#### 8.3.4 Case B: GW background with $\mu_1 : \mu_2 : \mu_3 = 1 : 1 : 1$ and $n_p = \frac{1}{3}$

The results of Case B are similar to Case A. The difference appears when reconnection probability is small, where we find the GW amplitude decreases more. As explained in Sec. 7.2.4, this is because the decrease of correlation length  $\gamma$  is milder compared to Case A and a more prominent effect of  $\psi_{\max}$  is seen.

#### 8.3.5 Case C: GW background with $\mu_1 : \mu_2 : \mu_3 = 1 : 10 : 10$ and $n_p = \frac{1}{3}$

In the same way as GWs from kink propagation in Sec. 7.2.5, we find that the power spectrum is slightly enhanced compared to the ordinary cosmic string case when  $p = 10^{-1}$ . This is again because the slope of the kink distribution is not entirely flattened by Y-junctions compared to Cases A and B and the value of  $\psi_{\max}$  is relatively large. The effect of small correlation length dominates the effect of small  $\psi_{\max}$  in case of  $p = 10^{-1}$  and  $10^{-2}$ , while the kink distribution becomes too gentle and the GW amplitude becomes very low when  $p = 10^{-3}$ .

By comparing between Fig. 7.2.2 and 8.3.6, we find that the amplitude of the GW background from kink-kink collisions is larger than the one from kink propagations. If kink sharpness is not smoothed out dramatically by Y-junctions, we may be able to detect GWs from kink-kink collisions by future GW experiments. As an example, in Fig. 8.3.7, we show the GW power spectrum for different tensions for Case C with  $p = 10^{-1}$ , which is the interesting case with a little enhancement of the GW power. The spectra are shown with sensitivity curves of various future experiments; SKA is the future pulsar timing array project, LISA and DECIGO are the future space-borne GW detectors, and Adv-LIGO describes the design sensitivity of cross-correlation between four ground-based GW detectors (Advanced-LIGO, Advanced-VIRGO, and KAGRA).

Fig. 8.3.8 shows the comparison between the gravitational wave background from kink-kink collisions on infinite cosmic superstrings and the ones from loops. If the loop size is small, the amplitude of the gravitational wave background from kink-kink collisions dominates the one from loops. Because the loop size is the unsolved topic, we may be able to observe the gravitational wave background from kink-kink collisions especially using the SKA and the satellite of observation of CMB polarization (LiteBIRD).

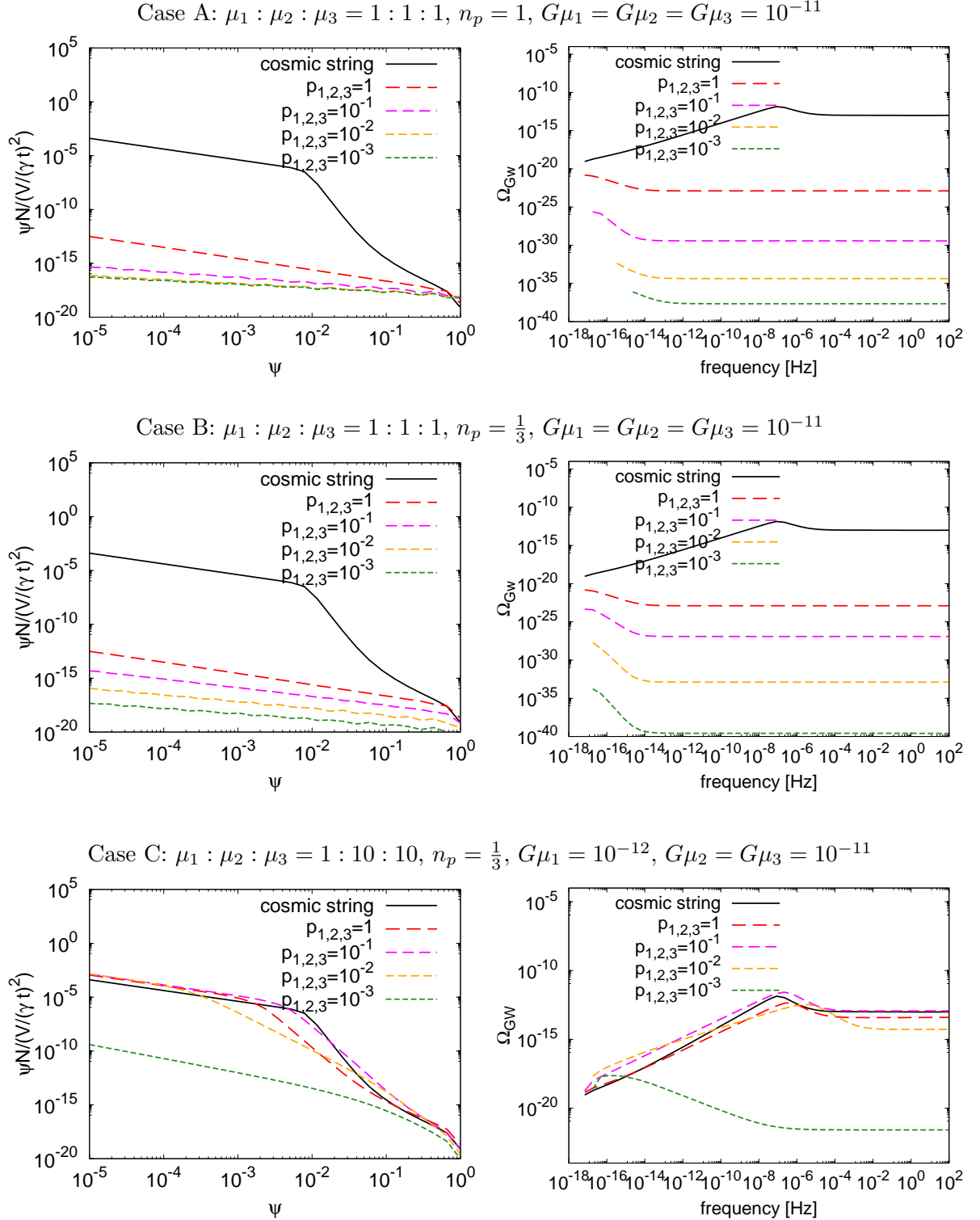


Fig. 8.3.6 Left: the distribution function of kinks on infinite cosmic superstrings calculated by taking into account the effects of GW emission. Right: the power spectrum of the GW background from kink-kink collisions on infinite cosmic superstrings for different reconnection probability. The red, magenta, orange and green broken lines represent  $p = 1, 10^{-1}, 10^{-2}$  and  $10^{-3}$ , respectively. In all panels, for comparison, we plot the case of ordinary cosmic strings with the black solid line ( $G\mu = 10^{-11}$ ).

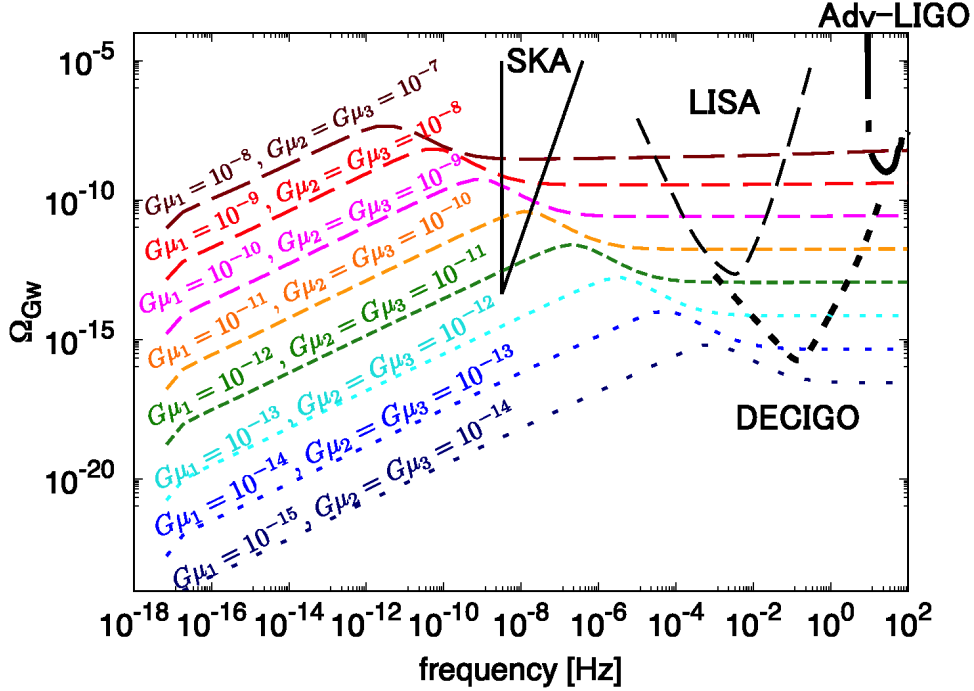


Fig. 8.3.7 The power spectrum of the GW background from kink-kink collisions on the infinite cosmic superstrings of Case C for different tensions. The reconnection probability is set to be  $p = 10^{-1}$ . The black solid and broken lines are the sensitivity curves of future experiments.

## 8.4 Summary

We estimate the power spectrum of the GW background from kink-kink collisions on infinite cosmic strings and superstrings by taking into account the GW emission effect, which reduces the kink's number at small sharpness. Because of this effect, the number of kinks contributing to the high frequency decrease and the GW amplitude is suppressed at the high-frequency. In the case of cosmic strings, the amplitude from kink-kink collisions is above the one from kink propagations. In the case of cosmic superstrings, when the tension ratio is 1 : 1 : 1, the amplitude becomes smaller with smaller reconnection probability and is weaker than the cosmic string one. On the other hand, in the case of 1 : 10 : 10, the GW amplitude is comparable to the cosmic string one because of the steeper kink distribution and larger sharpness contributing to the GW background.

Finally, let us comment on previous works. The GW spectrum from small structures on infinite strings has been calculated analytically in Refs. [55, 56] and numerical simulations for GWs from infinite strings are performed in Ref. [57]. They all predict a smaller GW amplitude compared to our result. We believe that the reason is that those previous studies considered only kinks with large sharpness  $\sim 1$  (for simplicity in the analytic study and because of the resolution in the simulation study), while our method based on solving the evolution

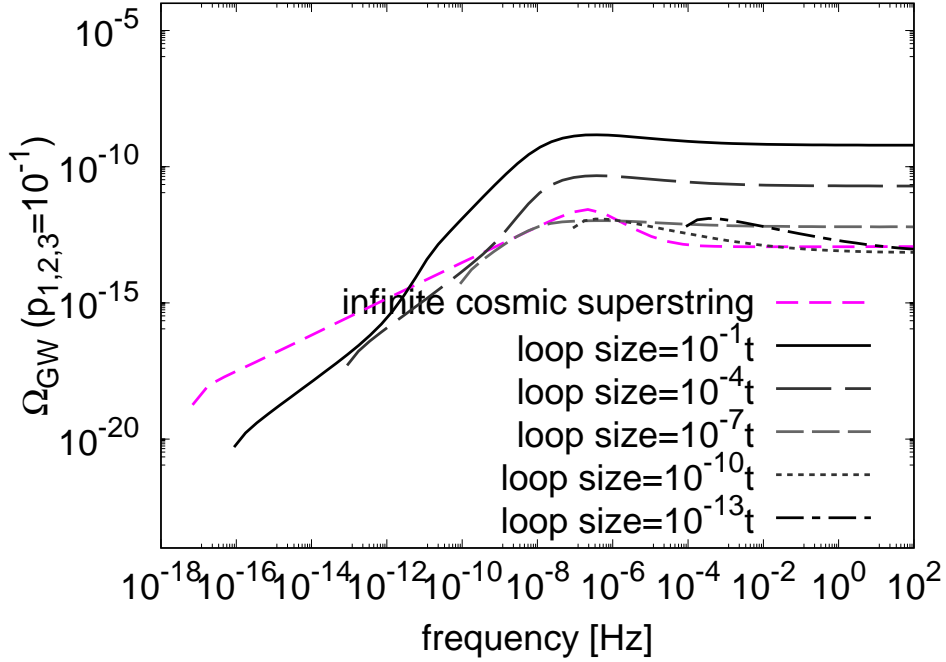


Fig. 8.3.8 The power spectrum of the GW background from kink-kink collisions on infinite cosmic superstrings for Case C with  $p = 10^{-1}$  (broken magenta line) and the ones from loops for different loop size (black and gray lines).

equation of kink distribution, established in Ref. [63], enables to take account of kinks with much smaller sharpness. In fact, we have seen that the enhancement of GWs occurs at high frequencies, which are mainly produced by kinks with small sharpness.

The GWs from kink-kink collisions on loops have been considered in Refs. [41, 124, 125]. Although their estimate has some uncertainty since the number of kinks on one loop is taken as a free parameter in their calculation, it has been shown that a large GW background can be expected by kink-kink collisions on loops. We would like to mention that our estimate of the kink number distribution may help to know the exact number of loops and may provide more concrete predictions.

## 9 Summary

We have investigated how the distribution function of kinks on infinite cosmic superstrings are affected by a small reconnection probability and Y-junctions. Then we have studied the power spectrum of the GW background created by propagating kinks and kink-kink collisions on infinite cosmic strings and infinite cosmic superstrings, taking into account the GW emission effect. We have also discussed the detectability of such a GW background by the current and future GW observations.

In Sec.2, we have briefly reviewed the basics of cosmology. Beginning with the FRWL metric, we have introduced the expansion history of the Universe. The expansion of the Universe can provide a huge impact on the dynamics of cosmic strings and cosmic superstrings. In Sec.3, we have introduced the generation mechanisms and the features of cosmic strings and cosmic superstrings. It is proposed that cosmic strings are generated by spontaneous symmetric breaking during a phase transition and at the end of inflation. On the other hand, cosmic strings can be produced at the end of the brane inflation. In Sec.4, we have presented the dynamics of both strings and the production of cusps and kinks. There are left-moving / right-moving modes on these strings as the solution of the string dynamics. When infinite strings intersect each other, they reconnect and make loops. Such loops have the transient singularity point, a so-called cusp. When loops are formed, kinks are generated on infinite strings. There exists another structure on infinite cosmic superstrings. Cosmic superstrings are composed of D-strings and F-strings. These two types of string can make a bound state, which is the third type of cosmic superstrings. The connection point of these three types of cosmic superstrings is called a Y-junction.

In Sec.5, we have described the string network dynamics. It is known that the cosmic string network obeys the scaling law in which the number of strings in the horizon stays constant. We have shown that the scaling law is valid even for cosmic superstrings. On the other hand, the smaller reconnection probability makes the loop production difficult in the case of cosmic superstrings. As a result, the number of strings inside the horizon becomes large and the correlation length decreases, compared with the case of cosmic strings.

In Sec.6, we have formulated the time evolution of the kink distribution function on cosmic superstrings. In the formulation, we introduce new terms that represent the effect of Y-junctions on the kink evolution. When a kink propagates through a Y-junction, three ‘daughter’ kinks are produced and the sharpness of these kinks is smaller than the original one. Including this effect on the kink evolution, we have numerically solved the evolutionary equation for the kinks on the cosmic superstrings. We have shown that the kink sharpness is reduced by Y-junctions and the distribution function of kinks becomes flatter with smaller reconnection probability. We have found that the kink distribution function is determined by the balance of the two effects; how much the number of kinks increases and how much the number of the Y-junction which kinks pass-through increases with smaller reconnection probability.

In Sec.7, using the distribution function of kinks obtained in the previous section, we have numerically calculated the power spectrum of the GW background from propagating kinks. We have shown that the GW background amplitude for cosmic strings becomes stronger towards the high frequency. In the case of comic superstrings, the power spectrum shape of the GW background strongly depends on the ratio of the three string tensions connected at a Y-junction. The GW amplitude is sensitive to the kink sharpness. As mentioned above, the tension of strings at the Y-junction provides a strong impact on the evolution of the kink sharpness. When the ratio of the three string tension is 1:1:1, the spectrum amplitude stays constant in a wide range of the GW frequency. In the 1 : 1 : 1 case, we found that the amplitude of the GW background is always suppressed by the existence of Y-junctions. We have also shown that the GW amplitude becomes smaller for smaller reconnection probability since the number of Y-junctions increases for small reconnection probability and the effect of smoothing kink sharpness is enhanced. Although the number of strings in the horizon and kink production is increased for small reconnection probability, the effect of Y-junction dominates and always reduces the GW amplitude. On the other hand, in the case of 1 : 10 : 10, one of the daughter kinks inherits the original sharpness and the kink distribution is not flattened compared to the 1 : 1 : 1 case. The resultant GW amplitude is comparable to the one in the case of cosmic strings.

In Sec.8, we have provided the formulation of the power spectrum of the GW background from kink-kink collisions. We have found that the power spectrum depends on the kink sharpness and kink number stronger than the propagating kinks case. We have calculated the power spectrum numerically and found that the GW amplitude is much larger compared to the one from propagating kinks on the cosmic strings. Moreover, we have investigated the effect of the GW radiation and backreaction on the scaling behavior and the kink distribution. We have found that these effects reduce the GW amplitude at high frequencies because the kinks contributing to the high-frequency GW decrease and the sharpness becomes small by the GW emission effect. We have compared the power spectrum including the GW emission effect with the upper bound on the GW background amplitude by ongoing experiments. We have obtained the constraints on the string tension  $G\mu \lesssim 10^{-5}$  from Advanced-LIGO, and  $G\mu \lesssim 4 \times 10^{-8}$  from NANOGrav. These bounds on the cosmic string tension are not stronger than the one obtained from the current pulsar timing constraint on the GW background. When getting this constraint on the tension, one adopts the GW background produced from loops. However, there exists the theoretical ambiguity on the loop distribution, which, in some scenarios, could weaken the pulsar timing constraint from loops. Therefore, we would like to emphasize that our constraint from GWs due to infinite cosmic strings does not have such uncertainty in the model. Similarly, we have calculated the GW power spectrum due to cosmic superstrings. We have found that, in the case of 1 : 10 : 10, the kink-kink collisions enhance the GW amplitude to the one in the case of cosmic strings. Especially, when  $p = 10^{-1}$ , we found the case in which the effect of small reconnection probability to increase the kink number dominates the one of Y-junction. Accordingly, the GW amplitude is slightly enhanced in this case. Therefore, we might observe the GW background from kink-kink collisions on infinite

cosmic superstrings by future GW experiments.

In general, when the reconnection probability is small, the loop production is not efficient and, as a result, the number density of strings is large. Therefore we can naively expect that cosmic superstrings can produce the GW background more than cosmic strings. However, this work shows that, depending on the tension ratio of strings, Y-junctions can smooth out sharp kinks efficiently. In this case, the resultant GW amplitude from infinite cosmic superstrings becomes smaller than the one from infinite cosmic strings. This result tells that our naive expectation that the constraint on the tension of cosmic superstrings is tighter than the one of ordinary cosmic strings is not always true. Depending on the tension ratio, the theoretical model predicting cosmic superstrings with a large tension could still survive. This may be also applicable for the GW background from kinks on loops, which are expected to be larger than the one from infinite strings at high frequencies. Previous works [124, 125] predicted a large amplitude of the GW background from kink-kink collisions on loops. In particular [54] showed that the amplitude could be enhanced with the existence of Y-junctions since it increases the kink number. However, the estimation was made in the assumption of the constant sharpness of kinks,  $\psi \sim 1$ , and the blunting of kinks is not taken into account. The evolution of the kink distribution, as performed in this work, would be necessary for a more accurate estimation of the GW background from loops with Y-junctions and it may result in a smaller amplitude than the expectation as in the case of infinite strings. We leave it for future work.

Finally, we found that the shape of the power spectra is quite different between the cases of cosmic strings and cosmic superstrings. Thus, the spectral shape may be useful to distinguish whether the origin is cosmic strings or cosmic superstrings. This could be possible by GW searches in a wide range of frequencies by using CMB polarization measurements, pulsar timing arrays, as well as the space-borne and ground-based direct detection experiments.

In this thesis, we focused on the cases where the string tensions have a ratio of  $1 : 1 : 1$  or  $1 : 10 : 10$  to demonstrate the characteristic effects of superstrings. If we can extend this work to explore the large parameter space of cosmic superstrings, we may be able to find cases where GW amplitude is enhanced more. With the beginning of the new era of multi-wavelength GW observations, GWs help us to get insight into the physics of the very early universe.

## Acknowledge

I am full of gratitude to all persons who concern with our work and my life. Before everything, I am indebted to professor Naoshi Sugiyama. When he taught the cosmology at the lesson eight years ago, his lesson fascinated me and I determined that I majored in the cosmology. For six years, he have taught me the basic of the cosmology and given me questions contributing to my work and discussed with me. I am much obliged to Dr. Sachiko Kuroyanagi. I have researched with her for five years. She always discuss politely and tenderly, so I have been able to study with a feeling of relief. I thank the member of our laboratory for arguing day-to-day, especially thanks to Arai-kun and Endo-kun. I express me appreciation for my husband Kazuki. He supports me; moreover He discuss with me at anytime and helps my work out. Finally, I am deeply grateful to my family, Yasunori, Keiko, Momoko and Tomohiro for supporting me.

## A Conservation of the kinks number

The kink sharpness ranges in  $0 \leq \psi \leq 1$ , and in this range, the number of kinks conserves as

$$\frac{d}{dt} \left\{ \int_0^1 d\psi(t) N(\psi, t) \right\} = 0. \quad (\text{A.0.1})$$

Using Eq.(6.1.6), we can rewrite

$$\begin{aligned} \frac{d}{dt} \left\{ \int_0^1 d\psi(t) N(\psi, t) \right\} &= \int_0^1 d\psi(t) \left( \frac{\partial N}{\partial t}(\psi, t) + \frac{\partial \psi}{\partial t} \frac{\partial N}{\partial \psi}(\psi, t) \right) + \int_0^1 d \left( \frac{d\psi}{dt} \right) N(\psi, t), \\ &= \int_0^1 \left( \frac{\partial N}{\partial t}(\psi, t) - \frac{2\zeta}{t} \psi \frac{\partial N}{\partial \psi} \right) + \int_0^1 d \left( -\frac{2\zeta}{t} \psi \right) N(\psi, t), \\ &= \int_0^1 d\psi(t) \left\{ \frac{\partial N}{\partial t} - \frac{2\zeta}{t} \left( \psi \frac{\partial N}{\partial \psi}(\psi, t) + N(\psi, t) \right) \right\}, \\ &= \int_0^1 d\psi(t) \left\{ \frac{\partial N}{\partial \psi}(\psi', t) - \frac{2\zeta}{t} \frac{\partial}{\partial \psi'}(\psi' N(\psi', t)) \right\} = 0. \end{aligned} \quad (\text{A.0.2})$$

Then, we get Eq.(6.2.20).

## B Analytic solution of kinks distribution function

\*5 In the RD era, Eq.(6.2.24) is expressed as

$$\frac{\partial N}{\partial t}(\psi, t) = \frac{\bar{\Delta}_r V}{\gamma_r^4 t^4} g(\psi) + \frac{2\zeta_r}{t} \frac{\partial}{\partial \psi}(\psi N(\psi, t)) - \frac{\eta_r}{\gamma_r t} N(\psi, t). \quad (\text{B.0.1})$$

We define  $\psi = \psi_*$  at  $t = t_*$  and rewrite the sharpness with  $t$  as

$$\psi = \psi_* \left( \frac{t_*}{t} \right)^{2\zeta_r}. \quad (\text{B.0.2})$$

We convert  $\psi$  into  $\psi_*$  in Eq.(B.0.1)

$$t \frac{\partial N}{\partial t}(\psi_*, t) + \left( \frac{\eta_r}{\gamma_r} - 2\zeta_r \right) N(\psi_*, t) = \frac{\bar{\Delta}_r V}{\gamma_r^4 t^3} g \left( \left( \frac{t_*}{t} \right)^{2\zeta_r} \psi_* \right). \quad (\text{B.0.3})$$

---

\*5 We write this subsection referring to [63].

We impose  $g(\psi) = 0$  for  $\psi > 1$  as the boundary condition. Multiplying the both side and  $t^{2-\beta_r}/V$ , we express it as

$$\frac{\partial}{\partial t} \left( t^{3-\beta_r} \frac{N(\psi_*, t)}{V(t)} \right) = \frac{\bar{\Delta}_r}{\gamma_r^4} t^{-\beta_r-1} g \left( \left( \frac{t_*}{t} \right)^{2\zeta_r} \psi_* \right), \quad (\text{B.0.4})$$

where

$$\beta \equiv 3 - 3\nu - \frac{\eta}{\gamma} + 2\zeta, \quad (\text{B.0.5})$$

$$\beta_r \simeq 1.1, \quad \beta_m \simeq 1.2. \quad (\text{B.0.6})$$

We assume that  $\bar{\Delta}$ ,  $\gamma$ ,  $\zeta$ ,  $\eta$  are constant and integrate Eq.(B.0.4) and return from  $\psi_*$  to  $\psi$ . Then, we obtain

$$\frac{N(\psi_*, t)}{V(t)} = \frac{\bar{\Delta}_r}{\gamma_r^4 t^{3-\beta_r}} \int_{\max\{t_*, t_k\}}^t \frac{dt'}{t'^{1+\beta_r}} g \left( \left( \frac{t_*}{t'} \right)^{2\zeta} \psi_* \right). \quad (\text{B.0.7})$$

Moreover, we integrate the equation with respect to time and get the distribution function of kinks analytically.  $t_k$  stands for the production time of kinks and we assume  $\psi = 1$  at that time, then,

$$\psi = \left( \frac{t_k}{t} \right)^{2\zeta_r}. \quad (\text{B.0.8})$$

Therefore, the kink generation time is described as

$$t_k = \psi^{1/2\zeta_r} t. \quad (\text{B.0.9})$$

The lower end of Eq.(B.0.7) is determined whether kinks are produced after the string formation or kinks and strings are generated at the same time. In the case of former,  $t_* < t_k = \psi^{1/2\zeta_r} t$  and the lower end of the integration is  $t_k$ . On the other hand,  $t_k < t_*$  and the lower end is  $t_*$  in the later. We assume that the kinks are generated in the RD era, using the sum as

$$g(\psi) = \sum_k g_k \psi^k \quad \left( k = \frac{1}{2}, \frac{3}{2}, \frac{5}{2} \right), \quad (\text{B.0.10})$$

$$g_{1/2} = \frac{525}{256}, \quad g_{3/2} = -\frac{105}{128}, \quad g_{5/2} = -\frac{35}{256}, \quad (\text{B.0.11})$$

in the RD era, the distribution function of kinks is written as

$$t^3 \frac{N(\psi, t)}{V(t)} = \sum_k \frac{g_k \bar{\Delta}_r}{(\beta_r + 2k\zeta_r) \gamma_r^4} (\psi^{-\beta_r/2\zeta_r} - \psi^k). \quad (\text{B.0.12})$$

In the MD era, we have

$$t^3 \frac{N(\psi, t)}{V(t)} = \begin{cases} \sum_k \frac{g_k \bar{\Delta}_m}{(\beta_m + 2k\zeta_m) \gamma_m^4} (\psi^{-\beta_m/2\zeta_m} - \psi^k) + \left(\frac{t}{t_{\text{eq}}}\right)^{\beta_m} t_{\text{eq}}^3 \frac{N\left(\left(\frac{t}{t_{\text{eq}}}\right)^{2\zeta_m} \psi, t_{\text{eq}}\right)}{V(t_{\text{eq}})} & \text{for } \psi > \left(\frac{t_{\text{eq}}}{t}\right)^{2\zeta_m}, \\ \sum_k \frac{g_k \bar{\Delta}_m}{(\beta_m + 2k\zeta_m) \gamma_m^4} \left\{ \left(\frac{t}{t_{\text{eq}}}\right)^{\beta_m + 2k\zeta_m} - 1 \right\} \psi^k + \left(\frac{t}{t_{\text{eq}}}\right)^{\beta_m} t_{\text{eq}}^3 \frac{N\left(\left(\frac{t}{t_{\text{eq}}}\right)^{2\zeta_m} \psi, t_{\text{eq}}\right)}{V(t_{\text{eq}})} & \text{for } \psi < \left(\frac{t_{\text{eq}}}{t}\right)^{2\zeta_m}, \end{cases} \quad (\text{B.0.13})$$

$t_{\text{eq}}^3 N\left(\left(t/t_{\text{eq}}\right)^{2\zeta_m} \psi, t_{\text{eq}}\right)/V(t_{\text{eq}})$  means the value of Eq.(B.0.12) at  $t = t_{\text{eq}}$ . Let us ignore the  $\mathcal{O}(1)$  coefficient and extract the leading term. Then, in the RD era,

$$\frac{N(\psi, t)}{V(t)/(\gamma t)^2} \sim \psi^{-\beta_r/2\zeta_r} t^{-1}, \quad (\text{B.0.14})$$

and the MD era,

$$\frac{N(\psi, t)}{V(t)/(\gamma t)^2} \sim \begin{cases} \psi^{-\beta_m/2\zeta_m} t^{-1} & \text{for } \psi > \left(\frac{t_{\text{eq}}}{t}\right)^{2\zeta_m}, \\ \left(\frac{t}{t_{\text{eq}}}\right)^{-B/\zeta_r} \psi^{-\beta_r/2\zeta_r} t^{-1} & \text{for } \psi < \left(\frac{t_{\text{eq}}}{t}\right)^{2\zeta_m}. \end{cases} \quad (\text{B.0.15})$$

## C Strain amplitude of GW from one kink

We formularize the motion of the general scalar fields at the distance  $r$  from the source  $S(\mathbf{x}, t)$  called the local wave zone [37], where  $r$  satisfies (remarking GW wavelength)  $\lambda < r < R_H$  (Hubble radius).

In an asymptotic metric to Minkowski spacetime

$$g_{\mu\nu} = \eta_{\mu\nu} + h_{\mu\nu}, \quad (\text{C.0.1})$$

where  $|h_{\mu\nu}| \ll 1$ , we consider a general scalar wave equation

$$\square\phi(\mathbf{x}, t) = -4\pi S(\mathbf{x}, t), \quad (\text{C.0.2})$$

where  $S$  is the source. We now treat the case where the source can be decomposed as

$$S(\mathbf{x}, t) = \int \frac{d\omega}{2\pi} e^{-i\omega t} S(\mathbf{x}, \omega) \quad (\text{C.0.3})$$

$$S(\mathbf{x}, t) = \sum_n e^{-i\omega_n t} S(\mathbf{x}, \omega_n) \quad (\text{C.0.4})$$

using Fourier integral or Fourier series. Focusing on one frequency  $\omega$  or  $\omega_n$ , we decompose the solution into  $\phi(\mathbf{x}, t) = \sum_{\omega} e^{-i\omega t} \phi(\mathbf{x}, \omega)$ . Then, we lead Eq. (C.0.2) to a Helmholtz equation

$$(\Delta + \omega^2)\phi(\mathbf{x}, \omega) = -4\pi S(\mathbf{x}, \omega), \quad (\text{C.0.5})$$

where the formulation of the equation is the same as the equation using the retarded Green function

$$(\Delta + \omega^2)G_\omega(\mathbf{x}, \mathbf{x}') = -4\pi\delta(\mathbf{x} - \mathbf{x}'). \quad (\text{C.0.6})$$

The retarded Green function

$$G_\omega(\mathbf{x}, \mathbf{x}') = \frac{e^{i\omega|\mathbf{x}-\mathbf{x}'|}}{|\mathbf{x} - \mathbf{x}'|} \quad (\text{C.0.7})$$

is well known, therefore the general scalar is described as

$$\phi(\mathbf{x}, \omega) = \int d^3x' \frac{e^{i\omega|\mathbf{x}-\mathbf{x}'|}}{|\mathbf{x} - \mathbf{x}'|} S(\mathbf{x}', \omega). \quad (\text{C.0.8})$$

We simply assume that there is the source at the origin. Here, we set  $r \equiv |\mathbf{x}|$  and  $\mathbf{n} \equiv \frac{|\mathbf{x}|}{r}$ . In the local wave zone ( $\omega|\mathbf{x}| \gg 1$ ), we can replace  $|\mathbf{x} - \mathbf{x}'|$  in the phase factor by  $r - \mathbf{n} \cdot \mathbf{x}'$  and in the denominator by  $r$ . Defining  $\mathbf{k} \equiv \omega\mathbf{n}$  (when  $\phi$  emits in the  $\mathbf{n}$  direction quadratically,  $k^\mu = (\mathbf{k}, \omega)$  is used as the four frequency), we can derive the space-time Fourier transform of the source

$$S(k^\mu) = S(\mathbf{k}, \omega) \equiv \int d^3x' e^{-i\mathbf{k} \cdot \mathbf{x}'} S(\mathbf{x}', \omega). \quad (\text{C.0.9})$$

Substituting this into  $\phi(\mathbf{x}, \omega)$ , we obtain the field  $\phi$  as

$$\phi(\mathbf{x}, \omega) \simeq \frac{e^{i\omega r}}{r} S(k^\mu), \quad (\text{C.0.10})$$

and integrating  $\omega$  or summing over  $\omega_n$ , it is rewritten as

$$\phi(\mathbf{x}, t) \simeq \frac{1}{r} \int d\omega e^{-i\omega(t-r)} S(k^\mu), \quad (\text{C.0.11})$$

$$\phi(\mathbf{x}, t) \simeq \frac{1}{r} \sum_{\omega_n} e^{-i\omega_n(t-r)} S(k^\mu). \quad (\text{C.0.12})$$

Applying the perturbation of the metric and the energy-momentum tensor of cosmic strings and superstrings to the formulation, we are able to obtain the strain amplitude of the GW from cosmic strings and superstrings.

## D Condition of sharpness mostly contributing to GW background of frequency $f$

We introduced the condition of  $\psi_{\max}$  as Eq.(7.1.14) and provided a brief explanation using Fig.7.1.2. Here, we describe in detail that the kinks whose interval is equal to the wavelength of the GW background contribute to the GW amplitude [58]. Since the  $T^{\mu\nu}$  of propagating

kinks and kink-kink collisions are expressed by using

$$I^\mu(\omega, \omega \mathbf{n}, v) \equiv \int_{u_A(v)}^{u_B(v)} du a'^\mu(u) e^{-\frac{i}{2}\omega(u + \mathbf{n} \cdot \mathbf{a}(u))}, \quad (\text{D.0.1})$$

where we introduce later (see Sec.E), we prove that the kinks satisfying Eq.(7.1.14) mainly contributes to  $I^\mu$ .

A kink is described as a discontinuity in  $a'^\mu$  and many sharp kinks and blunted kinks exist on infinite strings. We focus on the kinks whose interval are larger than the wavelength of the GW background  $\left\{ \psi \frac{N(\psi, t)}{V(t)/(\gamma t)^2} \right\}^{-1} \gtrsim \omega^{-1}$  called "big kinks". Then, the sharpness is  $\psi \gtrsim \psi_{\max}$ . Around each big kink, the integration range of  $I^\mu$  is divided into the wavelength  $\sim \omega^{-1}$  as

$$I^\mu(\omega, \omega \mathbf{n}) = \sum_l I_l^\mu(\omega, \omega \mathbf{n}), \quad (\text{D.0.2})$$

where  $l$  is the label of the big kink and  $l$ -th big kink contributes to  $I^\mu(\omega, \omega \mathbf{n})$ . There are many kinks with small sharpness around big kinks called "small kinks" whose sharpness are  $\psi \lesssim \psi_{\max}$ . Namely, these small kinks satisfy  $\left\{ \psi \frac{N(\psi, t)}{V(t)/(\gamma t)^2} \right\}^{-1} \lesssim \omega^{-1}$ . We decompose  $a'^\mu$  in the  $l$ -th interval as

$$a'^\mu(u) = \bar{a}_l'^\mu(u) + \delta a_l'^\mu(u), \quad (\text{D.0.3})$$

where  $\bar{a}_l'^\mu(u)$  is smooth except for the big kink. And the contribution of small kinks to  $a'^\mu(u)$  is expressed as  $\delta a_l'^\mu(u)$ . When  $\mu = 0$ , we have  $a'^0 = \bar{a}_l'^0 = -1$  and  $\delta a_l'^0(u) = 0$ .  $\delta a_l'^\mu(u)$  has discontinuities at each small kinks and using the sharpness definition (Eq.(6.1.1)), the discontinuity changes by  $\sim \sqrt{\psi}$  \*6. Since small kinks have different sharpness and they randomly interact with the big kink, the average of the small kink contribution becomes 0 ( $\langle \delta a_l'^\mu(u) \rangle = 0$ ). When we integrate Eq.(D.0.3),

$$a^\mu(u) = \bar{a}_l^\mu(u) + \delta a_l^\mu(u). \quad (\text{D.0.4})$$

To be sure,  $\bar{a}_l^\mu(u)$  and  $\delta a_l^\mu(u)$  are not differentiable at big kinks and small kinks. And we have  $a^0 = \bar{a}_l^0 = -u$  and  $\delta a_l^0(u) = 0$ . Therefore,  $I_l^\mu(\omega, \omega \mathbf{n})$  can be written as

$$I_l^\mu(\omega, \omega \mathbf{n}) = \int_l du \bar{a}_l'^\mu(u) e^{-\frac{i}{2}\omega(u + \mathbf{n} \cdot \bar{\mathbf{a}}_l(u) + \mathbf{n} \cdot \delta \mathbf{a}_l(u))} + \int_l du \delta a_l'^\mu(u) e^{-\frac{i}{2}\omega(u + \mathbf{n} \cdot \bar{\mathbf{a}}_l(u) + \mathbf{n} \cdot \delta \mathbf{a}_l(u))}, \quad (\text{D.0.5})$$

where the integration works for the  $l$ -th interval. In the  $l$ -th interval, we define the position of the  $j$ -th small kink as  $u = u_{l;j}$ . Let us rewrite the equation. In the range of  $[u_{l;j}, u_{l;j+1}]$ , we assume that the integrand of the first term of Eq.(D.0.5) can be approximated as constant

---

\*6 Using the definition of the sharpness Eq.(6.1.1), the solution of the cosmic string and cosmic superstring dynamics are written as  $\mathbf{a} \sim \sqrt{\psi}$ .

and  $\Delta u_{l;j} \equiv u_{l;j+1} - u_{l;j}$ . In order to decompose  $\delta a_l^{\mu'}(u)$  in the second term, we introduce

$$\delta a_l^{\mu'} = \sum_k F_l^{(k)\mu}(u), \quad (\text{D.0.6})$$

where kinks with  $\psi \sim \psi_k$  contribute to  $F_l^{(k)\mu}(u)$  and they are placed with the interval of  $\left\{ \psi_k \frac{N(\psi_k, t)}{V(t)/(\gamma t)^2} \right\}^{-1}$ . Therefore, the value of  $F_l^{(k)\mu}(u)$  jumps at each kink and the jump width is  $\sim \sqrt{\psi_k}$ . When there is a kink at  $u = u_{l,s}^k$ ,  $F_l^{(k)\mu}(u_{l,s}^k)$  is the probability distribution whose average is 0 and the dispersion is given by  $\psi_k$ . Using the decomposition, the first and the second terms of Eq.(D.0.5) is given as

$$\text{first term} \simeq \sum_j \bar{a}_l^{\mu'}(u_{l;j}) e^{-\frac{i}{2}\omega(u_{l;j} + \mathbf{n} \cdot \bar{\mathbf{a}}_l(u_{l;j}))} e^{-\frac{i}{2}\omega \mathbf{n} \cdot \delta \mathbf{a}_l(u_{l;j})} \Delta u_{l;j} \quad (\text{D.0.7})$$

$$\text{second term} \simeq \sum_k \sum_s F_l^{(k)\mu}(u_{l,s}^k) e^{-\frac{i}{2}\omega(u_{l,s}^k + \mathbf{n} \cdot \bar{\mathbf{a}}_l(u) + \mathbf{n} \cdot \delta \mathbf{a}_l(u))} (u_{l,s+1}^k - u_{l,s}^k) \quad (\text{D.0.8})$$

$T^{\mu\nu}$  is roughly expressed as  $\langle |I^\mu|^2 \rangle$ . Although there are cross-terms such as  $\langle |I_l^\mu I_m^\mu| \rangle$  ( $l \neq m$ ), the GW from a local kink is not affected by other kinks, and we can approximate  $T^{\mu\nu}$  as  $\langle |I_l^\mu|^2 \rangle$ . Then, it is written as

$$\begin{aligned} \langle |I^\mu|^2 \rangle &= \sum_{j,h} \left\langle \bar{a}_l^{\mu'}(u_{l;j}) \bar{a}_l^{\mu'}(u_{l;h}) e^{-\frac{i}{2}\omega(u_{l;j} + u_{l;h} + \mathbf{n} \cdot \bar{\mathbf{a}}_l(u_{l;j}) - \mathbf{n} \cdot \bar{\mathbf{a}}_l(u_{l;h}))} \right\rangle \\ &\quad \times \left\langle e^{-\frac{i}{2}\omega(\mathbf{n} \cdot \delta \mathbf{a}_l(u_{l;j}) - \mathbf{n} \cdot \delta \mathbf{a}_l(u_{l;h}))} \right\rangle \Delta u_{l;j} \Delta u_{l;h} \\ &+ \left\langle \left( \sum_k \sum_s F_l^{(k)\mu}(u_{l,s}^k) e^{-\frac{i}{2}\omega(u_{l,s}^k + \mathbf{n} \cdot \bar{\mathbf{a}}_l(u) + \mathbf{n} \cdot \delta \mathbf{a}_l(u))} (u_{l,s+1}^k - u_{l,s}^k) \right)^2 \right\rangle \\ &+ \sum_j \left\langle \bar{a}_l^{\mu'}(u_{l;j}) e^{-\frac{i}{2}\omega(u_{l;j} + \mathbf{n} \cdot \bar{\mathbf{a}}_l(u_{l;j}))} e^{-\frac{i}{2}\omega \mathbf{n} \cdot \delta \mathbf{a}_l(u_{l;j})} \right\rangle \Delta u_{l;j} \\ &\quad \times \sum_k \sum_s \left\langle F_l^{(k)\mu}(u_{l,s}^k) e^{-\frac{i}{2}\omega(u_{l,s}^k + \mathbf{n} \cdot \bar{\mathbf{a}}_l(u_{l,s}^k) + \mathbf{n} \cdot \delta \mathbf{a}_l(u_{l,s}^k))} (u_{l,s+1}^k - u_{l,s}^k) \right\rangle \\ &+ \text{c.c.}, \end{aligned} \quad (\text{D.0.9})$$

where c.c. denotes the complex conjugate. First, we focus on the first term and evaluate  $\langle |\delta \mathbf{a}_l(u_{l;j}) - \delta \mathbf{a}_l(u_{l;h})|^2 \rangle$ . We assume that the interval of kinks is extremely narrow and  $F_l^{(k)\mu}(u_{l,s}^k)$  is constant between kinks. In addition, there is no correlation between kinks,

namely,  $\langle F_l^{(k)\mu}(u_{l,s}^k) F_l^{(k')i}(u_{l,s'}^{k'}) \rangle = 0$  ( $k \neq k'$ ,  $s \neq s'$ ). Using eq.(D.0.6), we get

$$\begin{aligned} (\langle |\delta \mathbf{a}_l(u_{l;j}) - \delta \mathbf{a}_l(u_{l;h})|^2 \rangle)^{\frac{1}{2}} &\sim (\langle |\delta \mathbf{a}_l(u_{l;j}) - \delta \mathbf{a}_l(u_{l;h})|^2 \rangle)^{\frac{1}{2}} \\ &\sim \left\langle \left\langle \left( \sum_k \sum_s F_l^{(k)\mu}(u_{l,s}^k) (u_{l,s+1}^k - u_{l,s}^k) \right)^2 \right\rangle \right\rangle^{\frac{1}{2}} \\ &\sim \left\{ \sum_k \sum_s \langle (F_l^{(k)\mu}(u_{l,s}^k))^2 \rangle (u_{l,s+1}^k - u_{l,s}^k)^2 \right\}^{\frac{1}{2}}. \end{aligned} \quad (\text{D.0.10})$$

Substituting  $\sqrt{\psi_k}$  into  $F_l^{(k)\mu}(u_{l,s}^k)$  and  $\left\{ \psi_k \frac{N(\psi_k, t)}{V(t)/(\gamma t)^2} \right\}^{-1}$  into  $u_{l,s+1}^k - u_{l,s}^k$ , thus

$$\begin{aligned} (\langle |\delta \mathbf{a}_l(u_{l;j}) - \delta \mathbf{a}_l(u_{l;h})|^2 \rangle)^{1/2} &\sim \left[ \sum_k \psi_k \times \left\{ \psi_k \frac{N(\psi_k, t)}{V(t)/(\gamma t)^2} \right\}^{-2} \right. \\ &\quad \left. \times \left( |u_{l;a} - u_{l;b}| / \left\{ \psi_k \frac{N(\psi_k, t)}{V(t)/(\gamma t)^2} \right\}^{-1} \right) \right]^{\frac{1}{2}} \\ &\sim \left[ \sum_k \left\{ \frac{N(\psi_k, t)}{V(t)/(\gamma t)^2} \right\}^{-1} \right]^{\frac{1}{2}} |u_{l;j} - u_{l;h}|^{\frac{1}{2}} \end{aligned} \quad (\text{D.0.11})$$

where  $u_{l;j}$ ,  $u_{l;h}$  are kink positions and we convert the sum  $\sum_s$  to the kink number in  $|\delta \mathbf{a}_l(u_{l;j}) - \delta \mathbf{a}_l(u_{l;h})|$ , namely,  $|u_{l;j} - u_{l;h}| / \left\{ \psi_k \frac{N(\psi_k, t)}{V(t)/(\gamma t)^2} \right\}^{-1}$ . Last, we convert the sum  $\sum_k$  to the integral  $\int d \ln \psi = \int d\psi \psi^{-1}$ . From the definition of  $\psi_{\max}$  (Eq.(7.1.14)),  $|u_{l;j} - u_{l;h}| \lesssim \left\{ \psi_{\max} \frac{N(\psi_{\max}, t)}{V(t)/(\gamma t)^2} \right\}^{-1} \sim \omega^{-1}$  because  $\delta \mathbf{a}$  reflects the contribution from small kinks. Then,

$$\begin{aligned} (\langle |\delta \mathbf{a}_l(u_{l;j}) - \delta \mathbf{a}_l(u_{l;h})|^2 \rangle)^{\frac{1}{2}} &\sim \left[ \int^{\psi_{\max}} d\psi \psi^{-1} \left\{ \frac{N(\psi, t)}{V(t)/(\gamma t)^2} \right\}^{-1} \right]^{\frac{1}{2}} |u_{l;j} - u_{l;h}|^{\frac{1}{2}} \\ &\sim \left\{ \frac{N(\psi_{\max}, t)}{V(t)/(\gamma t)^2} \right\}^{-\frac{1}{2}} |u_{l;j} - u_{l;h}|^{\frac{1}{2}} \\ &\sim \left[ \psi_{\max} \left\{ \psi_{\max} \frac{N(\psi_{\max}, t)}{V(t)/(\gamma t)^2} \right\}^{-1} \right]^{\frac{1}{2}} |u_{l;j} - u_{l;h}|^{\frac{1}{2}} \\ &\lesssim \left\{ \psi_{\max} \omega^{-1} \right\}^{\frac{1}{2}} \omega^{-\frac{1}{2}} \\ &\sim \psi_{\max}^{\frac{1}{2}} \omega^{-1} \ll \omega^{-1}. \end{aligned} \quad (\text{D.0.12})$$

Therefore,  $\omega \mathbf{n} \cdot (\delta \mathbf{a}_l(u_{l;j}) - \delta \mathbf{a}_l(u_{l;h})) \ll 1$  and we find  $e^{-\frac{i}{2} \omega (\mathbf{n} \cdot (\delta \mathbf{a}_l(u_{l;j}) - \delta \mathbf{a}_l(u_{l;h})))} \simeq 1$ . Then,

we can approximate the first term of Eq.(D.0.9) as

$$\text{the first term of Eq.(D.0.9)} = \left\langle \left| \int_l du \bar{a}_l^{\mu'}(u) e^{-\frac{i}{2}\omega(u_l + \mathbf{n} \cdot \bar{\mathbf{a}}_l(u))} \right|^2 \right\rangle. \quad (\text{D.0.13})$$

Since there is no effect of small kinks in this approximation, we can evaluate it using Eq.(E.1.2)

$$\text{the first term of Eq.(D.0.9)} = \sum_l \left( \frac{\psi_l^{\frac{1}{2}}}{\omega} \right)^2, \quad (\text{D.0.14})$$

where  $\psi_l$  means the  $l$ -th big kink sharpness.

Next, we evaluate the second term of Eq.(D.0.9) as before,

$$\begin{aligned} & \text{the second term of Eq.(D.0.9)} \\ &= \left\langle \left( \sum_k \sum_s F_l^{(k)\mu}(u_{l,s}^k) e^{-\frac{i}{2}\omega(u_{l,s}^k + \mathbf{n} \cdot \bar{\mathbf{a}}_l(u) + \mathbf{n} \cdot \delta \mathbf{a}_l(u))} (u_{l,s+1}^k - u_{l,s}^k) \right)^2 \right\rangle \\ &= \sum_k \sum_s \left\langle \left( F_l^{(k)\mu}(u_{l,s}^k) \right)^2 \right\rangle (u_{l,s+1}^k - u_{l,s}^k)^2 \\ &\sim \sum_k \psi_k \left\{ \psi_k \frac{N(\psi_k, t)}{V(t)/(\gamma t)^2} \right\}^{-2} \left( |u_{l,j} - u_{l,h}| / \left\{ \psi_k \frac{N(\psi_k, t)}{V(t)/(\gamma t)^2} \right\}^{-1} \right) \\ &\sim \sum_k \psi_k \left\{ \psi_k \frac{N(\psi_k, t)}{V(t)/(\gamma t)^2} \right\}^{-1} \omega^{-1} \\ &\sim \int^{\psi_{\max}} d\psi \psi^{-1} \left\{ \frac{N(\psi, t)}{V(t)/(\gamma t)^2} \right\}^{-1} \omega^{-1} \\ &\sim \left\{ \frac{N(\psi_{\max}, t)}{V(t)/(\gamma t)^2} \right\}^{-1} \omega^{-1} \\ &\sim \psi_{\max} \omega^{-2}. \end{aligned} \quad (\text{D.0.15})$$

Because  $\psi_l$  describes the effect of big kinks in the first term of Eq.(D.0.9),  $\psi_{\max} < \psi_l$  and the first term dominates the second term.

Last, we describe the third term of Eq.(D.0.9). Since the average of  $F_l^{(k)\mu}(u_{l,s}^k)$  is 0, the third term vanishes. Then, the first term of Eq.(D.0.9) is the leading term. That is to say, the big kink only affects  $I_l^\mu$  and we can neglect the small kink effect.

To summarize, we obtain

$$\begin{aligned}
 \langle |I^\mu|^2 \rangle &\sim \sum_l \frac{\psi_l}{\omega^2} \\
 &\sim \int_{\psi_{\max}}^1 d\psi \left\{ \frac{N(\psi, t)}{V(t)/(\gamma t)^2} \right\}^{-1} \times \psi \omega^{-2} \times L \\
 &\sim \psi_{\max} \frac{N(\psi_{\max}, t)}{V(t)/(\gamma t)^2} \psi_{\max} \omega^{-2} \times L,
 \end{aligned} \tag{D.0.16}$$

where  $L$  is the range of the integration of  $I^\mu$ . This result suggests that kinks with the sharpness  $\psi_{\max}$  mainly contribute to  $\langle |I^\mu|^2 \rangle$ , namely, such kinks give the contribution to the GW whose frequency is  $\omega$ .

This is the case when  $\psi_{\max}$  satisfying Eq.(7.1.14) exists. If  $\psi \frac{N(\psi, t)}{V(t)/(\gamma t)^2} \ll \omega$ , all kinks are classified as big kinks. So,  $\langle |I^\mu|^2 \rangle$  can be approximated as Eq.(D.0.14) and we obtain

$$\begin{aligned}
 \langle |I^\mu|^2 \rangle &\sim \int_0^1 d\psi \left\{ \frac{N(\psi, t)}{V(t)/(\gamma t)^2} \right\}^{-1} \times \psi \omega^{-2} \times L \\
 &\sim \psi_{\text{peak}} \frac{N(\psi_{\text{peak}}, t)}{V(t)/(\gamma t)^2} \psi_{\text{peak}} \omega^{-2} \times L,
 \end{aligned} \tag{D.0.17}$$

where  $\psi_{\text{peak}}$  is the sharpness which is the peak of the distribution function of kink  $\psi \frac{N(\psi, t)}{V(t)/(\gamma t)^2}$ . Then, kinks with  $\psi_{\text{peak}}$  dominantly contribute to  $\langle |I^\mu|^2 \rangle$ .

## E Energy momentum tensor $T^{\mu\nu}$ of cusp and kink

Here, we obtain the energy-momentum tensor  $T^{\mu\nu}$  of cusp and kink. Since these are small scale structures, we will consider the energy-momentum tensor in Minkowski spacetime. In the spacetime, the energy momentum tensor is written as Eq.(4.1.11). We obtain Fourier transformation of  $T^{\mu\nu}(t, \mathbf{r})$  as [37, 118]

$$\begin{aligned}
 T^{\mu\nu}(k^\lambda) &= T^{\mu\nu}(\omega, \mathbf{k}) = \int d^4x e^{ik \cdot r} T^{\mu\nu}(t, \mathbf{r}) \\
 &= \mu \int dt \int d^3x e^{ik \cdot r} \int_{s_A(t)}^{s_B(t)} d\sigma (\dot{x}^\mu \dot{x}^\nu - x^{\mu'} x^{\nu'}) \delta^3(\mathbf{r} - \mathbf{x}(t, \sigma)) \\
 &= \mu \int dt e^{ik \cdot x} \int_{s_A(t)}^{s_B(t)} d\sigma (\dot{x}^\mu \dot{x}^\nu - x^{\mu'} x^{\nu'}),
 \end{aligned} \tag{E.0.1}$$

where  $k \cdot r = \eta_{\mu\nu} k^\nu r^\mu = \omega t - \mathbf{k} \cdot \mathbf{r}$ ,  $k \cdot x = \omega t - \mathbf{k} \cdot \mathbf{x}(t, \sigma)$ . Substituting  $x^\mu = \frac{1}{2}(a^\mu(u) + b^\mu(v))$  into  $T^{\mu\nu}(k^\lambda)$ , we transform  $(t, \sigma)$  to  $(u, v)$ , and then  $T^{\mu\nu}(k^\lambda)$  is rewritten as

$$T^{\mu\nu}(k^\lambda) = -\frac{\mu}{4} \int du \int dv e^{\frac{i}{2}\{\omega(v-u) - \mathbf{k} \cdot (\mathbf{a}(u) + \mathbf{b}(v))\}} (a^{\mu'} b^{\nu'} + a^{\nu'} b^{\mu'}) \tag{E.0.2}$$

using  $\dot{x}^\mu = \frac{1}{2}(-a^{\mu'} + b^{\mu'})$  and  $dt d\sigma = \frac{1}{2} du dv$ . We assume  $\mathbf{k} = \omega \mathbf{n}$ , then

$$\begin{aligned}
T^{\mu\nu}(\omega, \omega \mathbf{n}) &= -\frac{\mu}{4} \int_{-\infty}^{\infty} dv b^{\nu'} e^{\frac{i}{2}\omega(v-\mathbf{n}\cdot\mathbf{b}(v))} \int_{u_A(v)}^{u_B(v)} du a^{\mu'}(u) e^{-\frac{i}{2}\omega(u+\mathbf{n}\cdot\mathbf{a}(u))} \\
&\quad -\frac{\mu}{4} \int_{-\infty}^{\infty} dv b^{\mu'} e^{\frac{i}{2}\omega(v-\mathbf{n}\cdot\mathbf{b}(v))} \int_{u_A(v)}^{u_B(v)} du a^{\nu'}(u) e^{-\frac{i}{2}\omega(u+\mathbf{n}\cdot\mathbf{a}(u))} \quad (\text{E.0.3})
\end{aligned}$$

In order to integrate this energy momentum tensor, we introduce the integral

$$I(\omega) \equiv \int_A^B dt f(t) e^{-i\omega\phi(t)}. \quad (\text{E.0.4})$$

in the high frequency limit  $\omega \rightarrow \infty$ . When the integral satisfies these conditions

1. When an arbitrary  $m \geq 0$ ,  $f^{(m)}(A) = f^{(m)}(B)$ ,  $\phi^{(m)}(A) = \phi^{(m)}(B)$
2. On  $[A, B]$ ,  $f, \phi$  are smooth, namely  $f, \phi$  is  $C^\infty$
3. For an arbitrary  $t$  on  $[A, B]$ ,  $\dot{\phi}(t) \neq 0$

then, the integral becomes 0 faster than any power  $\frac{1}{\omega}$ . Namely, when the condition is violated,  $I(\omega)$  have a finite value. Using  $I(\omega)$ , the energy-momentum tensor is

$$\begin{aligned}
T^{\mu\nu}(\omega, \omega \mathbf{n}) &= -\frac{\mu}{4} \int_{-\infty}^{\infty} dv b^{\nu'} e^{\frac{i}{2}\omega(v-\mathbf{n}\cdot\mathbf{b}(v))} I^\mu(\omega, \omega \mathbf{n}, v) \\
&\quad -\frac{\mu}{4} \int_{-\infty}^{\infty} dv b^{\mu'} e^{\frac{i}{2}\omega(v-\mathbf{n}\cdot\mathbf{b}(v))} I^\nu(\omega, \omega \mathbf{n}, v), \quad (\text{E.0.5})
\end{aligned}$$

where

$$I^\mu(\omega, \omega \mathbf{n}, v) \equiv \int_{u_A(v)}^{u_B(v)} du a'^{\mu}(u) e^{-\frac{i}{2}\omega(u+\mathbf{n}\cdot\mathbf{a}(u))}. \quad (\text{E.0.6})$$

The varying scale of  $\mathbf{a}'$  is the same as the correlation length  $L$ . Then, from  $|\mathbf{a}'| = 1$ ,  $\mathbf{a}'' \sim \mathcal{O}(L^{-1})$ ,  $\mathbf{a}''' \sim \mathcal{O}(L^{-2})$ .

### E.1 $I^\mu$ for a discontinuity

First, when we assume that there is the discontinuity on  $\mathbf{a}'$  at  $u = u_*$ ,

$$\begin{aligned}
I^\mu(\omega, \omega \mathbf{n}, v) &= \int_{u_A(v)}^{u_*} du a^{\mu'}(u) e^{-\frac{i}{2}\omega(u+\mathbf{n}\cdot\mathbf{a}(u))} + \int_{u_*}^{u_B(v)} du a^{\mu'}(u) e^{\frac{i}{2}\omega(u-\mathbf{n}\cdot\mathbf{a}(u))}, \\
&= \left[ -\frac{2}{i\omega(1+\mathbf{n}\cdot\mathbf{a}'(u))} a^{\mu'}(u) e^{-\frac{i}{2}\omega(u+\mathbf{n}\cdot\mathbf{a}(u))} \right]_{u_A(v)}^{u_*} \\
&\quad + \left[ -\frac{2}{i\omega(1+\mathbf{n}\cdot\mathbf{a}'(u))} a^{\mu'}(u) e^{-\frac{i}{2}\omega(u+\mathbf{n}\cdot\mathbf{a}(u))} \right]_{u_*}^{u_B(v)} + \mathcal{O}\left(\frac{a^{\mu''}}{\omega}\right), \\
&= -\frac{2}{i\omega} \left( \frac{a_+^{\mu'}}{1+\mathbf{n}\cdot\mathbf{a}'_+} - \frac{a_-^{\mu'}}{1+\mathbf{n}\cdot\mathbf{a}'_-} \right) e^{-\frac{i}{2}\omega(u_*+\mathbf{n}\cdot\mathbf{a}(u_*))} \\
&\quad + (\text{the valu of the integration end}) + \mathcal{O}\left(\frac{a^{\mu''}}{\omega}\right). \tag{E.1.1}
\end{aligned}$$

Considering  $\mathcal{O}\left(\frac{a^{\mu''}}{\omega}\right) \sim 0$  and the periodic boundary condition, it is expressed as

$$I^\mu(\omega, \omega \mathbf{n}, v) \simeq -\frac{2}{i\omega} \left( \frac{a_+^{\mu'}}{1+\mathbf{n}\cdot\mathbf{a}'_+} - \frac{a_-^{\mu'}}{1+\mathbf{n}\cdot\mathbf{a}'_-} \right) e^{-\frac{i}{2}\omega(u_*+\mathbf{n}\cdot\mathbf{a}(u_*))}. \tag{E.1.2}$$

Since it does not depend on  $v$ , we can express it as  $I^\mu(\omega, \omega \mathbf{n})$ . When there is the discontinuity in  $\mathbf{a}$ , the energy-momentum tensor can be rewritten as

$$T^{\mu\nu}(\omega, \omega \mathbf{n}) = -\frac{\mu}{4} (I_-^\nu(\omega, \omega \mathbf{n}) I_+^\mu(\omega, \omega \mathbf{n}) + I_-^\mu(\omega, \omega \mathbf{n}) I_+^\nu(\omega, \omega \mathbf{n})), \tag{E.1.3}$$

where

$$I_+^\mu(\omega, \omega \mathbf{n}) \equiv \int_{u_A(v)}^{u_B(v)} du a^{\mu'}(u) e^{-\frac{i}{2}\omega(u+\mathbf{n}\cdot\mathbf{a}(u))}, \quad I_-^\nu(\omega, \omega \mathbf{n}) \equiv \int_{-\infty}^{\infty} dv b^{\nu'}(v) e^{\frac{i}{2}\omega(v-\mathbf{n}\cdot\mathbf{b}(v))}. \tag{E.1.4}$$

### E.2 $I^\mu$ for a stationary point

Second, if there is a stationary point of the phase  $u + \mathbf{n}\cdot\mathbf{a}(u)$  at  $u_s$ , using  $|\mathbf{a}'| = 1$ , the relations is satisfied

$$\left. \frac{d}{du} (u + \mathbf{n}\cdot\mathbf{a}(u)) \right|_{u=u_s} = 0 \quad \Rightarrow \quad \mathbf{a}'(u_s) = -\mathbf{n}. \tag{E.2.1}$$

Using this equation, the second derivative is given by

$$\left. \frac{d^2}{du^2} (u + \mathbf{n}\cdot\mathbf{a}(u)) \right|_{u=u_s} = \mathbf{n}\cdot\mathbf{a}''(u_s) = \mathbf{a}'(u_s)\cdot\mathbf{a}''(u_s). \tag{E.2.2}$$

Differentiating  $|\mathbf{a}'| = 1$  with respect to  $\sigma$ , we obtain  $\mathbf{a}'(u) \cdot \mathbf{a}''(u) = 0$ , then, we find  $\left. \frac{d^2}{du^2}(u + \mathbf{n} \cdot \mathbf{a}(u)) \right|_{u=u_s} = 0$ . Nearby the stationary point, we approximate the phase as

$$u + \mathbf{n} \cdot \mathbf{a}(u) \simeq u_s + \mathbf{n} \cdot \mathbf{a}(u_s) + \frac{1}{3!} \frac{d^3}{du^3}(u + \mathbf{n} \cdot \mathbf{a}(u)) \Big|_{u=u_s} (u - u_s)^3, \quad (\text{E.2.3})$$

$$\simeq u_s + \mathbf{n} \cdot \mathbf{a}(u_s) + \frac{\omega \mathbf{n} \cdot \mathbf{a}'''(u_s)}{6} (u - u_s)^3, \quad (\text{E.2.4})$$

and  $\mathbf{a}'$  as

$$a^{\mu'}(u) \simeq a^{\mu'}(u_s) + a^{\mu''}(u_s)(u - u_s). \quad (\text{E.2.5})$$

In this case, there is the only contribution to the integration from the nearby of the stationary point, then, the contribution from the interval of  $2\varepsilon$  nearby stationary point is written as

$$\begin{aligned} I_{+}^{\mu}(\omega, \omega \mathbf{n}) &\simeq a^{\mu'}(u_s) e^{-\frac{i}{2}\omega(u_s + \mathbf{n} \cdot \mathbf{a}(u_s))} \int_{u_s - \varepsilon}^{u_s + \varepsilon} du \exp\left(-i \frac{\omega \mathbf{n} \cdot \mathbf{a}'''(u_s)}{12} (u - u_s)^3\right), \\ &+ e^{-\frac{i}{2}\omega(u_s + \mathbf{n} \cdot \mathbf{a}(u_s))} \int_{u_s - \varepsilon}^{u_s + \varepsilon} du a^{\mu''}(u_s)(u - u_s) \exp\left(-i \frac{\omega \mathbf{n} \cdot \mathbf{a}'''(u_s)}{12} (u - u_s)^3\right). \end{aligned} \quad (\text{E.2.6})$$

We assume that there is the only stationary point at  $u = u_s$ , then, the integration becomes 0 as  $\omega \rightarrow \infty$  except the nearby point. Assuming that the boundaries  $u_s \pm \varepsilon$  are far from the stationary point, we change the integration range from  $[u_s - \varepsilon, u_s + \varepsilon]$  to  $[-\infty, \infty]$  in the second term of Eq.(E.2.6), then

$$\begin{aligned} &\text{Second term of Eq.(E.2.6)} \\ &= e^{-\frac{i}{2}\omega(u_s + \mathbf{n} \cdot \mathbf{a}(u_s))} \int_{-\infty}^{\infty} du a^{\mu''}(u_s)(u - u_s) \exp\left(-i \frac{\omega \mathbf{n} \cdot \mathbf{a}'''(u_s)}{12} (u - u_s)^3\right), \\ &\simeq e^{-\frac{i}{2}\omega(u_s + \mathbf{n} \cdot \mathbf{a}(u_s))} a^{\mu''}(u_s) \left(\frac{12}{\omega |\mathbf{n} \cdot \mathbf{a}'''(u_s)|}\right)^{2/3} \int_{-\infty}^{\infty} dw w e^{-iw^3}, \end{aligned} \quad (\text{E.2.7})$$

where

$$w = \left(\frac{\omega |\mathbf{n} \cdot \mathbf{a}'''(u_s)|}{12}\right)^{\frac{1}{3}} (u - u_s), \quad \int_{-\infty}^{\infty} dw w e^{-iw^3} = -\frac{i}{\sqrt{3}} \Gamma\left(\frac{2}{3}\right). \quad (\text{E.2.8})$$

Therefore, we can rewrite as

$$\text{Second term of Eq.(E.2.6)} \simeq -\frac{i}{\sqrt{3}} \Gamma\left(\frac{2}{3}\right) \frac{1}{\omega^{2/3}} a^{\mu''}(u_s) \left(\frac{12}{|\mathbf{n} \cdot \mathbf{a}'''(u_s)|}\right)^{2/3} e^{-\frac{i}{2}\omega(u_s + \mathbf{n} \cdot \mathbf{a}(u_s))} \quad (\text{E.2.9})$$

The first term of Eq.(E.2.6) is also the leading term. However, it is not physical because we

can remove the first term by the coordinate transformation

$$T_{\mu\nu}(k) \rightarrow T_{\mu\nu}(k) + k_\mu \xi_\nu + k_\nu \xi_\mu. \quad (\text{E.2.10})$$

Then, we only focus on the second term and rewrite Eq.(E.2.6) as

$$I_+^\mu(\omega, \omega \mathbf{n}) \simeq -\frac{1}{\omega^{2/3}} a^{\mu'''}(u_s) \left( \frac{12}{|\mathbf{n} \cdot \mathbf{a}'''(u_s)|} \right)^{2/3} \frac{i}{\sqrt{3}} \Gamma\left(\frac{2}{3}\right) e^{-\frac{i}{2}\omega(u_s + \mathbf{n} \cdot \mathbf{a}(u_s))}. \quad (\text{E.2.11})$$

Combining Eq.(E.1.2) and Eq.(E.2.11), we obtain the energy-momentum tensor for propagating kinks and kink-kink collisions. In order to make the former, we need Eq.(E.1.2) and Eq.(E.2.11). On the other hand, we use only Eq.(E.1.2) in order to make it later.

## References

- [1] Abbott, B. P., 2016, 061102(February), 1, doi: 10.1103/PhysRevLett.116.061102.
- [2] Abbott, B. P., 2017, Phys. Rev. Lett., 119(14), 1, doi: 10.1103/PhysRevLett.119.141101.
- [3] Abbott, B. P., 2017, Phys. Rev. Lett., 119(16), 30, doi: 10.1103/PhysRevLett.119.161101.
- [4] Aasi, J., 2015, Class. Quantum Gravity, 32(7), doi: 10.1088/0264-9381/32/7/074001.
- [5] Acernese, F., 2015, Class. Quantum Gravity, 32(2), doi: 10.1088/0264-9381/32/2/024001.
- [6] Kuroda, K., 2010, Class. Quantum Gravity, 27(8), doi: 10.1088/0264-9381/27/8/084004.
- [7] Kibble, T. W. B., 1976, J. Phys. A Gen. Phys., 9(8), 1387, doi: 10.1088/0305-4470/9/8/029.
- [8] Vilenkin, A. & Shellard, E. P. S., Cosmic Strings and Other Topological Defects, 2000.
- [9] Linde, A., 1994, Phys. Rev. D, 49(2), 748, doi: 10.1103/PhysRevD.49.748.
- [10] Lyth, D. H. & Riotto, A., 1997, (1), 1, doi: 10.1016/S0370-2693(97)01044-7, URL <http://arxiv.org/abs/hep-ph/9707273>{%}0Ahttp://dx.doi.org/10.1016/S0370-2693(97)01044-7.
- [11] Sarangi, S. & Tye, S. H., 2002, Phys. Lett. Sect. B Nucl. Elem. Part. High-Energy Phys., 536(3-4), 185, doi: 10.1016/S0370-2693(02)01824-5.
- [12] Jones, N. T., Stoica, H., & Tye, S. H., 2003, Phys. Lett. Sect. B Nucl. Elem. Part. High-Energy Phys., 563(1-2), 6, doi: 10.1016/S0370-2693(03)00592-6.
- [13] Dvali, G. & Tye, S. H., 1999, Phys. Lett. Sect. B Nucl. Elem. Part. High-Energy Phys., 450(1-3), 72, doi: 10.1016/S0370-2693(99)00132-X.
- [14] Dvali, G. & Vilenkin, A., 2004, J. Cosmol. Astropart. Phys., (3), 153, doi: 10.1088/1475-7516/2004/03/010.
- [15] Zeldovich, Y. B., 1980, Mon. Not. R. Astron. Soc., 192(4), 663, doi: 10.1093/mnras/192.4.663.
- [16] Vilenkin, A., 1981, Phys. Lett. B, 107(1-2), 47, doi: 10.1016/0370-2693(81)91144-8.
- [17] Silk, J. & Vilenkin, A., 1984, Phys. Rev. Lett., 53(17), 1700, doi: 10.1103/PhysRevLett.53.1700.
- [18] Kaiser, N. & Stebbins, A., 1984, Nature, 310(5976), 391, doi: 10.1038/310391a0.
- [19] Albrecht, A., Battye, R. A., & Robinson, J., 1997, Phys. Rev. Lett., 79(24), 4736, doi: 10.1103/PhysRevLett.79.4736.
- [20] Bouchet, F. R., Peter, P., Riazuelo, A., & Sakellariadou, M., 2002, Phys. Rev. D - Part. Fields, Gravit. Cosmol., 65(2), 213011, doi: 10.1103/PhysRevD.65.021301.
- [21] Wyman, M., Pogosian, L., & Wasserman, I., 2005, Phys. Rev. D - Part. Fields, Gravit. Cosmol., 72(2), 1, doi: 10.1103/PhysRevD.72.023513.
- [22] Bevis, N., Hindmarsh, M., Kunz, M., & Urrestilla, J., 2007, Phys. Rev. D - Part. Fields, Gravit. Cosmol., 76(4), 1, doi: 10.1103/PhysRevD.76.043005.

- [23] Rocher, J. & Sakellariadou, M., 2005, Phys. Rev. Lett., 94(1), 1, doi: 10.1103/PhysRevLett.94.011303.
- [24] Vilenkin, A., 1984, Astrophys. J., 282, L51, doi: 10.1086/184303.
- [25] Sazhin, M., Longo, G., Capaccioli, M., Alcalá, J. M., Silvotti, R., Covone, G., Khovanskaya, O., Pavlov, M., Pannella, M., Radovich, M., & Testa, V., 2003, Mon. Not. R. Astron. Soc., 343(2), 353, doi: 10.1046/j.1365-8711.2003.06568.x.
- [26] Sazhin, M. V., Khovanskaya, O. S., Capaccioli, M., & Longo, G., 2018, 9(December), 1.
- [27] Verbiest, J. P., 2016, Mon. Not. R. Astron. Soc., 458(2), 1267, doi: 10.1093/mnras/stw347.
- [28] Janssen, G. H., Hobbs, G., Mclaughlin, M., Bassa, C. G., Deller, A. T., Kramer, M., Lee, K. J., Mingarelli, C. M., Rosado, P. A., Sanidas, S. A., Sesana, A., Shao, L., Stairs, I. H., Stappers, B. W., & Verbiest, J. P., Gravitational wave astronomy with the SKA, In Proc. Sci., volume 9-13-June-, pages 1–19, 2014, doi: 10.22323/1.215.0037.
- [29] Amaro-Seoane, P., 2012, URL <http://arxiv.org/abs/1201.3621>.
- [30] Amaro-Seoane, P., Low-frequency gravitational-wave science with eLISA/NGO, 2012, ISSN 02649381.
- [31] Seto, N., Kawamura, S., & Nakamura, T., 2001, Phys. Rev. Lett., 87(22), 221103, doi: 10.1103/PhysRevLett.87.221103.
- [32] Kawamura, S., 2011, Class. Quantum Gravity, 28(9), doi: 10.1088/0264-9381/28/9/094011.
- [33] Harry, G. M., 2010, Class. Quantum Gravity, 27(8), doi: 10.1088/0264-9381/27/8/084006.
- [34] Accadia, T., 2011, Class. Quantum Gravity, 28(11), doi: 10.1088/0264-9381/28/11/114002.
- [35] Somiya, K., 2012, Class. Quantum Gravity, 29(12), doi: 10.1088/0264-9381/29/12/124007.
- [36] Damour, T. & Vilenkin, A., 2000, Phys. Rev. Lett., 85, 18, doi: 10.1103/PhysRevD.64.064008.
- [37] Damour, T. & Vilenkin, A., 2001, Phys. Rev. D - Part. Fields, Gravit. Cosmol., 64(6), 18, doi: 10.1103/PhysRevD.64.064008.
- [38] Binétruy, P., Bohé, A., Hertog, T., & Steer, D. A., 2009, Phys. Rev. D - Part. Fields, Gravit. Cosmol., 80(12), 1, doi: 10.1103/PhysRevD.80.123510.
- [39] Shellard, E. P., 1987, Nucl. Physics, Sect. B, 283(C), 624, doi: 10.1016/0550-3213(87)90290-2.
- [40] Jackson, M. G., Jones, N. T., & Polchinski, J., 2005, J. High Energy Phys., 10(10), 271, doi: 10.1088/1126-6708/2005/10/013.
- [41] Binétruy, P., Bohé, A., Hertog, T., & Steer, D. A., 2010, Phys. Rev. D - Part. Fields, Gravit. Cosmol., 82(8), 1, doi: 10.1103/PhysRevD.82.083524.
- [42] Damour, T. & Vilenkin, A., 2005, Phys. Rev. D - Part. Fields, Gravit. Cosmol., 71(6), 1, doi: 10.1103/PhysRevD.71.063510.
- [43] Siemens, X., Mandic, V., & Creighton, J., 2007, Phys. Rev. Lett., 98(11), 1, doi:

- 10.1103/PhysRevLett.98.111101.
- [44] DePies, M. R. & Hogan, C. J., 2007, Phys. Rev. D - Part. Fields, Gravit. Cosmol., 75(12), 1, doi: 10.1103/PhysRevD.75.125006.
- [45] Ölmez, S., Mandic, V., & Siemens, X., 2010, Phys. Rev. D - Part. Fields, Gravit. Cosmol., 81(10), 1, doi: 10.1103/PhysRevD.81.104028.
- [46] Sanidas, S. A., Battye, R. A., & Stappers, B. W., 2012, Phys. Rev. D - Part. Fields, Gravit. Cosmol., 85(12), 1, doi: 10.1103/PhysRevD.85.122003.
- [47] Sanidas, S. A., Battye, R. A., & Stappers, B. W., 2013, Astrophys. J., 764(1), 1, doi: 10.1088/0004-637X/764/1/108.
- [48] Binétruy, P., Bohé, A., Caprini, C., & Dufaux, J. F., 2012, J. Cosmol. Astropart. Phys., 2012(6), doi: 10.1088/1475-7516/2012/06/027.
- [49] Kuroyanagi, S., Miyamoto, K., Sekiguchi, T., Takahashi, K., & Silk, J., 2012, Phys. Rev. D - Part. Fields, Gravit. Cosmol., 86(2), 1, doi: 10.1103/PhysRevD.86.023503.
- [50] Kuroyanagi, S., Miyamoto, K., Sekiguchi, T., Takahashi, K., & Silk, J., 2013, Phys. Rev. D - Part. Fields, Gravit. Cosmol., 87(2), 111212, doi: 10.1103/PhysRevD.87.023522.
- [51] Siemens, X., Olum, K. D., & Vilenkin, A., 2002, Phys. Rev. D - Part. Fields, Gravit. Cosmol., 66(4), 4, doi: 10.1103/PhysRevD.66.043501.
- [52] Polchinski, J. & Rocha, J. V., 2006, Phys. Rev. D - Part. Fields, Gravit. Cosmol., 74(8), 1, doi: 10.1103/PhysRevD.74.083504.
- [53] Sousa, L. & Avelino, P. P., 2016, Phys. Rev. D, 94(6), 1, doi: 10.1103/PhysRevD.94.063529.
- [54] Binétruy, P., Bohé, A., Hertog, T., & Steer, D. A., 2010, Phys. Rev. D - Part. Fields, Gravit. Cosmol., 82(12), 1, doi: 10.1103/PhysRevD.82.126007.
- [55] Sakellariadou, M., 1990, Phys. Rev. D, 42(2), 354, doi: 10.1103/PhysRevD.42.354.
- [56] Hindmarsh, M., 1990, Phys. Lett. B, 251(1), 28, doi: 10.1016/0370-2693(90)90226-V.
- [57] Figueroa, D. G., Hindmarsh, M., & Urrestilla, J., 2013, Phys. Rev. Lett., 110(10), 1, doi: 10.1103/PhysRevLett.110.101302.
- [58] Kawasaki, M., Miyamoto, K., & Nakayama, K., 2010, Phys. Rev. D - Part. Fields, Gravit. Cosmol., 82(10), 1, doi: 10.1103/PhysRevD.82.103504.
- [59] Matsui, Y., Horiguchi, K., Nitta, D., & Kuroyanagi, S., 2016, J. Cosmol. Astropart. Phys., 2016(11), doi: 10.1088/1475-7516/2016/11/005.
- [60] Matsui, Y. & Kuroyanagi, S., 2019, Phys. Rev. D, 100(12), 123515, doi: 10.1103/PhysRevD.100.123515, URL <http://arxiv.org/abs/1902.09120>.
- [61] Avgoustidis, A. & Shellard, E. P., 2008, Phys. Rev. D - Part. Fields, Gravit. Cosmol., 78(10), 1, doi: 10.1103/PhysRevD.78.103510.
- [62] Avgoustidis, A. & Copeland, E. J., 2010, Phys. Rev. D - Part. Fields, Gravit. Cosmol., 81(6), 1, doi: 10.1103/PhysRevD.81.063517.
- [63] Copeland, E. J. & Kibble, T. W. B., 2009, Phys. Rev. D - Part. Fields, Gravit. Cosmol., 80(12), doi: 10.1103/PhysRevD.80.123523.
- [64] Penzias, A. A. & Wilson, R. W., 1965, Astrophys. J., 142, 419.
- [65] Mather, J. C., Cheng, E. S., Cottingham, D. A., Eplee, R. E., J., Fixsen, D. J.,

- Hewagama, T., Isaacman, R. B., Jensen, K. A., Meyer, S. S., Noerdlinger, P. D., Read, S. M., Rosen, L. P., Shafer, R. A., Wright, E. L., Bennett, C. L., Boggess, N. W., Hauser, M. G., Kelsall, T., Moseley, S. H., J., Silverberg, R. F., Smoot, G. F., Weiss, R., & Wilkinson, D. T., 1994, Astrophys. J., 420, 439, doi: 10.1086/173574.
- [66] Planck Collaboration, 2016, Astron. Astrophys., 594, doi: 10.1051/0004-6361/201525830.
- [67] Yadav, J., Bharadwaj, S., Pandey, B., & Seshadri, T. R., 2005, Mon. Not. R. Astron. Soc., 364(2), 601, doi: 10.1111/j.1365-2966.2005.09578.x.
- [68] Friedmann, A., 1922, Z. Phys, 10(1), 377.
- [69] Walker, A. G., 1936, 95(1935), 263.
- [70] Robertson, H. P., 1935.
- [71] Kolb, E. W. & Turner, M. S., The early universe, 2018, ISBN 9780429961410, doi: 10.1201/9780429492860.
- [72] Kirzhnits, D. A. & Linde, A. D., 1972, Phys. Lett. B, 42(4), 471, doi: 10.1016/0370-2693(72)90109-8.
- [73] Weinberg, S., 1974, Phys. Rev. D, 9(12), 3357, doi: 10.1103/PhysRevD.9.3357.
- [74] Goldstone, J., 1961, Nuovo Cim., 19(1), 154, doi: 10.1007/BF02812722.
- [75] Higgs, P. W., 1964, Phys. Rev. Lett., 13(16), 508, doi: 10.1103/PhysRevLett.13.508.
- [76] Guth, A. H., 1981, Phys. Rev. D, 23(2), 347, doi: 10.1103/PhysRevD.23.347.
- [77] Sato, K., 1981, Mon. Not. R. Astron. Soc., 195(3), 467, doi: 10.1093/mnras/195.3.467.
- [78] Armillis, R. & Pallis, C., Implementing hilltop F-term hybrid inflation in supergravity, 2013, ISBN 9781624179433.
- [79] Quevedo, F., Lectures on string/brane cosmology, In Class. Quantum Gravity, volume 19, pages 5721–5779, 2002, doi: 10.1088/0264-9381/19/22/304.
- [80] Yoneya, T., 1973, Lett. al Nuovo Cim., 8(16), 951, doi: 10.1007/BF02727806.
- [81] Yoneya, T., 1974, Prog. Theor. Phys., 51(6), 1907, doi: 10.1143/ptp.51.1907.
- [82] Scherk, J. & Schwarz, J. H., 1974, Nucl. Physics, Sect. B, 81(1), 118, doi: 10.1016/0550-3213(74)90010-8.
- [83] Polchinski, J., 2005, Gen. Relativ. Gravit., pages 142–160.
- [84] Sakellariadou, M., 2008, Philos. Trans. R. Soc. A Math. Phys. Eng. Sci., 366(1877), 2881, doi: 10.1098/rsta.2008.0068.
- [85] Randall, L. & Sundrum, R., 1999, Phys. Rev. Lett., 83, 4, URL [papers2://publication/uuid/E0B35896-79F4-438F-8D1C-053BBD0B7E50](https://arxiv.org/abs/hep-th/9810155).
- [86] Goddard, P., 1973, Nucl. Physics, Sect. B, 56(1), 109, doi: 10.1016/0550-3213(74)90249-1.
- [87] Nielsen, H. B. & Olesen, P., 1973, Nucl. Phys., B61, 45, doi: 10.1016/0550-3213(73)90350-7.
- [88] Vilenkin, A., 1985, Phys. Rep., 121(5), 263, doi: 10.1016/0370-1573(85)90033-X.
- [89] Turok, N., 1983, Phys. Lett., 126B.
- [90] Turok, N., 1984, Nucl. Physics, Sect. B, 242(2), 520, doi: 10.1016/0550-3213(84)90407-3.
- [91] Copeland, E. J. & Turok, N., 1986, Fermi Natl. Accel. Laboratory.

- [92] Albrecht, A. & Turok, N., 1989, Phys. Rev. D, 40(4), 973, doi: 10.1103/PhysRevD.40.973.
- [93] Martins, C. J. & Shellard, E. P., 1996, Phys. Rev. D - Part. Fields, Gravit. Cosmol., 54(4), 2535, doi: 10.1103/PhysRevD.54.2535, URL <https://arxiv.org/pdf/hep-ph/9602271.pdf>.
- [94] Pogosian, L. & Vachaspati, T., 1999, Phys. Rev. D - Part. Fields, Gravit. Cosmol., 60(8), 1, doi: 10.1103/PhysRevD.60.083504.
- [95] Vilenkin, A., 1981, Phys. Rev., D24, 2082, doi: 10.1103/PhysRevD.24.2082.
- [96] Hindmarsh, M. B. & Kibble, T. W. B., may 1995, Reports Prog. Phys., 58(5), 477, doi: 10.1088/0034-4885/58/5/001, URL <https://doi.org/10.1088/0034-4885/58/5/001>.
- [97] Shellard, E. P. & Ruback, P. J., 1988, Phys. Lett. B, 209(2-3), 262, doi: 10.1016/0370-2693(88)90944-6.
- [98] Moriarty, K. J., Myers, E., & Rebbi, C., 1988, Phys. Lett. B, 207(4), 411, doi: 10.1016/0370-2693(88)90674-0.
- [99] Matzner, R. A., 1988, Comput. Phys., 2(5), 51, doi: 10.1063/1.168306.
- [100] Witten, E., 1985, Phys. Lett., 153B, 243, doi: 10.1016/0370-2693(85)90540-4.
- [101] Davis, A. C. & Kibble, T. W. B., 2005, Contemp. Phys., 46(5), 313, doi: 10.1080/00107510500165204.
- [102] Kibble, T. W. B. & Turok, N., 1982, Phys. Lett. B, 116(2-3), 141, doi: 10.1016/0370-2693(82)90993-5.
- [103] Blanco-Pillado, J. J. & Olum, K. D., 1999, Phys. Rev. D - Part. Fields, Gravit. Cosmol., 59(6), 1, doi: 10.1103/PhysRevD.59.063508.
- [104] Kibble, T. W. B. & Copeland, E., 1991, Phys. Scr., 1991(T36), 153, doi: 10.1088/0031-8949/1991/T36/017.
- [105] Schwarz, J. H., 1995, Phys. Lett. B, 360(1-2), 13, doi: 10.1016/0370-2693(95)01138-G.
- [106] Witten, E., 1996, Nucl. Phys. B, 460(2), 335, doi: 10.1016/0550-3213(95)00610-9.
- [107] Polchinski, J., 2005, pages 229–253, doi: 10.1007/1-4020-3733-3\_10.
- [108] Copeland, E. J., Kibble, T. W. B., & Steer, D. A., 2006, Phys. Rev. Lett., 97(2), 1, doi: 10.1103/PhysRevLett.97.021602.
- [109] Copeland, E. J., Kibble, T. W. B., & Steer, D. A., 2007, Phys. Rev. D - Part. Fields, Gravit. Cosmol., 75(6), 1, doi: 10.1103/PhysRevD.75.065024.
- [110] Kibble, T. W. B., 1985, Nucl. Phys. B, pages 227–244.
- [111] Avgoustidis, A. & Shellard, E. P., 2006, Phys. Rev. D - Part. Fields, Gravit. Cosmol., 73(4), 1, doi: 10.1103/PhysRevD.73.041301.
- [112] Pourtsidou, A., Avgoustidis, A., Copeland, E. J., Pogosian, L., & Steer, D. A., 2011, Phys. Rev. D - Part. Fields, Gravit. Cosmol., 83(6), 1, doi: 10.1103/PhysRevD.83.063525.
- [113] Martins, C. J. & Shellard, E. P., 2002, Phys. Rev. D - Part. Fields, Gravit. Cosmol., 65(4), 11, doi: 10.1103/PhysRevD.65.043514.
- [114] Sakellariadou, M., 2005, J. Cosmol. Astropart. Phys., 2005, 003.

- [115] Jackson, M. G., 2007, J. High Energy Phys., 2007(9), doi: 10.1088/1126-6708/2007/09/035.
- [116] Tye, S. H., Wasserman, I., & Wyman, M., 2005, Phys. Rev. D - Part. Fields, Gravit. Cosmol., 71(10), 1, doi: 10.1103/physrevd.71.103508.
- [117] Austin, D., Copeland, E. J., & Kibble, T. W. B., 1993, Phys. Rev. D, 48(12), 5594, doi: 10.1103/PhysRevD.48.5594.
- [118] Binétruy, P., Bohé, A., Hertog, T., & Steer, D. A., 2009, Phys. Rev. D - Part. Fields, Gravit. Cosmol., 80(12), 1, doi: 10.1103/PhysRevD.80.123510.
- [119] Cabass, G., Pagano, L., Salvati, L., Gerbino, M., Giusarma, E., & Melchiorri, A., 2016, Phys. Rev. D, 93(6), 1, doi: 10.1103/PhysRevD.93.063508.
- [120] Copeland, E. J., Magueijo, J., & Steer, D. A., 2000, Phys. Rev. D - Part. Fields, Gravit. Cosmol., 61(6), 1, doi: 10.1103/PhysRevD.61.063505.
- [121] Siemens, X. & Olum, K. D., 2001, Nucl. Phys. B, 611(1-3), 125, doi: 10.1016/S0550-3213(01)00353-4.
- [122] Abbott, B. P., 2017, Phys. Rev. Lett., 118(12), 1, doi: 10.1103/PhysRevLett.118.121101.
- [123] NANOGrav Collaborator, 2018, Astrophys. J., 859(1), 47, doi: 10.3847/1538-4357/aabd3b.
- [124] Ringeval, C. & Suyama, T., 2017, J. Cosmol. Astropart. Phys., 2017(12), doi: 10.1088/1475-7516/2017/12/027.
- [125] Jenkins, A. C. & Sakellariadou, M., 2018, Phys. Rev. D, 98(6), 63509, doi: 10.1103/PhysRevD.98.063509, URL <https://doi.org/10.1103/PhysRevD.98.063509>.